Doctoral Dissertation

Development of Plasma Chemical Process for Sensor and Bio-chem Devices

Nina Andreeva

2012

Department of Materials, Physics and Energy Engineering

Graduate School of Engineering

Nagoya University

Contents

Chapter 4:

Synthesis and surface modification of carbon nanoballs (CNBs)

Chapter 5:

Characterization of platinum catalyst supported on carbon nanoballs prepared by solution plasma processing

Acknowledgements

This doctoral dissertation has been carried out under the supervision of Professor Nagahiro Saito at Nagoya University from 2008 to 2011. I would like to thank for his appropriate advices, his continuous guidance and generous supports throughout my work. Without his appropriate guide and helpful advices, this dissertation would not have been completed. This dissertation has been greatly advanced and developed by the advices of Professor Ryoichi Ichino (Nagoya University), Professor Katsuya Teshima (Shinshu University), Professor Tatsuru Shirafuji (Osaka City University) and Associate Professor Takuya Fujima (Tokyo City University). I am grateful to their appropriate guidance with enthusiasm. I thank my advisor, Dr. Takahiro Ishizaki (AIST) and Dr. Pavel Baroch (West Bohemia University) for teaching me your thought as a researcher and their helpful discussions.

January, 2012

Nina Andreeva

Chapter 1

Introduction

1.1 Preface

1.2 Objectives

1.3 Outlines

1.4 References

1.1 Preface

1.1.1 Background

In moving into the 21st century, global warming becomes a major issue all over the world. To depress the global warming, technological developments for lowering fuel consumption and reducing CO_2 emission are essential. Solar cells, fuel cells, and secondary batteries are devices on green innovation for producing energy required in our daily life. These devices have been fabricated by various methods [1]. However, in these devices there are many problems on electric generation efficiency, life time, costs and so on. To overcome these problems, it is necessary to functionalize highly materials used in the devices. Surface modification would be an effective means for this purpose. Plasma technology has been used to modify material surfaces [2]. Thus, the plasma process would be a key technology for developing the energy materials.

Life innovation for healthcare, and decontamination and sterilization of water is also one of the most important issues on the environmental and medical fields. Plasma healthcare or plasma medicine is an emerging field that has its roots, quite naturally, in plasma science [3]. It has grown rapidly and is now the subject of a broad interdisciplinary research involving medicine, biology, physics, chemistry and engineering. On the other hand, in the field of water treatment plasma technologies under atmospheric conditions are emerged as potential alternative methods for the

sterilization of the bacteria in water [4-11]. The advantages of the methods have their stability to sterilize at relatively low temperatures within a short time and non-toxic nature in comparison to more traditional methods. Unlike chemical based biocides such as chlorine and ozone, the plasma treatment is a physical method used to kill all bacteria without adding any biocidal chemical.

As above-mentioned, plasma technology would be a key technology to realize green and life innovations, and then it is very important to advance the plasma technology.

1.1.2 Plasma technology

Irving Langmuir first used the term “plasma” in 1926 to describe the inner region of an electrical discharge [12]. Later, the definition was broadened to define a state of matter in which a significant number of atoms and/or molecules are electrically charged or ionized. The components in plasma are ions, free electrons, photons, and neutral atoms and molecules in ground and excited states. In order to maintain a steady state, it is necessary to apply an electric field to the gas plasma, which is generated in a chamber at low pressure.

Plasma, as a very reactive material, can be used to modify the surface of a certain substrate, depositing chemical materials to impart some desired properties, removing substances, which were previously deposited on the substrate, and so on.

Plasma is any substance (usually a gas) whose atoms have one or more electrons detached and therefore become ionized. The detached electrons remain, however, in the gas volume that in an overall sense remains electrically neutral. Thus, any ionized gas that is composed of nearly equal numbers of negative and positive ions is called plasma. The ionization can be effected by the introduction of large concentrations of energy, such as bombardment with fast external electrons and irradiation with laser light, or by heating the gas to very high temperatures.

A gas becomes plasma when the kinetic energy of the gas particles rises to equal the ionization energy of the gas. When this level is reached, collisions of the gas particles cause a rapid cascading ionization, resulting in plasma. If the necessary energy is provided by heat, the threshold temperature is from 50,000 to 100,000 K and the temperatures for maintaining plasma range up to hundreds of millions of degrees. Another way of changing a gas into plasma is to pass high-energy electrons through the gas. The individually charged plasma particles respond to electric and magnetic fields and can therefore be manipulated and contained. The atmospheres of most stars, the gas within the glass tubing of neon advertising signs, and the gases of the upper atmosphere of the earth are examples of plasmas. On the earth, plasmas occur naturally in the form of lightning bolts and in parts of flames.

There are many different ways to induce the ionization of gases; (1) glow discharge, (2) corona discharge, (3) arc discharge and (4) dielectric barrier discharge

(DBD). Generation of plasma can be created by applying an electric field to a low-pressure gas, as in neon or fluorescent tubes. Plasma can also be created by heating a neutral gas to very high temperatures. Usually the required temperatures are too high to be applied externally, and the gas is heated internally by the injection of high-speed ions or electrons that collide with the gas particles, increasing their thermal energy. The electrons in the gas can also be accelerated by external electric fields. Ions from such plasmas are used in the semiconductor industry for etching surfaces and otherwise altering the properties of materials. Here, electric current is passed through a gas and electrons from the electrical current become part of the gas causing the gas atoms and molecules to become ionized, or charged. The degree of ionization, α is defined as

$$\alpha = n_i / (n_i + n_a) \quad (1.1)$$

Where, n_i is the number density of ions and n_a is the number density of neutral atoms. The amount, or degree, of ionization is called the "plasma density".

Generally, high plasma densities are desirable, because electrons impact gas molecules and create the excited-state species used for textile treatment. Having more electrons generally equates to faster treatment time. However, very high plasma densities (greater than 10^{17} electrons cm^{-3}) can only exist with very high gas temperature. This extremely high level of plasma density is unsuitable for textile treatment, because the plasma's energy will burn almost any material. These plasmas,

often called thermal plasmas, are used for incineration.

Plasma properties are dependent on the plasma parameters like degree of ionization, the plasma temperature, the density and the magnetic field in the plasma region. Different range of plasma depending on density and temperature is shown in Fig. 1.1.

1.1.3 Principle of plasma processing

Plasma technology is a surface-sensitive method that allows selective modification from μm to nm ranges. By introducing energy into a gas, quasi-neutral plasma can be generated consisting of neutral particles, electrically charged particles and highly reactive radicals. If a material to be functionalized is placed in a reaction chamber with any gas and the plasma is then ignited, the generated particles interact with the surface of the material. In this way, the surface is specifically structured, chemically functionalized or even coated with thin film depending on the type of gas and control of the process.

The plasma consists of free electrons, radicals, ions, UV-radiation and a lot of different excited particles in dependence upon the used gas. Different reactive species in the plasma chamber interact with the substrate surface. Cleaning, modification or coating is dependent on the used parameters. Plasma treatments have been used to induce both surface modifications and bulk property enhancements of materials,

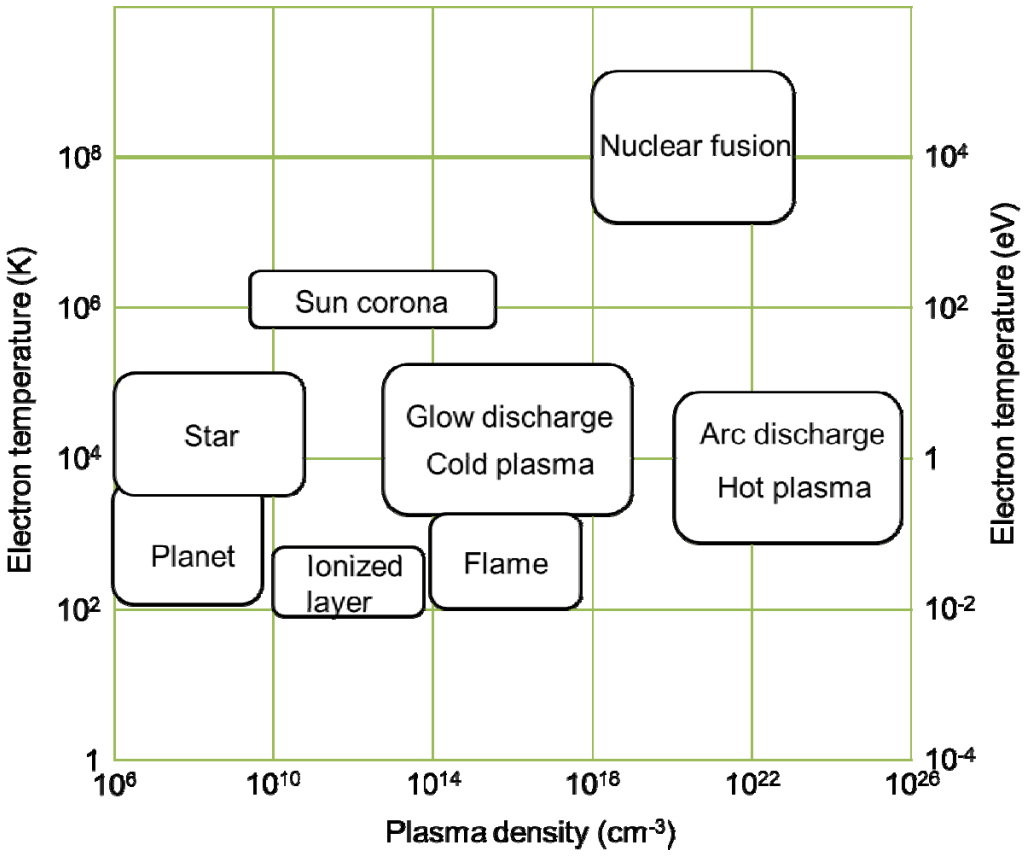

Fig. 1.1 Relationship among plasma, electron temperature and plasma density.

resulting in improvements to products ranging from conventional materials to advanced composites. These treatments have been shown to enhance dyeing rates of polymers, to increase adhesion of coatings, and to modify the wettability of materials. Research has shown that improvements in toughness and tenacity can be achieved by subjecting various materials to plasma. Recently, plasma treatments have produced increased moisture absorption in fibers, altered degradation rates of biomedical materials (such as sutures), and deposition of low friction coatings.

1.1.4 Various plasmas

There are many different ways to induce the ionization of gases; (1) glow discharge, (2) corona discharge, (3) arc discharge, (4) dielectric barrier discharge (DBD) and (5) solution plasma. The details of these plasmas are described below.

1.1.4.1 Glow discharge

It is the oldest type of plasma technique. It is produced at reduced pressure (low-pressure plasma technique) and provides the highest possible uniformity and flexibility of any plasma treatment. The plasma is formed by applying a DC, low frequency (50 Hz) or radio frequency (40 kHz, 13.56 MHz) voltage over a pair or a series of electrodes. Alternatively, a vacuum glow discharge can be made by using microwave (GHz) power supply.

1.1.4.2 Corona discharge

It is formed at atmospheric pressure by applying a low frequency or pulsed high voltage over an electrode pair, the configuration of which can be one of many types. Typically, both electrodes have a large difference in size. The corona consists of a series of small lightning-type discharges; the high local energy levels make the classical corona treatment of materials problematic in many cases.

1.1.4.3 Arc discharge

It is formed at atmospheric pressure or higher pressures by applying a DC, AC low frequency or radio frequency voltage over electrodes. It is thermal plasma or high temperature plasma, and in an equilibrium state. It is applied to melting, welding, material syntheses and so on.

As discussed earlier, there are various forms of plasma depending on the range of temperature and electron density. Generally, high plasma densities are desirable, because electrons impact gas molecules and create the excited-state species used for surface treatments of materials. Having more electrons generally equates to faster treatment time. However, very high plasma densities (greater than 10^{17} electrons cm^{-3}) can only exist with very high gas temperature ("thermal plasma"). This extremely high level of plasma density is unsuitable for polymer treatment, because the plasma's energy will burn almost any organic material. Hence for polymer material processing,

the plasma needs to do its job at room temperature, thus the name “cold plasma”. This is due to the fact that the energy of the plasma is mainly confined to the energy of low mass electrons. Nonthermal plasma or cold plasma is characterized by a large difference in the temperature of the electrons relative to the ions and neutrals. Thus, $T_e >> T_i \approx T_n$. As the electrons are extremely light, they move quickly and have almost no heat capacity. Ionization is maintained by the impact of electrons with neutral species. These plasmas are maintained by passing electrical current through a gas. The low temperature makes them suitable for textile processing. However, nonthermal plasmas generally require low-pressure or vacuum conditions.

1.1.4.4 Dielectric barrier discharge (DBD)

DBD is formed by applying a pulsed voltage over an electrode pair of which at least one is covered by a dielectric material. Though also here lightning-type discharges are created, a major advantage over corona discharges is the improved textile treatment uniformity.

1.1.4.5 Solution plasma

Solution plasma means discharge in liquid phase and has been developed by our laboratory. This solution plasma would be reasonable to expect a higher reaction rate under lower-temperature conditions with greater chemical reaction variability because

the molecular density of the liquid phase is much higher than that of the gas phase. We can generate a variety of plasmas by choosing the combinations of solvents and solutes in solutions. This approach would allow us to functionalize various materials in liquids within a short time.

Fig. 1.2 shows three categories of plasma corresponding to the pressure–temperature relationship of three phases. This figure summarizes the present status of plasma research too.

1.2 Objectives

The aim of this doctoral dissertation is to establish the basic process conditions for high functionalization of biomaterial, sensor device, energy material, and sterilization treatment using plasma chemical process and to investigate their characteristics.

The details of the objectives are shown as follows:

(a) Investigation of hydrophilicity and bioactivity of polymer surfaces modified by plasma-initiated graft polymerization.

(b) Investigation of sensitive detection of volatile organic compounds on quartz crystal microbalance coated with superhydrophobic film prepared by plasma enhanced chemical vapor deposition method.

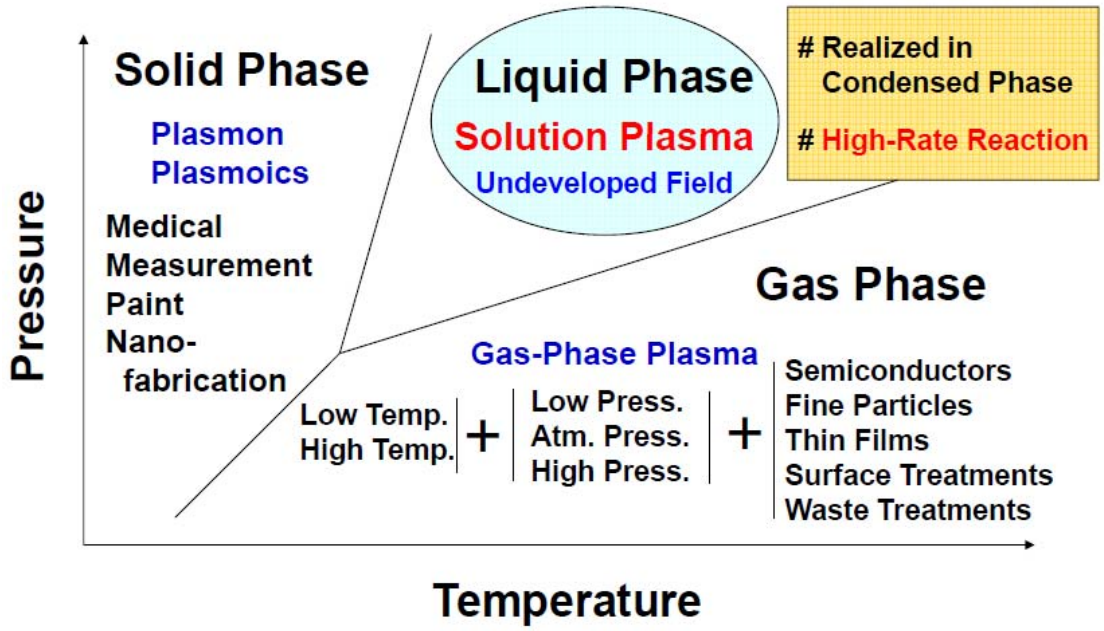

Fig. 1.2 Three categories of plasma corresponding to the pressure-temperature relation of three phases.

(c) Establishment of synthesis process of carbon nanoballs and investigation of surface states of carbon nanoballs modified by solution plasma.

(d) Characterization of platinum catalyst supported on carbon nanoballs prepared by solution plasma processing.

(e) Development of rapid sterilization process of *Escherichia coli* by solution plasma.

1.3 Outlines

In this Chapter 1 entitled “Introduction”, the background of the present study, and the necessity and category of plasma processes are described. The motivation, the objectives and the outlines of this research work are also stated.

In Chapter 2 entitled “Hydrophilicity and bioactivity of polymer surfaces modified by plasma-initiated graft polymerization”, mouse 3T3 fibroblast cell adhesion behaviors on various polymer surfaces modified by plasma treatment have been investigated in terms of the plasma process conditions. By controlling the plasma process conditions, the polymer surface became hydrophilic and the hydrophilicity was maintained for a long time. On the modified polyethylene terephthalate (PET) surfaces the 3T3 fibroblast cells were cultured for the evaluation of cell adhesion behaviors.

In Chapter 3 entitled “High sensitive detection of volatile organic compounds using superhydrophobic quartz crystal microbalance”, the correlation between

detection sensitivities of quartz crystal microbalance (QCM) for volatile organic compounds (VOCs) and wettability of QCM surface has been studied by changing the preparation conditions of hydrophobic or superhydrophobic surface. It has been revealed that the QCM sensor coated with the superhydrophobic film were more sensitive to the VOCs than the conventional QCM sensor. In addition, the adsorption mechanisms of VOCs on the superhydrophobic film were suggested.

In Chapter 4 entitled “Synthesis and surface modification of carbon nanoballs (CNBs)”, the synthesis conditions of CNBs have been investigated in terms of the gas flow rate for raw material and reaction temperature. In addition, the plasma conditions in liquid phase for surface modification of the CNBs have been established. It has been revealed that the CNBs could be synthesized at the temperature of more than 850^{o}C and the C_2H_4 gas flow rate of more than 175 sccm. The carboxyl acid groups were successfully introduced to the CNB surface by the plasma treatment in liquid phase. The COOH-terminated CNBs were uniformly dispersed in water, ethanol, acetone, and toluene.

In Chapter 5 entitled “Characterization of platinum catalyst supported on carbon nanoballs prepared by solution plasma processing”, the fabrication conditions of Pt nanoparticles supported on CNBs by solution plasma processing has been studied by changing plasma process conditions and protection agents. In addition, catalytic activities of the Pt/CNB covered with different protection agents have been examined

using cyclic voltammetry. It has been revealed that the sodium dodecyl sulfate (SDS)-containing Pt/CNB showed the higher activity than the carbon material used conventionally.

In Chapter 6 entitled “Rapid sterilization of *Escherichia coli* by solution plasma process”, the sterilization performances of the solution plasma have been investigated by changing the distance between electrodes and applied voltage. It has been revealed that the decimal reduction time of *Escherichia coli (E.coli)* (D value) of this system set at electrode distance of 1.0 mm were estimated to be approximately 1.0 min. In addition, it has been clarified that the UV light generated by the discharge was an important factor for sterilization of the *E.coli*.

In Chapter 7 entitled “Conclusions”, the conclusions of the research achieved for this dissertation are described.

Fig. 1.3 summarizes the plasma chemical process studied in this dissertation.

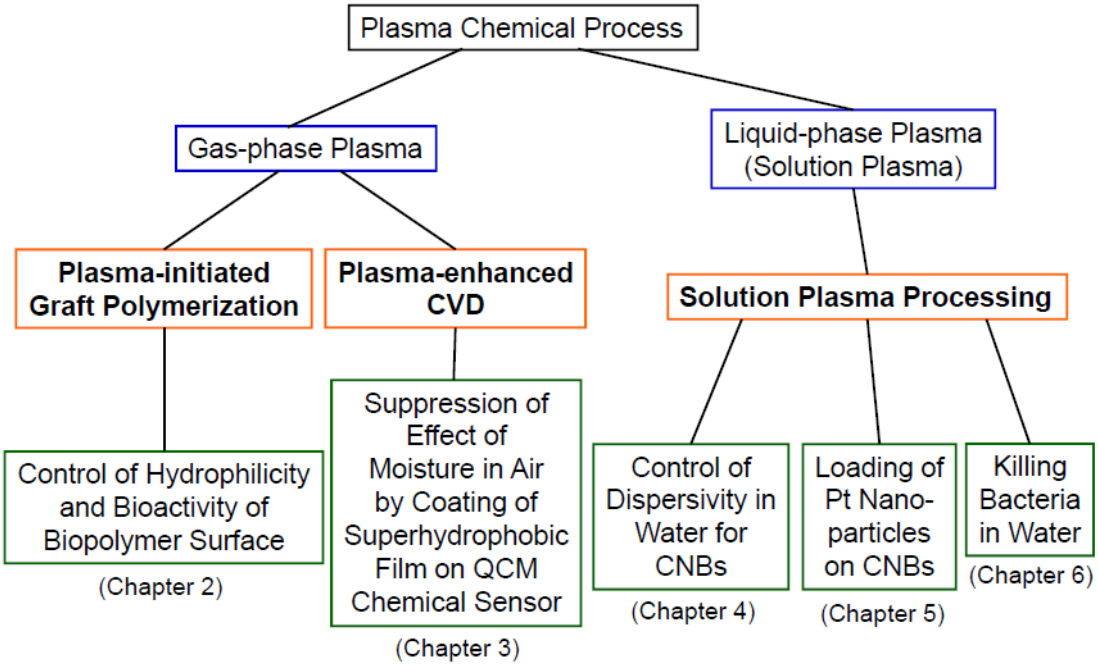

Fig. 1.3 Plasma chemical process studied.

1.4 References

[1] T. Suezaki, P.G. O'Brien, J.I.L. Chen, E. Loso, N.P. Kherani, G.A. Ozin, Adv. Mater., 21, 559 (2009).

[2] E. Endo, T. Yasuda, A. Kita, K. Yamaura, K. Sekai, J. Electrochem. Soc., 147, 1291 (2000).

[3] M. G. Kong, G. Kroesen, G. Morfill, T. Nosenko, T. Shimizu, J. van Dijk, J. L. Zimmermann, New J. Phys., 11, 115012 (2009).

[4] A. Sharma, A. Pruden, Z. Yu, G.J. Collins, Environ. Sci. Technol., 39, 339 (2005).

[5] T. Montie, K.K.-Wintenberg, R. Roth, IEEE Trans. Plasma Sci., 28, 41 (2000).

[6] M. Moisan, J. Barbeau, S. Moreau, M. Tabrizian, J. Pelletier, A. Ricard, L.H. Yahia, Int. J. Pharm., 226, 1 (2001).

[7] M. Laroussi, IEEE Trans. Plasma Sci., 30, 1409 (2002).

[8] M. Laroussi, J.P. Richardson, F.C. Dobbs, Appl. Phys. Lett., 81, 772 (2002).

[9] Y. Akishev, V. Chugunov, M. Grushin, V. Karal'nik, V. Kholodenko, N. Trushkin, Biomedical Aspect of Plasma Physics, APP Spring meeting, Bad Honnef, Germany, 37 (2003).

[10] M. Moisan, J. Barbeau, M.-C. Crevier, J. Pelletier, N. Philip, B. Saoudi, Pure Appl. Chem. 74, 349 (2002).

[11] M. Boudam, M. Moisan, B. Saodi, C. Popovici, N. Gherardi, F. Massines, J. Phys.

D: Appl. Phys. 39, 3494 (2006).

[12] H. M. Mott-Smith, Nature, 233, 219 (1971).

Chapter 2

Hydrophilicity and bioactivity of polymer surfaces modified by plasma-initiated graft polymerization

2.1 Introduction

As stated previous Chapter 1, one of my research targets is to establish the basic process conditions for high functionalization of biomaterial using plasma process and to investigate their characteristics. In this chapter, surface modification of polyethylene terephthalate (PET) was performed using plasma process. In addition, the bioactivity of the PET modified by plasma-initiated graft polymerization was also investigated. Because of its biocompatibility and good mechanical properties, PET has found new developments in the field of medical devices, such as surgical suture material, tendon and ligament replacement material, drug/cell delivery system, and cell culturing support. However, one main issue for biomedical applications of PET concerns low surface hydrophilicity. For better performance in biomedical applications, the PET surface still needs to be improved by functionalization, particularly controlling the hydrophilicity. Thus, it is necessary to establish the surface modification process to impart the hydrophilicity to the PET surface.

The PET film is widely used in a variety of applications because it has some excellent material properties, such as a high melting point and high tensile strength; other characteristics include very good barrier properties, crease resistance, solvent resistance, and resistance to fatigue. However, bonding and finishing of the PET film presents a problem due to low surface hydrophilicity. For example, this affects

wettability, biocompatibility, adhesion and various other surface treatments. Among them, biocompatibility is very important for biomedical applications of the PET film, since it greatly affects on protein adsorption and cell cultures. Thus, controlling the hydrophilicity of the PET surface is crucial for the biomedical applications. In order to impart hydrophilicity to the PET surface, many methods have been devised and used commercially. Among them, plasma treatment is a promising means of enhancing the hydrophilicity of the polymer surface [1–4]. For example, surface oxidation by plasma treatment (e.g., O_2 and H_2O) improves the wettability of polymers such as polyethylene (PE) and poly(methyl methacrylate) (PMMA) [5]. However, these treatments lack permanence because of surface rearrangement. Indeed, previous attempts to make polysulfone membranes hydrophilic by plasma treatment, primarily with O_2 plasma, resulted in only transient hydrophilicity, as demonstrated by contact angle changed within 24 h after plasma treatment.

Plasma is a complex mixture of charged (electrons and ions) and neutral (atoms, molecules and radicals) species. The excited molecular and atomic species in the plasma, in turn, can emit photons over a very broad span of the electromagnetic spectrum, ranging from X-rays to the infrared. The radiation in the vacuum ultraviolet or ultraviolet region is sufficiently energetic to cause modification of surface layers by breaking bonds or initiating photochemical reactions in the polymer [6]. Many researchers have explained that improvement in surface hydrophilicity was generated

by introducing new oxygen-containing functional groups, such as –OH and –COOH, to the surface. These functional groups are hydrophilic [3,4,7–9], so the plasma surface modification should be able to increase the hydrophilicity of the PET surface. However, surface modification by the plasma process introduces two complications. First, polymers are damaged by plasma irradiation [10]; this induces polymer chain scission, thereby contaminating the polymer surfaces. Second, surface hydrophilicity decreases over time due to surface reorientation [11]. In order to overcome these problems when using plasma treatments, it is necessary to introduce organic molecules with hydrophilic functional groups without causing surface damage. Surface-wave plasma (SWP) is a promising method for this purpose, because it allows treatment of polymer surfaces on a large scale at a low electron temperature [12]. In addition, plasma-initiated graft polymerization can attach functional groups or long alkyl chains to the polymer surfaces.

In this study, we demonstrate surface modification of the PET film to provide hydrophilicity through plasma-initiated graft polymerization using surface-wave plasma. The wettability of the modified PET surface was estimated using contact angle measurements. The surface composition was analyzed using X-ray photoelectron spectroscopy (XPS). The roughness of the polymer surface was observed with atomic force microscopy (AFM). Bioactivity was investigated by culturing mouse fibroblast cells on the modified PET film.

2.2 Experimental procedures

2.2.1 Materials

PET films were purchased from Tsutsunaka Plastic Industry Co., Ltd., Japan. The surface of the film was cleaned with ethanol and subsequently rinsed with ultrapure water for 5 min before use. Acrylic acid (AA), (2-hydroxyethyl) methacrylate (HEMA), and styrene (St) monomers were purchased from WAKO Pure Chemical Industries, Ltd., Japan.

2.2.2 Surface modification

The PET surface was modified by SWP excited by microwave radiation. The schematic diagram of the SWP system is shown in Fig. 2.1. The SWP system consisted of a waveguide attached to a microwave generator, a coaxial waveguide, and a stainless steel chamber. A curved reflective plate was attached to the waveguide to efficiently introduce microwaves to the coaxial waveguide. The top of the chamber was sealed with a quartz plate 12 mm in thickness and 140 mm in diameter. The coaxial waveguide was connected vertically to the quartz plate as the dielectric. The generated microwave passed through the waveguide and reached the quartz plate, leading to the formation of the plasma. The cleaned PET substrates were placed at the center of the substrate stage in the chamber. The distance between the quartz plate and

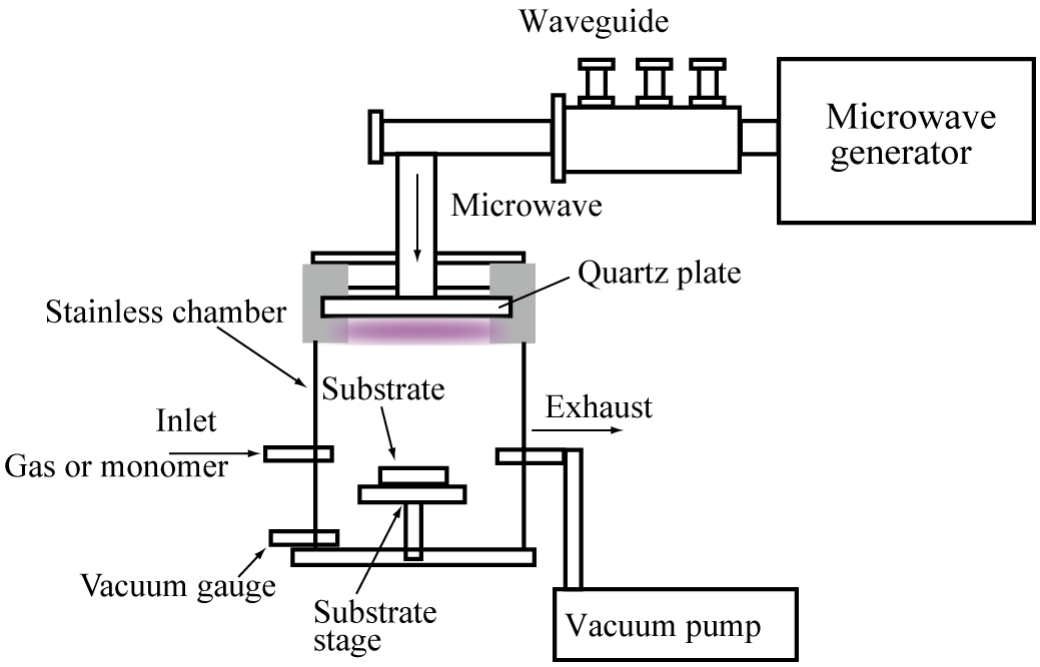

Fig. 2.1 Schematic diagram of the SWP system.

substrate stage was kept constant at 50 mm. The chamber was evacuated to 0.5 Pa with a rotary pump prior to surface modification and Ar gas was subsequently introduced. The total pressure in the chamber varied from 20 to 100 Pa. A microwave power of 200 W was applied to generate plasma for 5 min using a 2.45 GHz generator. The PET surface was irradiated with Ar plasma that generated radicals on the polymer surface [13]. The polymer films were then exposed to AA, HEMA, or St monomer in the vapor phase. The gas pressures for AA, HEMA, and St monomer were 2000, 80, and 400 Pa, respectively. Each gas pressure was kept constant for 60 min, leading to the graft polymerization of the monomer. After exposure to the gas, the polymer films were ultrasonically cleaned in ultrapure water or ethanol for 10 min.

2.2.3 Surface characterization

Topographic images of PET surfaces before and after plasma irradiation were acquired with AFM in the tapping mode; a micro cantilever type SI-DF3 with a spring constant of 1.1 N/m and a resonance frequency of 24 kHz were used for all measurements. The scanning area was a square 10 μm on one side. The hydrophilicity of the polymer surface was characterized using a static water contact angle measurement. A 2 μL water droplet was placed on the sample surface. The chemical bonding states and chemical composition of the polymer surfaces were analyzed using XPS. The MgKα X-ray source was operated at 10 mA and 12 kV.

2.2.4 Cell culture

In order to characterize the bioactivity of the modified PET surface, mouse fibroblast cells (NIH-3T3) were cultured onto both untreated and modified PET surfaces by immersing them into the culture medium (DMEM, pH: 7.0) in a humidified atmosphere containing 5.0 % CO_2 at 37.0°C for 72 h. The initial cell seeding number was 5000 cells/cm^2. The cultured cells were observed with optical and phase-contrast microscopes at intervals of 12 h and were counted using a blood cell counting chamber.

2.3 Results and discussion

In order to provide hydrophilicity to the PET surface without incurring damage, surface modification of the PET film was conducted using varied gas pressures and treatment times. Fig. 2.2 (a) shows the water contact angles of the PET surface modified at different Ar gas pressures. The water contact angle of the untreated PET surface was estimated to be 76.9°, while those modified by Ar gas pressures from 20 to 100 Pa ranged from 34° to 37°. The Ar plasma treatments greatly improved the hydrophilicity of the PET surface. However, the hydrophilicity of the modified PET surface decreased over a period of 70 h after the plasma treatment, which could have been caused by surface reorientation of the PET film. It should be noted that Ar gas

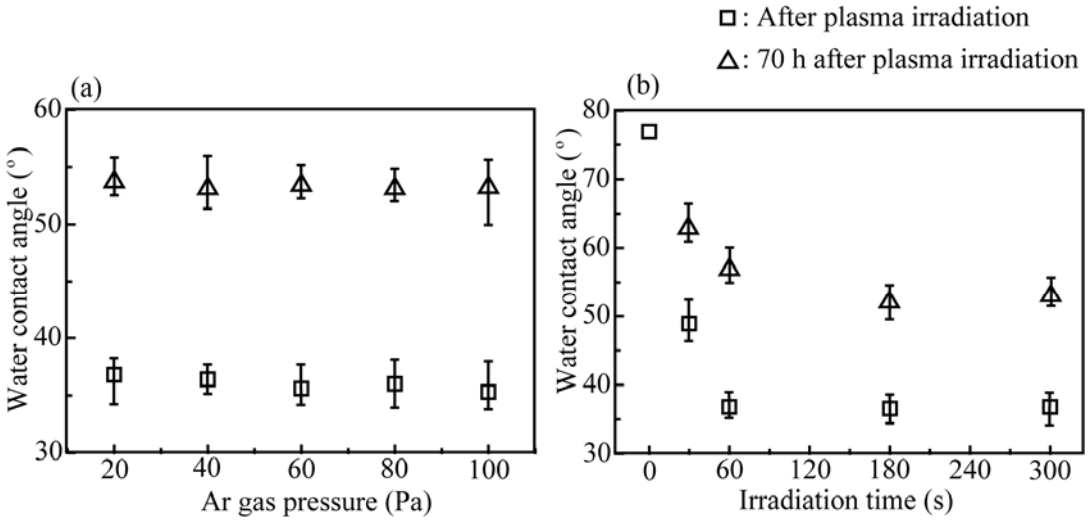

Fig. 2.2 (a) Water contact angles of the PET surface modified at different Ar gas pressures. (b) Effect of plasma irradiation time on water contact angles of the PET surface modified by Ar plasma at 20 Pa.

pressures had no effect on the chemical properties of the modified PET film surface. Fig. 2.2 (b) shows the effects of the plasma irradiation time on the water contact angles of the PET surface modified by Ar plasma at 20 Pa. The hydrophilicity of the PET surface was greatly improved by the Ar plasma treatment for 60 s. The hydrophilicity of the modified PET film remained almost constant with treatment times longer than 60 s. The decrease in the degree of hydrophilicity with time after the treatment of the modified PET surfaces remained almost the same, independent of the plasma treatment time.

Fig. 2.3 shows topographic images of (a) the untreated PET surface, (b) the PET surface modified by Ar plasma at 20 Pa, and (c) the PET surface modified by Ar plasma at 100 Pa. The surface of the untreated PET film appeared to be comparatively smooth with a root-mean-square roughness (R_{rms}) of 1.2 nm (Fig. 2.3(a)). No change in the topography was observed on the PET surface treated by Ar plasma at 20 and 100 Pa, and the R_{rms} were estimated to be 1.0 and 0.7 nm, respectively. This indicated that Ar plasma treatments using SWP did not etch the PET surface. Thus, we were successful in altering the hydrophilicity of the PET surface without any physical damage. However, there was still a lack of permanence of the hydrophilicity of the PET surface modified by Ar plasma.

Plasma-initiated graft polymerization was carried out to enhance the permanence of the hydrophilicity on the PET surface. Fig. 2.4 shows a time course of the water

(a) Untreated

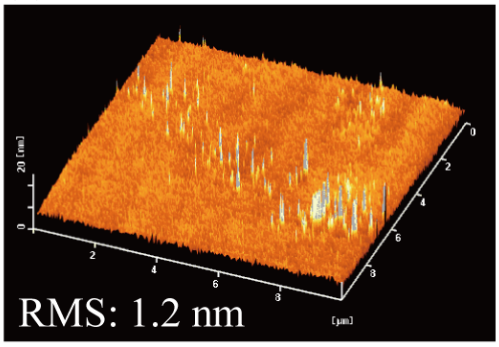

(b) Plasma irradiation (Ar pressure: 20 Pa)

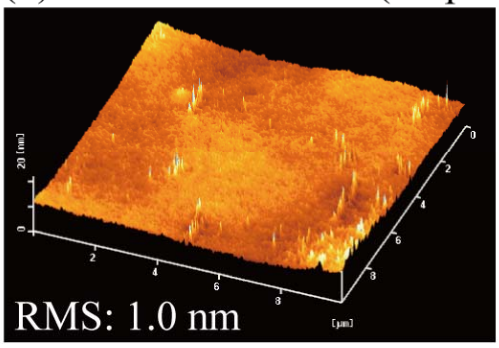

(c) Plasma irradiation (Ar pressure: 100 Pa)

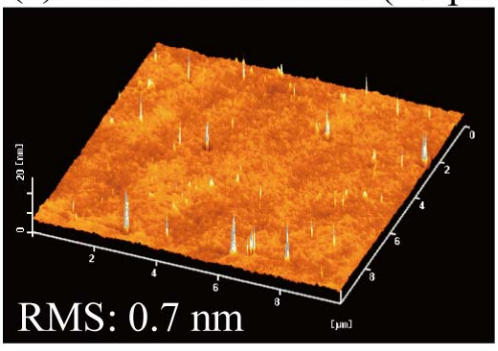

Fig. 2.3 Topographic images of (a) the untreated PET surface, (b) the PET surface modified by Ar plasma at 20 Pa, and (c) the PET surface modified by Ar plasma at 100 Pa.

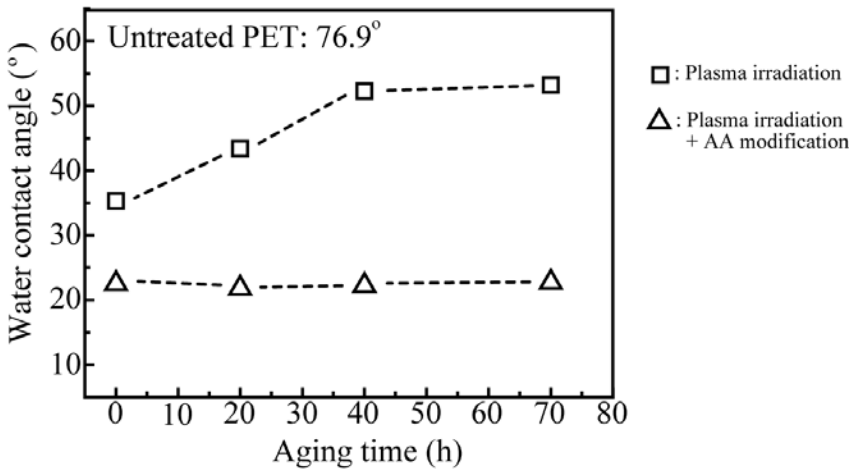

Fig. 2.4 Time course of water contact angles of the PET surface modified by Ar plasma treatment and plasma-initiated graft polymerization using hydrophilic AA monomer.

contact angles of the PET surface modified by (i) Ar plasma treatment and (ii) plasma-initiated graft polymerization using hydrophilic AA monomer. The water contact angles of the PET surface after Ar plasma treatment and Ar plasma followed by hydrophilic AA modification were 35° and 23°, respectively, indicating that plasma-initiated graft polymerization slightly improved the hydrophilicity. In addition, there was a noticeable difference between the treatments in the permanence of the hydrophilicity. The water contact angles of the Ar plasma-treated PET surface increased over time as a result of the instability of hydrophilic groups, such as –OH and –COOH groups, on the polymer surface. In contrast, those on the PET surface after Ar plasma followed by hydrophilic AA modification remained constant at approximately 20°, thereby showing stable hydrophilicity.

In order to test the chemical bonding state of the PET surface, XPS measurements were performed. Fig. 2.5 shows XPS C 1*s* spectra obtained from (a) the untreated PET surface, (b) the PET surface after Ar plasma treatment, and (c) the PET surface after Ar plasma followed by hydrophilic AA modification. The C 1*s* spectrum of the untreated PET surface (Fig. 2.5 (a)) was deconvoluted into three peaks corresponding to carbon atoms of the benzene rings unbonded to the ester group (peak C1 at 284.7 eV), carbon atoms singly bonded to oxygen (peak C2 at 286.5 eV), and ester carbon atoms (peak C3 at 289.1 eV) [13–23]. The relative component concentrations determined from these peak areas were 58.9 % for C1, 21.9 % for C2,

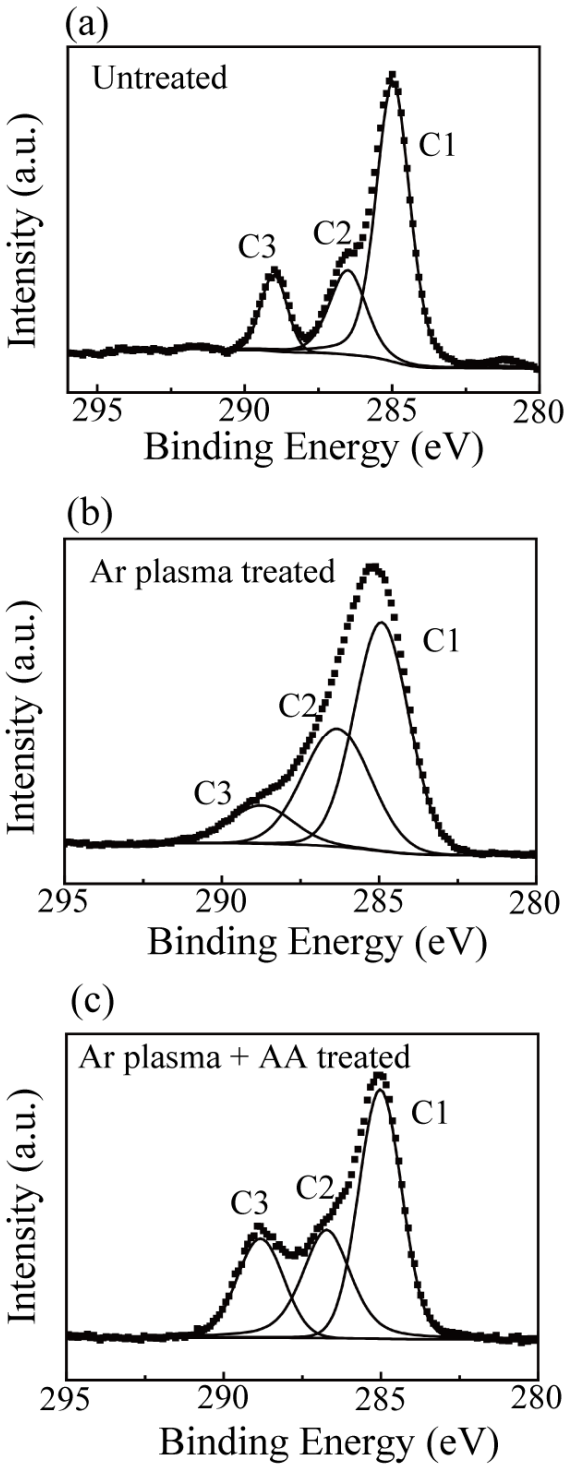

Fig. 2.5 XPS C 1*s* spectra obtained from (a) the untreated PET surface, (b) the PET surface after Ar plasma, and (c) the PET surface after Ar plasma followed by hydrophilic AA modification.

and 19.2 % for C3. However, the C 1*s* spectrum (Fig. 2.5 (b)) reveals that the PET surface was chemically altered by the Ar plasma treatment. The relative component concentrations determined from these peak areas were 54.8 % for C1, 34.1 % for C2, and 11.1 % for C3. The C1–C3 peaks of the untreated PET were broadened by the Ar plasma treatment, indicating that each peak included more than one unique species. These species are ascribed to be formed through a chemical reaction of the polymer chains with activated ion species and radicals. The broadening of C1 and C2 peaks has been associated with the destruction of aromatic rings in PET [19,20,24]. These peaks are assumed to include signals from polar groups such as –C–C=O, –C–COO, or –C–C–O [17,19]. The C 1*s* spectrum (Fig. 2.5 (c)) reveals that the intensities of the C2 and C3 peaks originating from polyacrylic acid have become stronger than those of the plasma-treated PET surface. This indicates that many AA monomers were adsorbed onto the PET surface and then polymerized by plasma-initiated radicals. Thus, polyacrylic acid was successfully grafted onto the PET surface, resulting in increased hydrophilicity. The modified PET surfaces maintained stable hydrophilicity for 70 h because two functional groups in polyacrylic acid (the –COOH group and the hydrocarbon chain) strongly affect the surface properties.

Thus, we successfully provided a PET surface with stable hydrophilicity using plasma-initiated graft polymerization. However, to control the bioactivity of the PET surface, it is necessary to produce PET surfaces with various other physicochemical

properties. Hence, we performed additional surface modifications of the PET film through the plasma-initiated graft polymerization using two different monomers, i.e., HEMA and St.

Fig. 2.6 (a) shows a time course of the water contact angles of the PET surface modified by Ar plasma treatment and plasma-initiated graft polymerization using hydrophilic HEMA monomer. The water contact angles of the PET surface after Ar plasma treatment and Ar plasma followed by hydrophilic HEMA modification were 35° and 29°, respectively. The plasma-initiated graft polymerization of HEMA also slightly improved the hydrophilicity of the PET surface. We observed a noticeable difference between the treatments in the permanence of the hydrophilicity. The water contact angles of the Ar plasma-treated PET surface increased over time, while those on the PET surface after Ar plasma followed by hydrophilic HEMA modification remained almost constant, ranging from 30° to 35°. The XPS C 1*s* spectrum of the PET surface after Ar plasma followed by hydrophilic HEMA modification (Fig. 2.6 (d)) is deconvoluted into three peaks corresponding to the carbon atoms of the benzene rings unbonded to the ester group (peak C1 at 284.7 eV), carbon atoms singly bonded to oxygen (peak C2 at 286.5 eV), and ester carbon atoms (peak C3 at 289.1 eV), as well as the untreated PET surface (Fig. 2.6 (c)). The relative component concentrations determined from these peak areas were 47.3 % for C1, 31.4 % for C2, and 21.3 % for C3. The intensity of the C2 peak attributed to HEMA increased compared to that of the

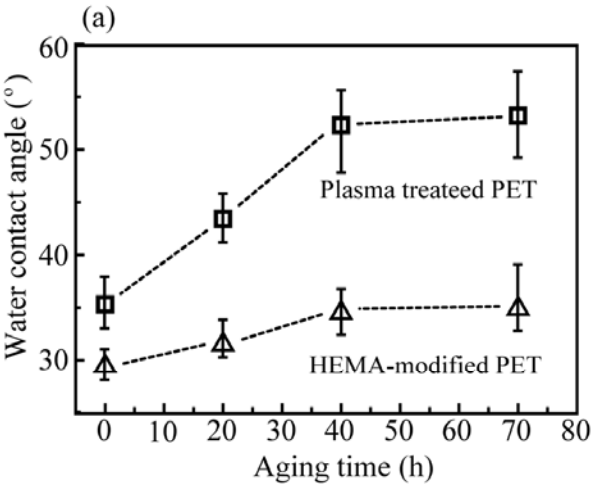

(b)

	Composition (at%)		C1*s* Peak Fitting (%)		
	C	O	C1 C-C, C-H	C2 C-O	C3 O=C-O
Untreated	74.0	26.0	58.9	21.9	19.2
Plasma-treated	71.9	28.1	54.8	34.1	11.1
HEMA-modified	60.5	39.5	47.3	31.4	21.3

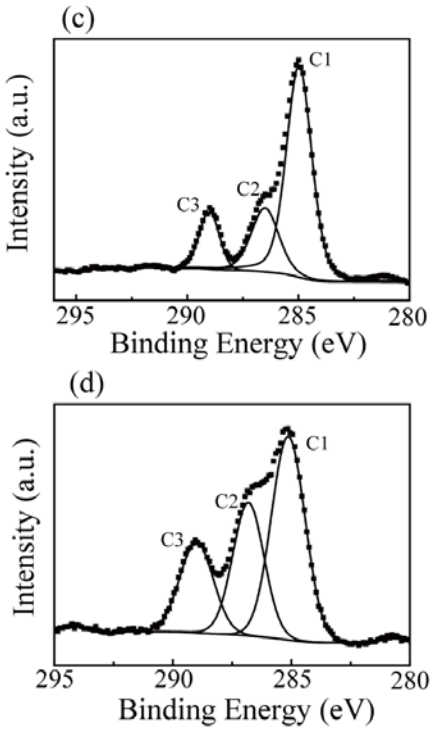

Fig. 2.6 (a) Time course of water contact angles of the PET surface modified by Ar plasma treatment and plasma-initiated graft polymerization using hydrophilic HEMA monomer. (b) Chemical composition and area rates of C1, C2, and C3 peaks obtained from C 1*s* peak fitting. (c) XPS C 1*s* spectrum of the untreated PET surface. (d) XPS C 1*s* spectrum of the PET surface after Ar plasma followed by hydrophilic HEMA modification.

untreated PET surface. This indicates that many HEMA monomers were grafted and polymerized on the PET surface, leading to the formation of a stable hydrophilic surface. Fig. 2.7 (a) shows a time course of the water contact angles of the PET surface modified by Ar plasma treatment and plasma-initiated graft polymerization using the hydrophobic St monomer. The water contact angle of the PET surface after Ar plasma followed by hydrophobic St modification was 53° and increased up to more than 60° over time. The St-modified PET surface was hydrophilic even though the St monomer is hydrophobic. This indicates that the St monomers might not have been sufficiently adsorbed at the reaction sites on the PET surface because of the steric hindrance between the St monomers. Based on the Cassie–Baxter equation, the ideal water contact angles of a surface covered by St polymers and the Ar plasma-treated PET surface should be 90° and 37°, respectively; the St surface coverage was estimated to be about 20 %. This surface coverage might be insufficient to provide the chemical properties of the St polymer. Thus, the water contact angle of the St-modified PET surface was lower than the expected value and increased greatly over time. Figs. 2.7 (c) and (d) show the XPS C 1*s* spectra of the untreated PET surface and the PET surface after Ar plasma followed by hydrophobic St modification, respectively. The XPS C 1*s* spectrum after St modification is deconvoluted into three peaks corresponding to the carbon atoms of the benzene rings unbonded to the ester group (peak C1 at 284.7 eV), carbon atoms singly bonded to oxygen (peak C2 at 286.5 eV),

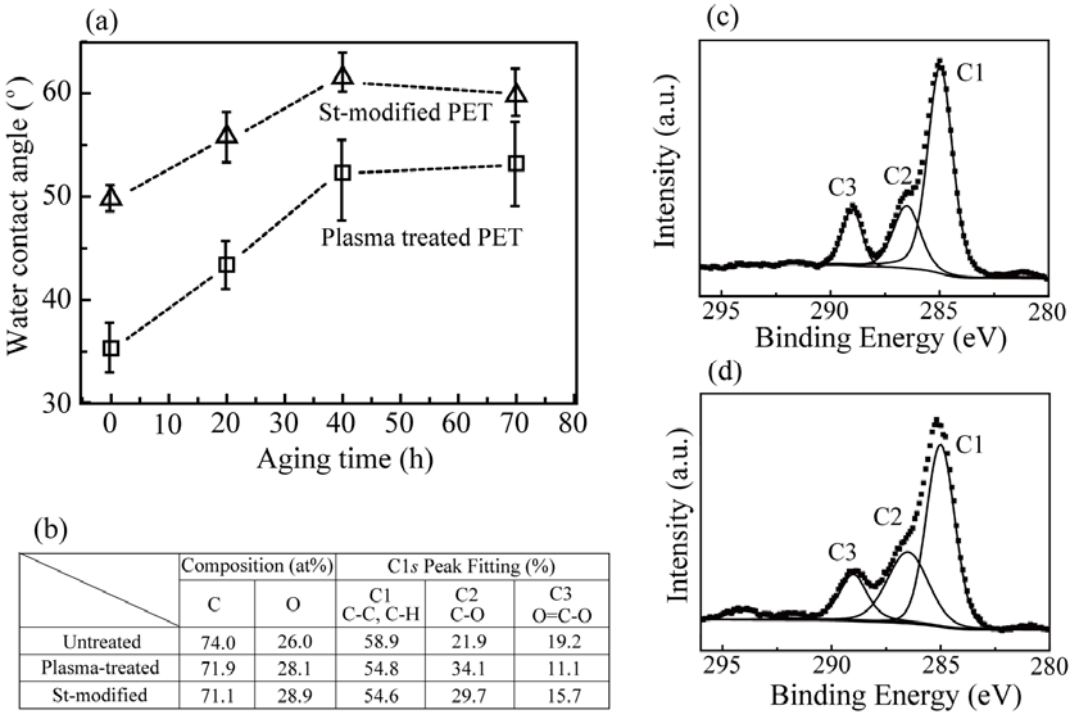

(b)

	Composition (at%)		C1*s* Peak Fitting (%)		
	C	O	C1 C-C, C-H	C2 C-O	C3 O=C-O
Untreated	74.0	26.0	58.9	21.9	19.2
Plasma-treated	71.9	28.1	54.8	34.1	11.1
St-modified	71.1	28.9	54.6	29.7	15.7

Fig. 2.7 (a) Time course of water contact angles of the PET surface modified by Ar plasma treatment and plasma-initiated graft polymerization using hydrophobic St monomer. (b) Chemical composition and area rates of C1, C2, and C3 peaks obtained from C 1*s* peak fitting. (c) XPS C 1*s* spectrum of the untreated PET surface. (d) XPS C 1*s* spectrum of the PET surface after Ar plasma followed by hydrophobic St modification.

and ester carbon atoms (peak C3 at 289.1 eV), as well as a weak peak at around 294.0 eV resulting from a $\pi \rightarrow \pi^*$ shake-up process. The peak resulting from the $\pi \rightarrow \pi^*$ transition, attributable to the phenyl groups, appeared as a result of the reaction of St monomers on the PET surface. Thus, three types of monomers with hydrophilic or hydrophobic functional groups were polymerized on the PET surface. The water contact angle of the PET surface modified with hydrophilic AA and HEMA monomers decreased from approximately 80° before treatment to less than 35°. The hydrophilicity of the PET surface modified with hydrophilic AA and HEMA monomers was maintained for 70 h.

Finally, 3T3 fibroblast cells were cultured on the untreated and modified PET surface to investigate bioactivity. Fig. 2.8 shows the number of cells cultured on the Ar plasma or AA-modified PET surface and the phase-contrast microscopic images for the cell growth behavior at 12 and 48 h after the cell culture. Initial cell growth was depressed on the AA-modified PET surface compared with the untreated and Ar plasma-treated PET surfaces. Phase-contrast microscopic images showed that the 3T3-fibroblast cells did not adhere well to the AA-modified surface. The number of cells cultured for 12 h correlated to some extent with the hydrophilicity of the PET surface. The cells increased as the water contact angles of the PET surface increased. After the cells were cultured for 48 h, the cell numbers increased on all PET surfaces, i.e., untreated, Ar plasma-treated, and AA-treated PET surfaces. The growth rate

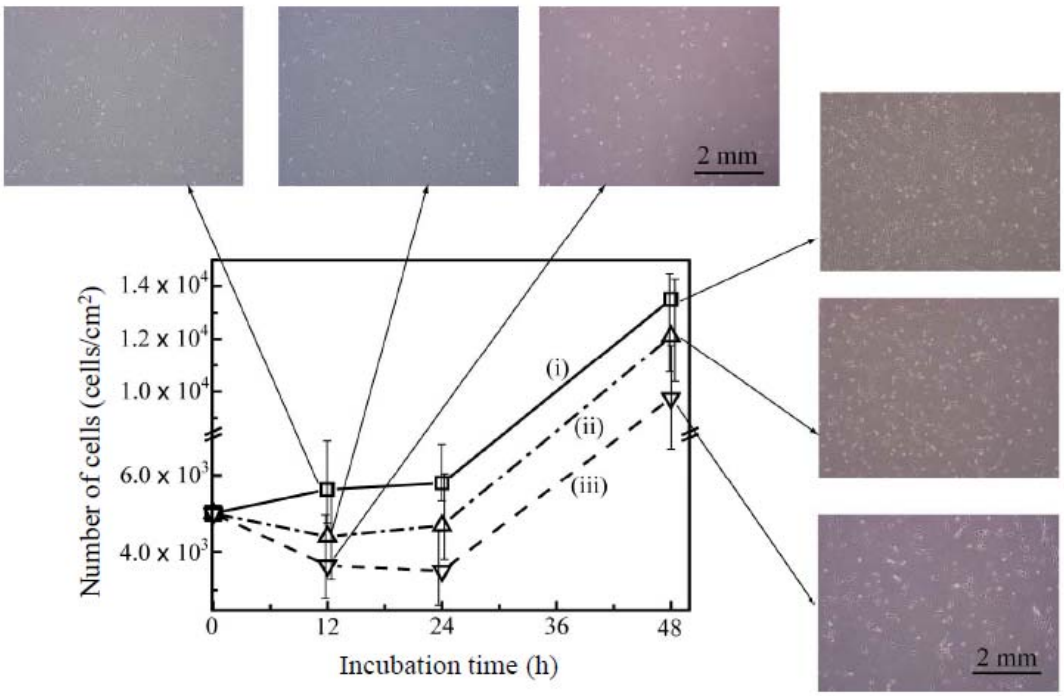

Fig. 2.8 Numbers of cells cultured on the Ar plasma or AA-modified PET surface and the phase-contrast microscopic images for the behaviors of the cell growth at 12 and 48 h after the cell culture. (i) Untreated PET surface. (ii) Ar plasma-treated PET surface. (iii) AA-modified PET surface.

remained almost constant on all PET surfaces. This indicates that the number of cultured cells might depend on the cell adhesion behavior after cell seeding. Fig. 2.9 shows the number of 3T3 fibroblast cells cultured for 24 h on the untreated, Ar plasma-treated, AA-modified, HEMA-modified, and St-modified PET surfaces. On the untreated and St-modified PET surfaces, the number of cultured cells was higher than the initial number of seeded cells. Despite the low coverage of the St monomer, the number of cultured cells increased on the St-modified PET surface. This indicates that hydrophobic functional groups in the polystyrene could affect adsorption of proteins that are necessary for cell adhesion. These proteins have hydrophobic functional groups in their molecular structure, so hydrophobic interaction between grafted polystyrene and proteins must have occurred, resulting in an increase in the number of cultured cells. In contrast, the number of cells cultured on the AA-modified and HEMA-modified surfaces was much lower than the initial number of seeded cells. It should be noted that the AA-modified and HEMA-modified surfaces had polar groups (–C–C=O, –C–COO, or –C–C–O) and maintained stable hydrophilicity. These results suggest that these negative polar groups might suppress adsorption of proteins resulting from repulsive electrostatic interaction.

2.4 Summary

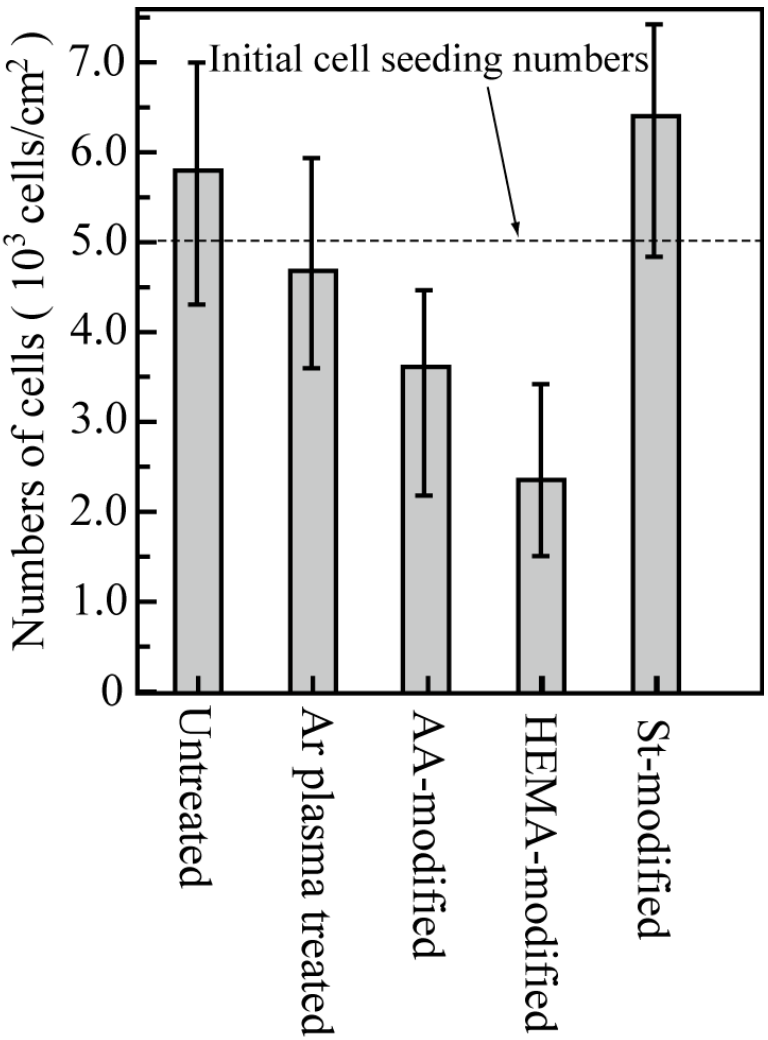

Fig. 2.9 Numbers of the 3T3 fibroblast cells cultured for 24 h on the untreated, Ar plasma-treated, AA-modified, HEMA-modified, and St-modified PET surfaces.

In this study, we successfully realized stable hydrophilicity on the PET surface through plasma-initiated graft polymerization using a SWP process. The water contact angles of the PET surfaces modified with hydrophilic AA and HEMA monomers decreased from approximately 80° before treatment to less than 35°. The hydrophilicity of the PET surface modified with hydrophilic AA and HEMA monomers was maintained for 70 h. In contrast, the water contact angle of the PET surface after Ar plasma treatment followed by hydrophobic St modification was 53° and increased up to more than 60° over time. 3T3 fibroblast cells were cultured on the modified PET surface. After the cells were cultured for 24 h, on the untreated and St-modified PET surfaces, the number of cultured cells was higher than the initial number of seeded cells. In contrast, the number of cells cultured on AA-modified and HEMA-modified surfaces was much lower than the initial number of seeded cells. The developed surface modification method can provide a way to control hydrophilicity and bioactivity of various polymer surfaces.

2.5 References

[1] M. Noeske, J. Degenhardt, and S. Strudthoff, et al. Int. J. Adhes. Adhes. 24 (2004) 171–177.

[2] S. Han, Y. Lee, H. Kim, et al. Surf. Coating Technol. 93 (1997) 261–264.

[3] N.-Y. Cui and N. M. D. Brown, Appl. Surf. Sci. 189 (2002) 31.

[4] E. E. Johnston and B. D. Ratner, J. Elec. Spec. 81 (1996) 303.

[5] F. D. Egitto and L. J. Matienzo, IBM J. Res. Develop. 38 (1994) 423.

[6] J. Li and J. W. McConkey, J. Vac. Sci. Technol. A 14 (1996) 2102.

[7] M. Keil, C.S. Rastomjee, A. Rajagopal, and H. Sotobayashi, Appl. Surf. Sci. 105 (1998) 273.

[8] N. Sakudo, D. Mizutani, Y. Ohmura, et al. Nucl. Instrum. Methods B 206 (2003) 687–690.

[9] M. Toufik, A. Mas, V. Shkinev, A. Nechaev, A. Elharfi, and F. Schue, Eur. Polym. J. 38 (2002) 203–209.

[10] N. Sprang, D. Theirich, and J. Engemann, Surf. Coat. Technol., 74-75, (1995) 689.

[11] M. Ballauf and O. Borisov, Curr. Opi. In Col. and Inter. Sci., 11, (2006) 316.

[12] J. Kudela, T. Terebessy, and M. Kando, Appl. Phys. Lett., 76, (2000) 1249.

[13] G. R. Llanos and M. V. Seastom, J. Biomed, Mater. Res., 27, 1383 (1993).

[14] A. Lippitz. J. F. Friedrich, W. E. S. Unger, A. Schertel, and Ch. Wöll, Polymer, 37, 3151 (1996).

[15] M. Chataib, E. M. Roberfroid, Y. Novis, J. J. Pireaux, R. Caudano, P. Lutgen, and G. Feyder, J. Vac. Sci. Technol., A, 7, 3233 (1989).

[16] L. J. Gerenser, J. Vac. Sci. Technol., A, 8, 3682 (1990).

[17] P. C. Wong, Y. S. Li, and K. A. R. Mitchell, Appl. Surf. Sci., 84, 245 (1995).

[18] R. Cueff, G. Band, M. Benmalek, J. P. Besse, J. R. Butruille, and M. Jacquet, Appl. Surf. Sci., 115, 292 (1997).

[19] R. W. Paynter, Surf. Interface Anal., 26, 674 (1998).

[20] I. Koprinarov, A. Lippitz, J. F. Friedrich, W. E. S. Unger, and Ch. Wöll, Polymer, 39, 3001 (1998).

[21] L. Sandrin, E. Sacher, Appl. Surf. Sci., 135, 339 (1998).

[22] A. M. Ektessabi and K. Yamaguchi, Thin Solid Films, 377, 793 (2000).

[23] S. Vasquez-Borucki, C. A. Achete, and W. Jacob, Surf. Coat. Technol., 138, 256 (2001).

[24] N. Médard, J. C. Soutif, and F. Poncin-Epaillard, Langmuir, 18, 2246 (2002).

Chapter 3

High sensitive detection of volatile organic compounds using superhydrophobic quartz crystal microbalance

3.1 Introduction

3.2 Experimental procedures

3.3 Results and discussion

3.4 Summary

3.5 References

3.1 Introduction

In previous Chapter 2, using plasma-initiated graft polymerization, the hydrophilicity was imparted to the PET surface. The PET surface modified by plasma process showed different bioactivity to 3T3 fibroblast cells, evidencing that the plasma process was effective for improving the functional capability of biomaterials.

In this Chapter 3, high functionalization of a quartz crystal microbalance (QCM) sensor was performed by plasma enhanced chemical vapor deposition (PECVD). The QCM sensor surface modified by PECVD showed superhydrophobicity. The detection sensitivity of superhydrophobic QCM sensor to volatile organic compounds (VOCs) such as formaldehyde and toluene were examined. In addition, the adsorption mechanism of the VOCs to the superhydrophobic QCM sensor was discussed.

Solid-state chemical sensors play a major role in medical diagnosis, environmental sensing, personal safety, automotive applications, and air conditions in airplanes and houses [1-3]. A current major goal in the evolving field of chemical sensors is to improve its sensitivity, so that they can detect very low concentrations of biomolecules and pollutants [4]. To realize this goal, many methods to increase the specific surface have been developed [5-7]. Many sensors have been operated under ambient conditions on the basis of changes in the electric properties of an active element brought about by the adsorption of an analyte on the sensor surface. The

ambient conditions thus provide moisture to the sensor surface. Here, conventional chemical sensors face their sensitivity limits due to the adsorption of the ambient moisture. Therefore, it is crucial to control wettability of the sensor surface without losing the sensitivity, because the adsorption of moisture originating from ambient conditions lowers the sensitivity. Promising strategies for achieving the above goal will likely come out of nanoscience technologies. Superhydrophobicity is based on the nanoscience technologies in terms of controlling the surface structures in nano-meter scale [8]. Currently, superhydrophobic surfaces with water contact angle greater than 150^{o} are attracting much attention because they will bring great convenience in daily life as well as in many industrial processes [9,10]. The superhydrophobic surfaces are controlled by two factors, i.e., the surface energy and the three-dimensional microgeometry, i.e., rough surface, of the solid surface [11,12]. The rough surface leads to the enhancement of specific surface area. This characteristic is important to effectively improve their performances not only for chemical sensors but also for another type of sensor.

QCM is one of the promising sensor devices, because the QCM sensor can precisely measure substance amounts adsorbed on the sensor in real time due to changes in resonance frequency of microbalance. The QCM sensors coated with film have enabled the detection of various individual pollutants [13-15] and are used for the online detection system of organic compounds [16]. In addition, the QCM sensor has

high detection sensitivity, so the application researches of the QCM sensors to chemical- and bio-sensors have been actively studied [17-20]. Therefore, the QCM sensor coated with superhydrophobic film would allow us to effectively operate as chemical sensor with high sensitivity under ambient conditions.

In this chapter, we aimed to fabricate a superhydrophobic film with water contact angle more than 150^{o} on the gold electrode of the conventional QCM sensor with by means of microwave plasma-enhanced chemical vapor deposition (MPECVD). In addition, the sensitivities of the QCM sensor coated and uncoated with the superhydrophobic film to VOCs such as formaldehyde and toluene were also investigated. The detection sensitivity of the QCM sensor was improved due to the superhydrophobicity and was maintained after the sensing examinations was repeated at more than 30 times. The nanostructured morphology combined with the chemical composition strongly contributes to high sensitivity of the QCM chemical sensor under ambient conditions.

3.2 Experimental procedures

3.2.1 Materials

Formaldehyde and toluene were purchased from Wako Pure Chemical Industries. Trimethylmethoxysilane (TMMOS) was purchased from Gelest Inc. All the chemicals

used in this study were of analytical reagent grade and used as received. AT-cut 9MHz quartz crystals with gold as electrodes of the QCM were purchased from Hertz.

3.2.2 Preparation of superhydrophobic film

A superhydrophobic film was deposited on a gold-covered QCM sensor head by the MPECVD method. The MPECVD system consisted of a Vycor glass discharge tube with an attached microwave cavity and a stainless steel deposition chamber, which was evacuated down to 6.7 Pa prior to the deposition. A 2.45 GHz generator supplied a microwave power of 300 W. A gas mixture of TMMOS and Ar was used as raw materials. Ar was needed to stabilize the microwave discharge. The partial pressures of TMMOS and Ar were changed from 10 to 93 Pa and from 40 to 50 Pa, respectively, and the total pressures were changed from 50 to 133 Pa to fabricate the superhydrophobic film. A gold electrode of the QCM sensor was used as the substrate for the film deposition. The substrate temperature did not exceed above 333 K during the film preparation. The deposition time was 5 min.

3.2.3 Preparation of flat hydrophobic surface

First, the bare gold electrode was ultrasonically cleaned for 10 min in toluene, acetone, and ultrapure water in that order to remove physical contaminations. After the cleaning, the substrates were dried with inert N_2 gas. Next, UV/O_3 cleaning was

performed on the cleaned substrate for 10 min at atmospheric pressure using vacuum ultraviolet (VUV) light of a wavelength of 172 nm. After the UV/O_3 cleaning, the substrate surface showed a water contact angle of less than 5^o. A self-assembled monolayer (SAM) was prepared on the cleaned gold electrode from *n*-octadecyltrimethoxysilane (ODS: $C_{18}H_{37}Si(OCH_3)_3$) molecules by a chemical vapor deposition (CVD) method. The cleaned substrate and the molecules were placed in a Teflon vessel with a volume of 60 cm^3. The vessel was maintained at 423 K in an electric oven for 3 h. After the SAM preparation, the samples were ultrasonically cleaned for 10 min in toluene, ethanol, ultrapure water and were dried with inert N_2 gas.

3.2.4 Film characterization

The water contact angles on the sample surface were estimated with a contact angle meter (Kyowa Interface Science, CA-D), which is based on a sessile drop measurement method. The diameter of the water droplet was 2 mm. The measurements were conducted in air at 298 K. The surface morphologies of ultra water repellent films were observed using a field-emission scanning electron microscope (FE-SEM; JEOL, JSM-6330F) at an accelerating voltage of 5 to 10 keV. Prior to the SEM imaging, the sample surface was coated with Pt layer with a thickness of ca. 5 nm using an ion sputter coater (Hitachi Ltd., E-1030). The film thickness was measured

using cross-sectional FE-SEM images. An atomic force microscope (AFM; Models SPA300HV & SPI-3800N, Seiko Instruments, Inc.) equipped with a silicon probe (NANOSENSORS; the force constant 42 N/m) was used in a dynamic mode at a scanning rate of 0.5 Hz to determine the root mean square roughness (R_{rms}) of the films. Specific surface area was calculated by the Brunauer-Emmett-Teller (BET) method using nitrogen adsorption isotherms (Gas Absorption Analyzer; Shimadzu, Tristar 3000).

3.2.5 Detection of volatile organic compounds (VOCs)

Formaldehyde and toluene were used as sensing substances. For all QCM measurements, changes in resonance frequency, that is, mass change, due to adsorption of organic substances were measured using the QCM sensor uncoated and coated with the superhydrophobic film. According to Sauerbrey [21], the deposition of a coating layer promotes the frequency shift of the crystal, which is described by the following linear relationship:

$$\Delta f = (f_0 / A\rho_q d_q) \Delta m \quad (3.1)$$

Here, Δf is the frequency shift, f_0 the fundamental oscillation frequency of the crystal, A the area of the electrode on the crystal, ρ_q the density of the crystal, d_q the thickness of the crystal, and Δm the mass change due to the deposition.

The QCM sensor, a syringe and a hygrometer were attached into a Teflon vessel

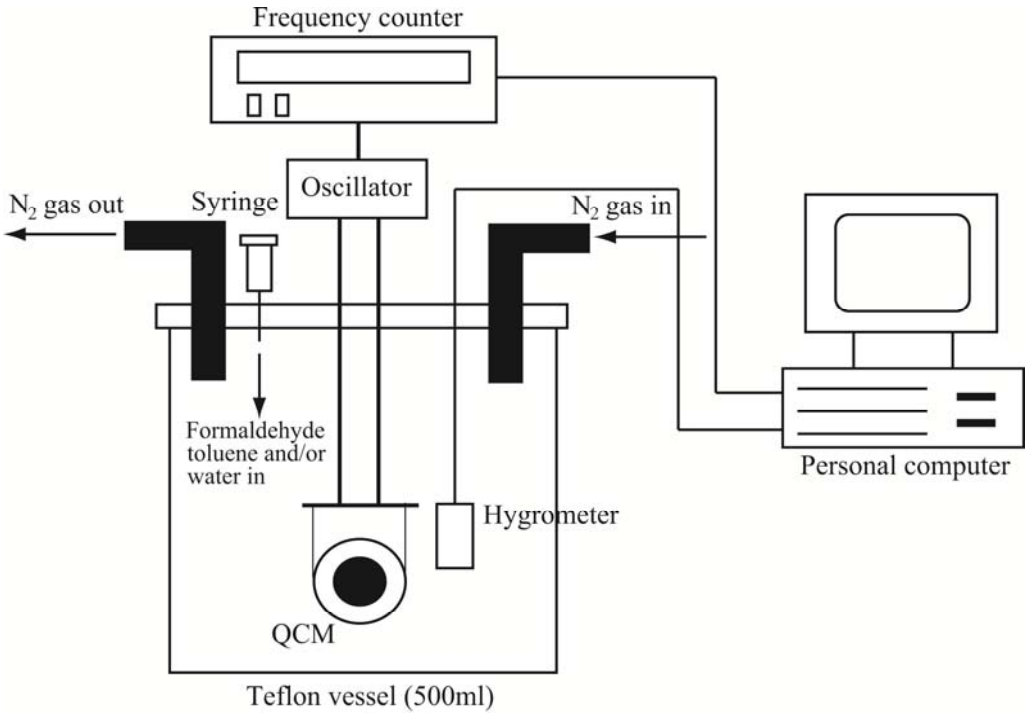

Fig. 3.1. Schematic diagram of the lab-made evaluation system using QCM chemical sensor for volatile organic compounds.

with a volume of 500 ml. Fig. 3.1 illustrates the schematic diagram of the lab-made evaluation system using QCM chemical sensor for VOCs. Three types of solutions were used as analytes. The solution (i) was only distilled water. The solution (ii) consisted of distilled water and formaldehyde, and the formaldehyde concentration was 10 vol% (2.5×10^{-2} mol/l). The solution (iii) consisted of distilled water and toluene, and the toluene concentration was 10 vol% (1.9×10^{-2} mol/l). The syringe was used to introduce 1 ml of the above-mentioned solutions into the vessel. After the introduction of each solution, it was vaporized, and the Teflon vessel was filled with the organic and/or water molecules. The vessel was located in thermostatic chamber controlled at a temperature of 24^{o}C. The humidity in the vessel was measured using the hygrometer. Although the humidity before the introduction of each solution was ca. 13 %, it increased with time evolution after introduction of each solution and was reached at 90 %. Nitrogen gas was used to remove adsorbed organic and water molecules to the sensor surface. The nitrogen gas was introduced in the vessel after the adsorption measurements for 20 min.

3.3 Results and discussion

Fig. 3.2 shows FE-SEM images (a) before and after the film deposition at (b) 50 and (c) 133 Pa on the Au electrode of the QCM, respectively. Before the film

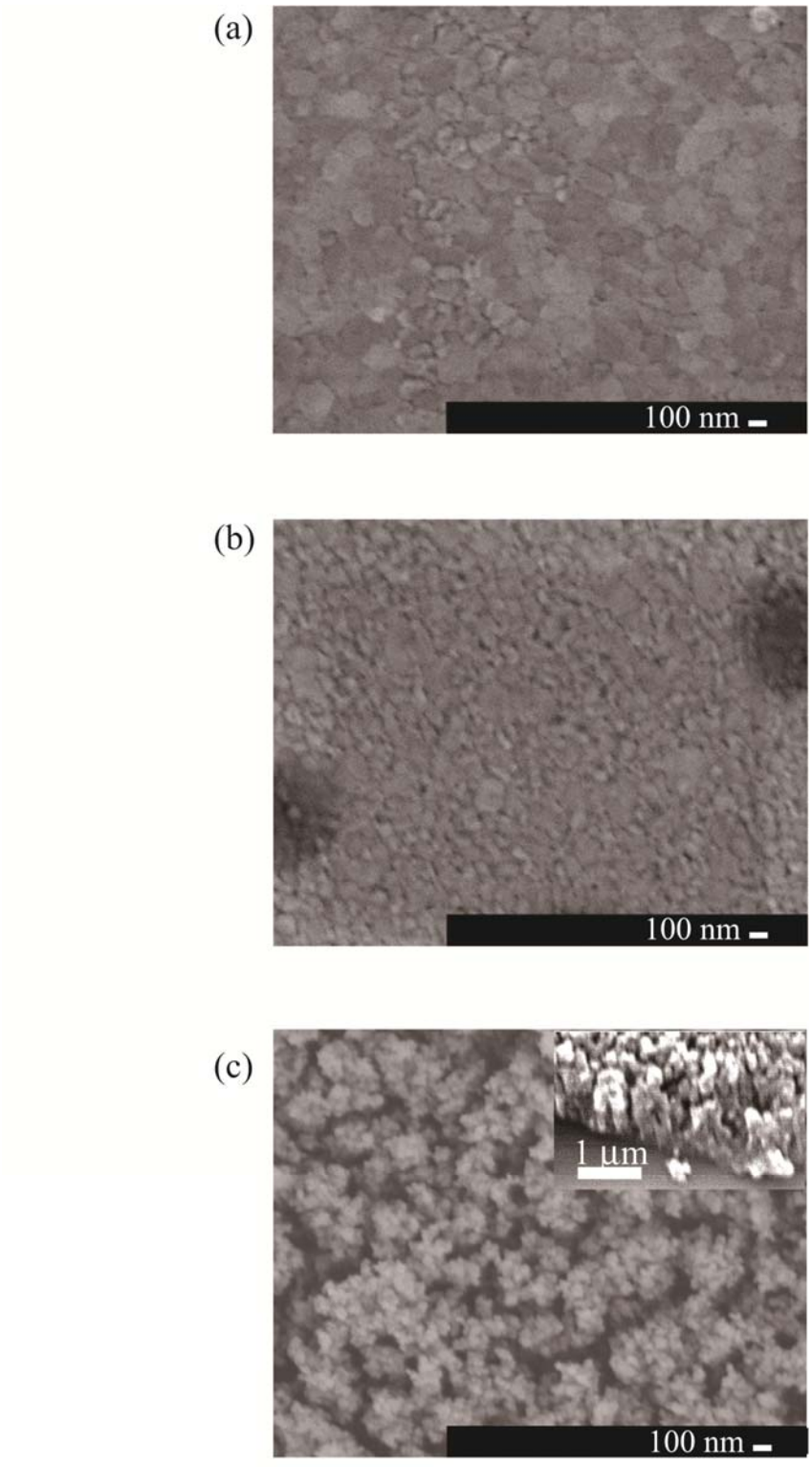

Fig. 3.2. FE-SEM images (a) before and after the film deposition at (b) 50 and (c) 133 Pa on the Au electrode of the QCM.

deposition, the Au electrode had compact surface and was relatively smooth. The AFM observation revealed that the R_{rms} value was less than 10 nm. After the film deposition at 50 Pa, the surface was covered with the film composed of minute particles with diameter of 30 to 150 nm. The R_{rms} value and film thickness were ca. 20 nm and ca. 110 nm, respectively. When the total pressure was 133 Pa, the surface had rough microstructures comprised of fine granular particles with sizes of several ten nanometers. The film thickness was estimated to be ca. 550 nm. The film had many pores of approximately 50 to 100 nm, as shown in Fig. 3.2 (c). Most of these particles would be prepared in a clustering process in the gas phase and condensed on the substrate. The clusters led to the irregular surface topography composed of granular particles and nanoscale pores with a few hundred nanometers in diameter, as estimated by AFM. The R_{rms} value of the QCM coated with the film was estimated to be ca. 70 nm. The increase of the surface roughness also lowers film density. Such surface roughness results in numerous asperities which lead to a highly reduced true contact area when the surface is brought into contact with water. Such topography can impart superhydrophobicity to the surface and leads to the increase of the specific surface area. The changes in the surface wettability before and after the deposition of the film were investigated using water contact angle measurements. Fig. 3.3 shows photographs of water droplet behaviors on QCM chemical sensor (a) uncoated and (b) coated with the film prepared at 133 Pa. The QCM surface before the deposition of the

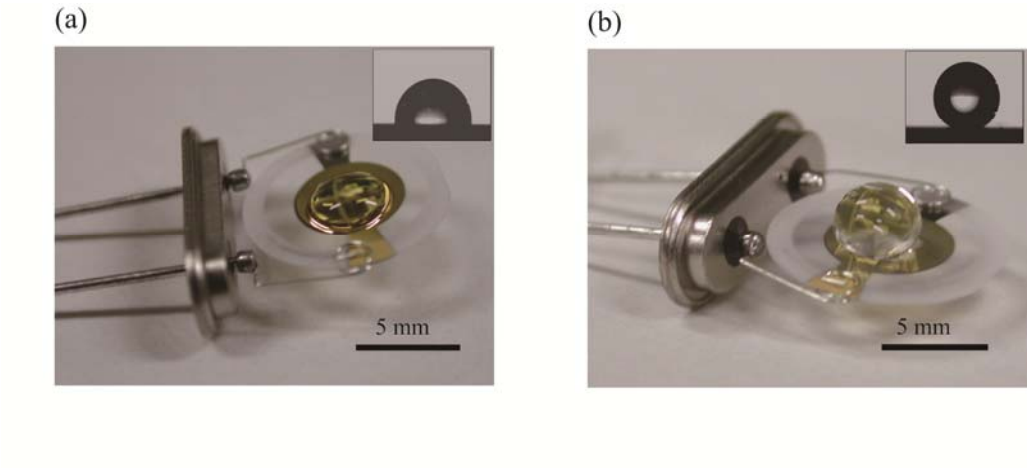

Fig. 3.3. Photographs of water droplet behaviors on QCM chemical sensor (a) uncoated and (b) coated with the film prepared by MPECVD at 133 Pa. Each inset shows the images of water drop on the respective surface.

superhydrophobic film showed a water contact angle of ca. 72^{o} , while the water contact angle of the QCM surface coated with the film prepared at 50 Pa was estimated to be ca. 92^{o}. The water contact angle of the film deposited QCM surface increased and the surface showed a hydrophobic property. With an increase in the total pressure, the surface had a water contact angle more than 150^{o}, that is, superhydrophobicity, as clearly shown by the water drop on the QCM sensor in Fig. 3.3 (b). The advancing and receding contact angles of the superhydrophobic surface were measured to be c.a. 157 and 153^{o}, respectively. This indicates that the contact angle hysteresis is less than 5^{o}. These values are in good agreement with those reported for various superhydrophobic surfaces [22-24]. The water contact angles increased with an increase in the total pressures during the film deposition because of the enhancement of the surface roughness. This agrees well with our previous results [25,26]. In previous study, the analyses using Fourier transform infrared spectroscopy (FT-IR) provided information that all the films fabricated by MPECVD using TMMOS and Ar mainly consisted of SiOx and $–CH_3$, indicating that the surfaces were covered with hydrophobic $–CH_3$ groups. Thus, the superhydrophobic film also consists of SiOx and $–CH_3$ groups. From these results, it was concluded that the total pressure of 133 Pa was suitable for fabricating the superhydrophobic silica film on the gold electrode of the QCM.

The specific surface areas of the QCM sensor coated and uncoated with the superhydrophobic film were calculated based on BET method using nitrogen gas

adsorption. The specific surface area for the QCM sensor coated with the superhydrophobic film, which was 440 cm^2/g, was thirteen times larger than that of a bare Au electrode surface of a QCM one (33 cm^2/g). Due to the larger specific surface area, it would be expected that the QCM sensor coated with the superhydrophobic film has much more active sites operating as adsorption sites than the sensor without the coating. From these results, it would be expected that the QCM sensor coated with the superhydrophobic film can detect VOCs high-sensitively with depressing any effect of water molecule adsorption from ambient conditions because of the large specific surface area and superhydrophobicity. In order to confirm this, we firstly measured an adsorption amount of water molecules and compared the sensitivity for the QCM sensor coated with the superhydrophobic film to that of a bare gold electrode surface of a QCM one by using lab-made evaluation system as shown in Fig. 3.1. The humidity in the evaluation system was changed from 14 % to 90 % by introducing water of 1 ml. After the 20 min, the frequency shift for the QCM sensor coated with the superhydrophobic film was c.a. 120 Hz, while that of a bare gold electrode surface was 85 Hz. Although the increase in frequency shifts of the QCM sensor coated with the superhydrophobic film is higher than that of a bare gold electrode surface, it should be noted that the specific surfaces of the both sensors are remarkably different. The adsorption amounts per unit area of the water molecules for the QCM sensor coated and uncoated with the superhydrophobic film were 0.19 and 1.34 g/m^2, respectively,

indicating that an adsorption amount of water molecules for the QCM sensor coated with the superhydrophobic film is much lower than that of a bare gold surface although the surface area is remarkably large. Accordingly, the QCM sensor coated with the superhydrophobic film would allow us to highly detect VOCs with reducing any effect of the water molecule adsorption from ambient conditions.

Next, we investigated the effect of surface chemistry and surface roughness on the water molecule adsorption using QCM sensor coated with ODS because the functional groups on the superhydrophobic and ODS surfaces are same. By using this molecule, flat hydrophobic surface with methyl groups was prepared on the gold electrode. The R_{rms} value of the hydrophobic surface was less than 10 nm and the specific surface area of the hydrophobic surface was estimated to be ca. 35 cm^2/g. These values were comparable to those of the bare gold electrode. The surface water contact angle of ODS surface was ca. 105^o. After 20 min from introducing water of 1 ml in the vessel, the frequency shift for the QCM sensor coated with the ODS film showed c.a. 45 Hz. The increase in the frequency shifts of the QCM sensor coated with ODS molecules was much lower than that of the bare gold electrode although the surface specific area of the QCM sensor coated with ODS molecules was comparable to that of the bare gold electrode. This indicates that the water adsorption to the QCM sensor coated with ODS molecules is suppressed due to the hydrophobicity of the sensor surface. On the other hand, the increase in the frequency shift of the QCM

sensor coated with superhydrophobic film was much higher than that of the QCM sensor coated with ODS molecules in spite of having same functional groups and high hydrophobicity. This means that the superhydrophobic surface have more active sites operating as adsorption sites than ODS surface due to the large specific surface area. Thus, it would be expected that the QCM sensor coated with the superhydrophobic film could detect highly VOCs.

Formaldehyde and toluene are extremely harmful to human organism, so it is vital to develop high sensitive chemical sensors for detecting a slight amount of formaldehyde and toluene. Therefore, we measured adsorption amounts of formaldehyde and toluene to QCM sensors coated with and without the superhydrophobic film. 1 ml of formaldehyde or toluene was separately diluted with 9 ml of distilled water. Each diluted solution was introduced separately into the evaluation system through the syringe. Fig. 3.4 shows the sensitivity of the QCM sensors coated and uncoated with the superhydrophobic film. The sensitivity was determined using the maximum frequency shift. It is clear that the sensitivity of the QCM coated with the superhydrophobic film is significantly higher than that of the QCM uncoated with the superhydrophobic film. It should be noted that in case of the water molecule adsorption the frequency shift for the QCM coated with the superhydrophobic film is larger than that of the QCM uncoated with the superhydrophobic film. As above mentioned, this is due to that the specific surface

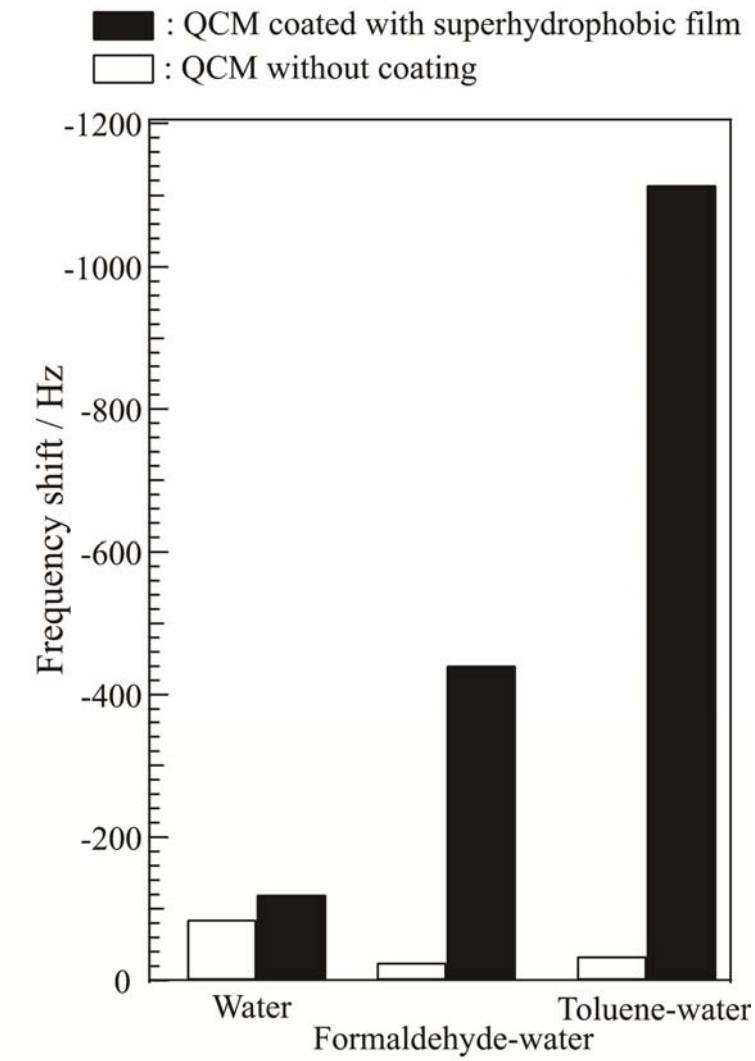

Fig. 3.4. Sensitivity of the QCM sensors coated and uncoated with the superhydrophobic film to water, formaldehyde-water, and toluene-water.

area of the QCM coated with the superhydrophobic film is much higher than that of the uncoated QCM. Fig. 3.5 (a) shows the frequency shifts of the QCM sensors coated (i) without and (ii) with the superhydrophobic film to formaldehyde-water and (iii) humidity changes as a function of measurement times. The oscillating frequency lowers due to an adsorption of formaldehyde and/or water molecules vaporized. The frequency shifts of the both QCM sensors decreases gradually with an elapse time. In case of using QCM sensor coated with the superhydrophobic film, the frequency shift decreased progressively with increasing measurement time from 3 to 5 min. The maximum frequency shift of the QCM sensor coated with superhydrophobic film is 441 Hz, while that of a naked Au electrode is less than 30 Hz. In addition, we investigated the frequency shift of the QCM sensor coated with ODS molecules to formaldehyde-water. The maximum frequency shift of the QCM sensor coated with ODS molecules is estimated to be 44 Hz. These results indicate that the sensitivity for the QCM sensor coated with the superhydrophobic film shows higher sensitivity compared to those of bare and ODS coated Au electrodes. Thus, it could be concluded that the surface chemistry could affect the adsorption of formaldehyde and toluene due to the hydrophobic interaction and the surface roughness could be closely related to the increase of active sites operating as adsorption sites. Fig. 3.5 (b) shows the frequency shifts of the QCM sensors coated with the superhydrophobic film to (i) formaldehyde-water and (ii) toluene-water as a function of measurement times. The

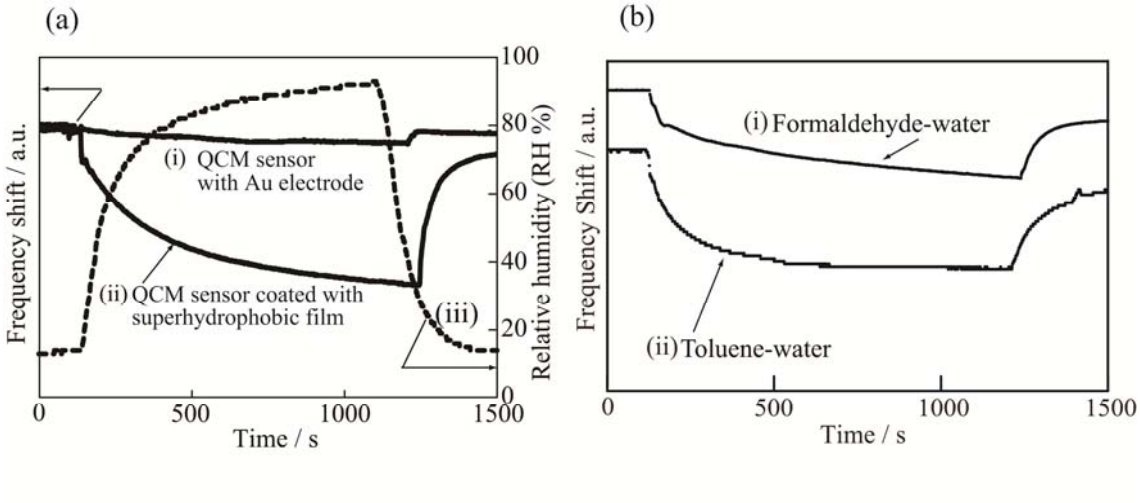

Fig. 3.5. (a) Frequency shifts of the QCM sensors coated (i) without and (ii) with the superhydrophobic film to formaldehyde-water and (iii) humidity changes as a function of measurement times. (b) Frequency shifts of the QCM sensors coated with the superhydrophobic film to (i) formaldehyde-water and (ii) toluene-water as a function of measurement times.

frequency shift of the toluene-water decreased markedly with increasing measurement time and was stable with increasing measurement times from 10 to 20 min. The frequency shift of the QCM sensor coated with superhydrophobic film for toluene-water was 1114 Hz. From these results, in the case of using the QCM sensor coated with the superhydrophobic film, it is concluded that the detection sensitivity for toluene molecules is much higher than that of formaldehyde molecules. The difference in the detection sensitivity could be caused by difference in electric charges and molecular structures of the formaldehyde and toluene molecules. The adsorption mechanisms of formaldehyde and toluene molecules to the superhydrophobic surface are considered to be as follows; Formaldehyde and toluene molecules have methylene and methyl groups in the molecular frameworks, respectively, as shown in Fig. 3.6. The superhydrophobic film also has methyl groups on the surface. The attractive forces would occur between methyl-methyl groups and methylene-methyl groups, respectively, due to hydrophobic interaction because the methylene and methyl groups are hydrophobic. In addition, the superhydrophobic film can depress the adsorption of water molecules on the superhydrophobic film. Thus, formaldehyde and toluene molecules are easily attached to the adsorption sites of the superhydrophobic film. The electric charges of formaldehyde, toluene, and water could be related to the adsorption of formaldehyde or toluene to the superhydrophobic surface. In the case of adsorption of formaldehyde-water, hydrophilic coating might be formed on the superhydrophobic

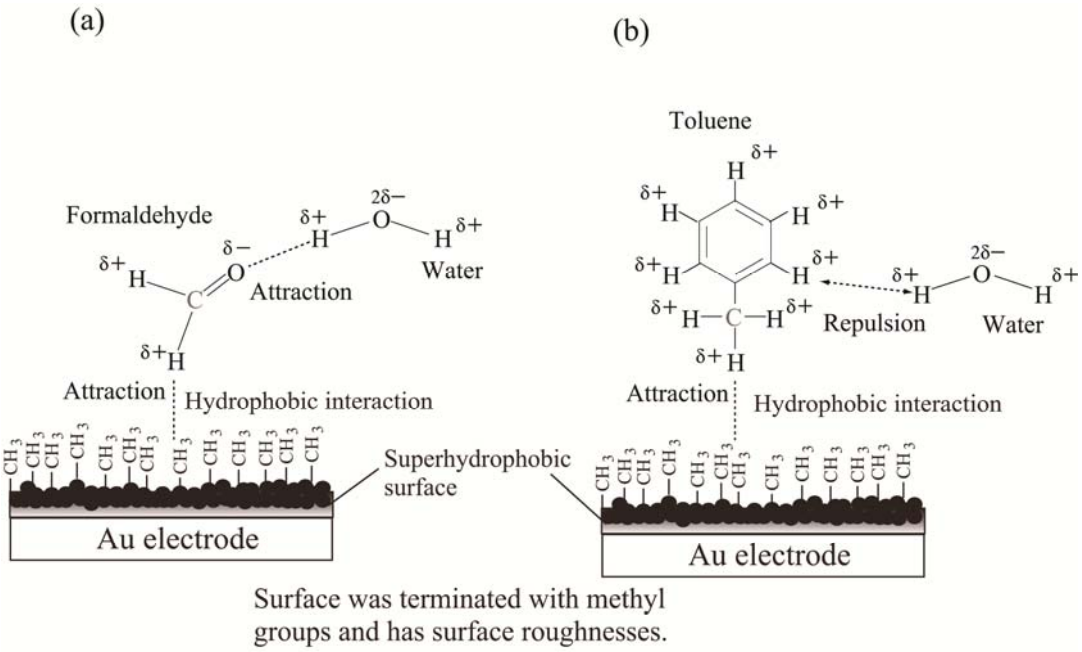

Fig. 3.6. Adsorption and bonding models of (a) water and formaldehyde molecules, and (b) water and toluene molecules to superhydrophobic surfaces.

film because the methylene units would attach to the methyl groups of the superhydrophobic film due to the hydrophobic interaction. Due to the formation of the hydrophilic coating, water molecules can attach to the formaldehyde molecules. This could induce the gradual decrease with time evolution in the frequency shift. On the other hand, in the case of adsorption of toluene-water, hydrogen atoms of toluene and water molecules have minute positive electric charges as shown in Fig. 3.6 (b). Due to the electrostatic repulsive force, water molecules could not attach to the toluene molecules and toluene molecules are in adsorption equilibrium when the frequency shift of the toluene-water is stable from 10 to 20 min.

From these results, we find that the QCM sensor coated with the superhydrophobic film effectively suppresses the adsorption of water molecules because of the superhydrophobicity and selectively responds to the formaldehyde and toluene, that is, VOCs, so it can act as a high sensitive chemical sensor for detecting formaldehyde and toluene. After the adsorption test, we confirmed that the frequency shifts of the QCM sensor coated with the superhydrophobic film were recovered to become an initial frequent value immediately after introducing a nitrogen gas into the evaluation system. This suggests that the adsorption of formaldehyde and toluene on the QCM sensor coated with the superhydrophobic film would be not chemical adsorption but physical one. Moreover, we confirmed that the adsorption/desorption tests of formaldehyde and toluene molecules could be performed repeatedly at more

than 30 times without lowering the detection sensitivity.

3.4 Summary

In this study, a superhydrophobic film with a water contact angle more than 150^{o} was successfully fabricated on the gold electrode of the QCM by MPECVD method. The specific surface area after the deposition of the superhydrophobic film was thirteen times larger than that of uncoated gold electrode. The QCM sensor coated with the superhydrophobic film were more sensitive to VOCs than the conventional QCM sensor. Moreover, the adsorption mechanisms of formaldehyde-water and toluene-water molecules to the superhydrophobic film were discussed. For the sensors described here, the high sensitivity and reversibility of the QCM sensor coated with the superhydrophobic film under ambient conditions can be attributed to the intrinsically small grain size and high specific surface associated with superhydrophobicity. The QCM sensor coated with the superhydrophobic film can be portable and sensitive sensor for detecting VOCs such as formaldehyde and toluene in ng-level at room temperature under ambient conditions. With the advantage of the superhydrophobicity the QCM chemical sensor becomes a good candidate for miniaturized, high sensitive chemical sensors in many applications. Further improvement in detection sensitivity for VOCs should be achievable by increasing the

specific surface, controlling the pore size and decorating these surfaces with catalysts. With such innovations, the chemical detection of single molecule on chemical sensors may soon be within reach.

3.5 References

[1] N. Yamazoe, *Sens. Actuators B,* 5 (1991) 7.

[2] M. Lei, Y. Gu, A. Baldi, R. A. Siegel, B. Ziaie, *Langmuir*, 20 (2004) 8947.

[3] G. Sberveglieri, *Sens. Actuators B*, 23 (1995) 103.

[4] M. Law, H. Kind, B. Messer, F. Kim, P. Yang, *Angew. Chem. Int. Ed.*, 41 (2002) 2405.

[5] Y. Cui, Q. Q. Wei, H. K. Park, C. M. Lieber, *Science*, 293 (2001) 1289.

[6] F. Favier, E. C. Walter, M. P. Zach, T. Benter, R. M. Penner, *Science*, 293 (2001) 2227.

[7] E. Comini, G. Faglia, G. Sberveglieri, Z. Pan, Z. L. Wang, *Appl. Phys. Lett.*, 81 (2002) 1869.

[8] Y. Wu, H. Sugimura, Y. Inoue, O. Takai, *Chem. Vap. Deposition*, 8 (2002) 47.

[9] W. Chen, Y. Fadeev, M. C. Heieh, D. Öner, J. Youngblood, T. J.McCarthy, *Langmmuir*, 15 (1999) 3395.

[10] T. Onda, S. Shibuichi, N. Satoh, K. Tsujii, *Langmuir*, 12 (1996) 2125.

[11] H. Gau, S. Herminghaus, P. Lenz, R. Lipowsky, *Science*, 283 (1999) 46.

[12] M. Hui, M. J. Blunt, *J. Phys. Chem B,* 104 (2000) 3833.

[13] J.F. Alder, J.J. McCallum, *Analyst*, 108 (1983) 1169.

[14] G. G. Guilbgoldlt, J. M. Jordan, *CRC Crit. Rev. Anal. Chem*., 19 (1988) 1.

[15] A. Mierzwinski, Z. Witkiewicz, *Environ. Pollut*., 57 (1989) 181.

[16] W. H. King, *Anal. Chem*., 36 (1964) 1735.

[17] I. Sugimoto, M. Nakamura, H. Kuwano, R. Shimada, *Thin Solid Films*, 310 (1997) 303.

[18] S. Okamura, M. Shimada, K. Okuyama, *Jpn. J. Appl. Phys*, 43 (2004) 4135.

[19] K. Bonroy, J. M. Friedt, F. Frederix, W. Laureyn, S. Langerock, A. Campitelli, M. Sara, G. Borghs, B. Goddeeris, P. Declerck, *Anal. Chem*., 76 (2004) 4299.

[20] A. Dupont-Filliard, M. Billon, T. Livache, S. Guillerez, *Anal. Chim. Acta*, 515 (2004) 271.

[21] G. Sauerbrey, *Z. Phys*., 155 (1959) 206.

[22] F. Shi, Y.Y. Song, X. Xia, Z. Wang, X. Zhang, *Chem. Mater*., 18 (2006) 1365.

[23] C. Cheng, L. Feng, L. Jiang, *Adv. Func. Mater*., 18 (2008) 3219.

[24] P.N. Manoudis, I. Karapanagiotis, A. Tsakalof, I. Zuburtikudis, C. Panayiotou, *Langmuir*, 24 (2008) 11225.

[25] T. Ishizaki, N. Saito, Y. Inoue, M. Bekke, O. Takai, *J. Phys. D: Appl. Phys*., 40 (2006) 192.

[26] T. Ishizaki, J. Hieda, N. Saito, N. Saito, O. Takai, *Electrochim. Acta*, 55 (2010) 7094.

Chapter 4

Synthesis and surface modification of carbon nanoballs (CNBs)

4.1 Introduction

In previous Chapters 2 and 3, plasma processes in gas phase has been established to functionalize bio- and environmental materials highly. In this chapter, the synthesis of carbon nanoballs (CNBs) was performed by thermal CVD. Next the surfaces of the synthesized CNBs were modified by plasma in liquid phase, or solution plasma.

Carbon materials have attracted much attention all over the world since the discovery of fullerenes [1]. This has led to the discovery of a number of novel carbon materials with unique structures such as carbon nanotubes (CNTs) [2], carbon onions [3], cone-shaped graphitic structures [4], carbon nanowalls [5], and carbon micro-trees [6], depending on the techniques and the carbon precursors used. Among the various carbon materials with unique structures, CNTs are potential candidates for use in many fields such as catalysis [7], storage of hydrogen and other gases [8], biological cell electrodes [9], nanoscale electronic and mechanical devices [10], and electron field emission tips [11]. Thus, the CNTs have been synthesized by many techniques such as arc discharge [12], laser ablation [13], and catalytic methods [14]. Synthesis of the carbon by chemical vapor deposition (CVD) from molecular precursors, assisted by the catalytic activity of transition metal particles, has been considered as one of synthesis methods toward mass production.

Carbon nanoballs (CNBs) can be also synthesized by the techniques that are

normally used to produce CNTs [15-20]. CNBs are becoming increasingly important as catalyst or as an anode material in secondary lithium battery. He et al [21] reported that the charge-discharge curves of CNBs produced by arc discharge showed that the cell electrode had a high reversible capacity and the capacity retention could reach 73.7 %. In addition, the CNBs have been expected to apply polymer composites and biological systems. In the case of the application to the polymer composites, it is necessary to tailor the chemical property of the CNB walls. Using the CNBs as a reinforcing component in polymer composites requires the ability to tailor the property of the CNB walls in order to control the interfacial interactions between the CNBs and the polymer chains. Several studies have reported on the mechanical properties of the CNTs-polymer composites where the CNTs were used without surface modification [22-24]. These results showed the increase in the elastic modulus of the composite. This indicates the potential of the CNTs as reinforcing components, so the CNBs would also work as reinforcing components of the polymer composites materials. In order to fabricate the CNBs-polymer composites, it is crucial to modify the CNBs surface in order to covalently bind the polymer to the CNBs surface. This can lead to the improvement of the efficiency of load transfer. However, there are few reports on the surface modification of the CNBs.

In this study, we aimed to synthesize the CNBs by thermal CVD method and to modify the CNBs surfaces to carboxylic acid groups using plasma treatment in liquid

phase. The presence of the carboxylic acid groups on the CNB surfaces would be convenient for applications to biomaterials and energy materials because the carboxylic acid can be utilized in a variety of chemical reactions.

4.2 Experimental procedures

n-type Si (100) wafers with a resistivity of 30 to 40 Ωcm were used as substrates. The substrates were sonically cleaned for 10 min with acetone, ethanol, and ultra pure water in that order. Prior to synthesis of CNTs and CNBs, Fe was deposited on the cleaned substrates with a radio-frequency magnetron sputtering apparatus (JEOL: JEH-430RS). A tubular quartz reactor with a 32 mm in diameter and a 450 mm long was placed horizontally in an electric furnace as shown in Fig. 4.1. The furnace temperature was under electronic control. The CVD synthesis was carried out at atmospheric pressure in the quartz reactor. The sputtered substrates were put in the middle of the quartz reactor. The reactor was heated at the temperature of 750 to 990 ^{o}C with an Ar gas flow of 150 sccm. Controlled amount of water vapor was also introduced to the reactor by bubbling Ar gas in order to promote and preserve the catalytic activity [25]. After the tube reached at the growth temperature, H_2 gas was introduced at the flow rate of 100 sccm. The C_2H_4 gas was then introduced at the flow rate of 25 to 175 sccm in order to synthesis CNTs and CNBs. The reaction time was 30

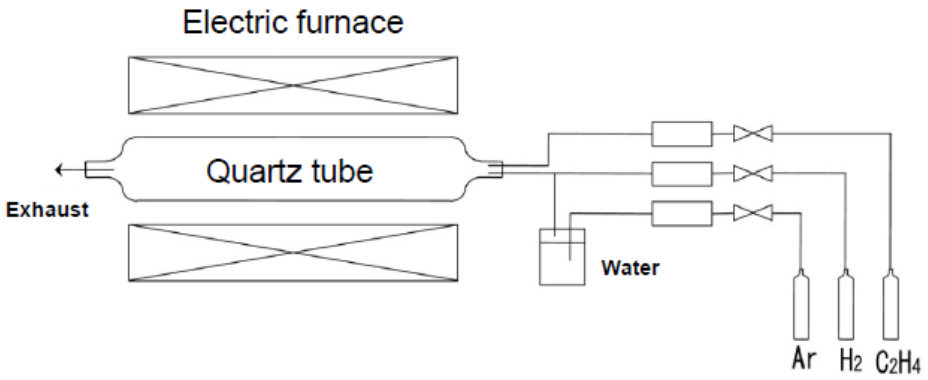

Fig. 4.1 A schematic illustration of apparatus for thermal CVD.

min. After the synthesis, the furnace was cooled down under the Ar gas flow of 150 sccm to room temperature.

To introduce carboxylic acid groups to the CNB surfaces, a carboxylation procedure was performed using plasma in liquid phase as follows: the as-prepared CNBs were added to 150 ml of ultrapure water with a resistivity of 18.2 MΩ. The conductivity of the solution was adjusted to be 500 μS/cm using KCl. Two tungsten electrodes with a diameter of 1.0 mm were set in the aqueous solution as shown in Fig. 4.2. The gap between electrodes was 0.5 mm. The bipolar-pulsed voltages were applied between the electrodes by pulsed power supply (Kurita Seisakusho Co. Ltd., MPS-06K-01C). The applied voltage was 2.4 kV. The pulse width and frequency were 2 μs and 15 kHz, respectively. After 2.4 kV of the voltage was applied between the electrodes, the discharge occurred. The discharge was kept for 60 min. After the carboxylation procedure, the CNBs were characterized by Fourier transform infrared spectroscopy (FT-IR).

The morphology of the resulting samples were observed with a field emission scanning electron microscope (FE-SEM, JEOL: JSM-6330F), operating at accelerating voltage of 5 kV and an emission current of 12 mA. The microstructures of the samples were observed with a transmission electron microscope (TEM, JEOL: JEM-2500TS) operated at an accelerating voltage of 200 kV. The crystal structures of the samples were examined by X-ray diffraction (XRD) (Rigaku, RINT2200V). The XRD data

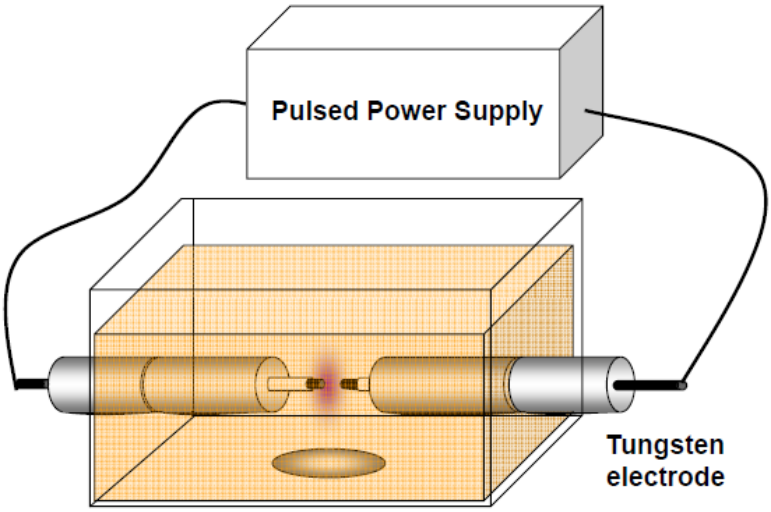

Fig. 4.2 A schematic illustration of apparatus for plasma in liquid phase.

were recorded on a powder diffractometer with CuKα radiation (40 kV, 40 mA) within the range of 10° and 90° at a scanning rate of $2\theta = 4°$ (min^{-1}). The XRD peaks were assigned to the appropriate phases on the basis of the JCPDS data. Raman spectroscopy was performed using Tokyo Instruments Nanofinder with 514.5 nm Ar laser excitation.

4.3 Results and discussion

4.3.1 Synthesis and characterization of CNBs

Table 4.1 lists CVD reaction conditions and resulting carbon products. Most of CNTs were synthesized below the temperature of 850 ^{o}C. On the other hand, CNBs were produced at 990 ^{o}C. This indicates that the morphologies of carbon products strongly depend on the reaction temperature. In addition, the flow rate of the C_2H_4 gas could affect the shapes of the resulting carbon products. When the flow rate was more than 175 sccm, the resulting carbon products were CNBs in spite of the reactor temperature. Figs. 4.1 (a)-(d) show FE-SEM images of CNTs and CNBs synthesized under the C_2H_4 gas flow rate of 75 sccm at 750, 800, 850, and 990 ^{o}C, respectively. The diameters of CNTs at 750 ^{o}C were ca. 100 nm, whereas those at 800 and 850 ^{o}C were ca. 70 to 80 nm. These CNTs are slightly curved in shape. On the other hand, the carbon products at 990 ^{o}C were CNBs. The diameters of the CNBs range from 800 to

Table 4.1 Summary of the carbon products and reaction conditions.

Sample number	Reaction Temp. (℃)	C_2H_4 gas flow rate (sccm)	Carbon product
1	750	25	CNTs
2	750	75	CNTs
3	750	100	CNTs
4	750	125	CNTs
5	750	175	CNBs + Carbon nanobeads
6	800	25	CNTs
7	800	75	CNTs
8	800	100	CNTs
9	800	125	CNTs
10	800	175	CNTs
11	850	25	CNTs
12	850	75	CNTs
13	850	100	CNTs
14	850	125	CNTs + CNBs
15	850	175	CNBs
16	990	25	CNTs
17	990	75	CNBs
18	990	100	CNBs
19	990	125	CNBs
20	990	175	CNBs

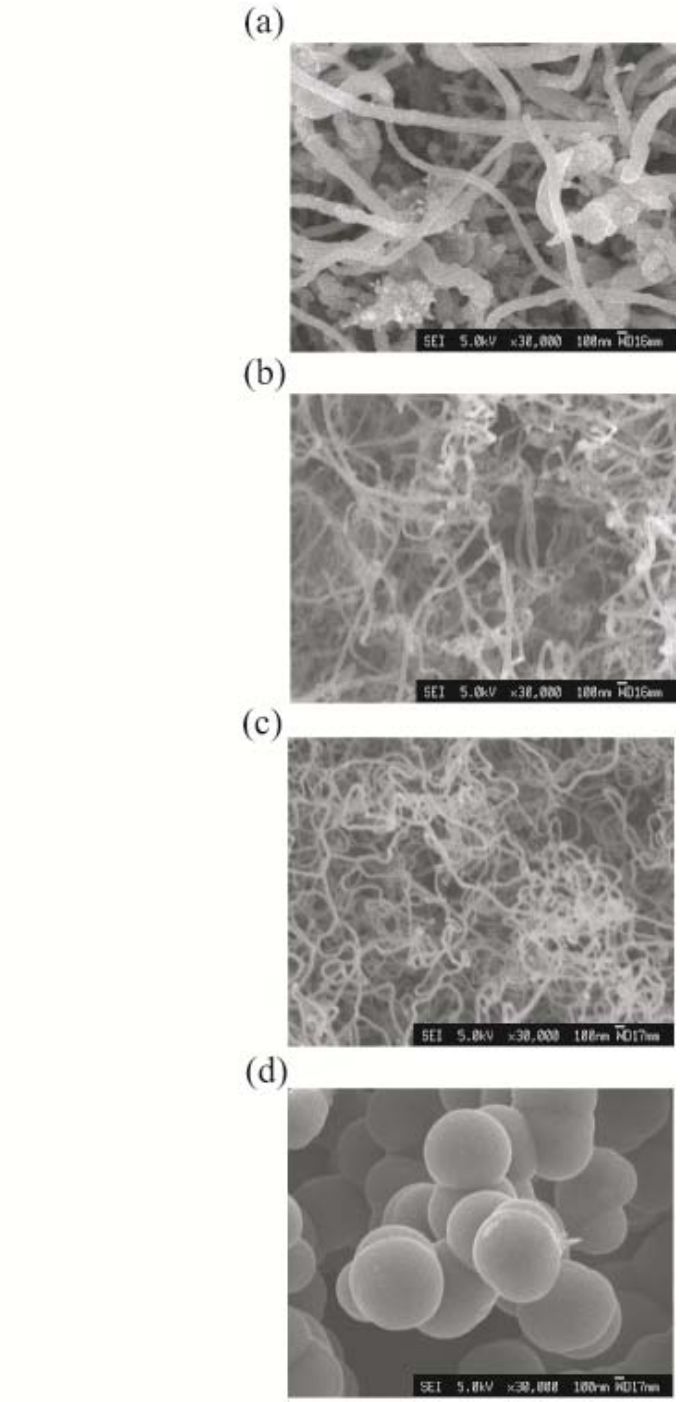

Fig. 4.3. FE-SEM images of CNTs and CNBs synthesized under the C_2H_4 gas flow rate of 75 sccm at various temperatures. (a) 750, (b) 800, (c) 850, and (d) 990 ^{o}C.

900 nm. Fig. 4.4 (a) shows a TEM image of CNTs at 850 ^{o}C. The CNTs have a hollow structure inside. The outside and inside diameters of the CNTs were ca. 80 nm and 15 to 20 nm, respectively. Fig. 4.4 (b) shows a high-resolution TEM (HRTEM) image of the wall of the CNTs. The wall was composed of multi graphite sheets, that is, multiwalled carbon nanotubes (MWNTs). The interplaner spacing of the graphite sheet was 0.34 nm, which agreed with the spacing of the 002 plane in graphite [26]. Fig. 4.4 (c) shows a TEM image of the CNTs with nanoparticle encapsulated. The TEM-EDX (energy dispersive X-ray spectroscopy) revealed that the nanoparticle was Fe. This indicates that the Fe particle plays a key role in the nucleation and growth of graphite layer. The presence of the Fe particle at the end of the CNT shows that the CNTs formation is originated from the Fe working catalyst. Indeed, Fe has been shown to be a catalyst for CNTs formation and growth. Thus, our CVD synthesis of CNTs could involve transport of C atoms toward and Fe atoms away from the graphite-Fe interface [26].

Figs. 4.5 (a)-(d) show FE-SEM images of CNTs and CNBs synthesized under the C_2H_4 flow rate of 175 sccm at 750, 800, 850, and 990 ^{o}C. The CNTs with a diameter of 30 to 40 nm were synthesized at 800 ^{o}C, while the CNBs were produced at the temperature of 850 and 990 ^{o}C. The diameters of the CNBs at 850 and 990 ^{o}C were 800 to 900 nm and 300 to 400 nm, respectively. This means that the diameter of the CNBs increases with the decrease of the reaction temperature. Comparing Fig. 4.3

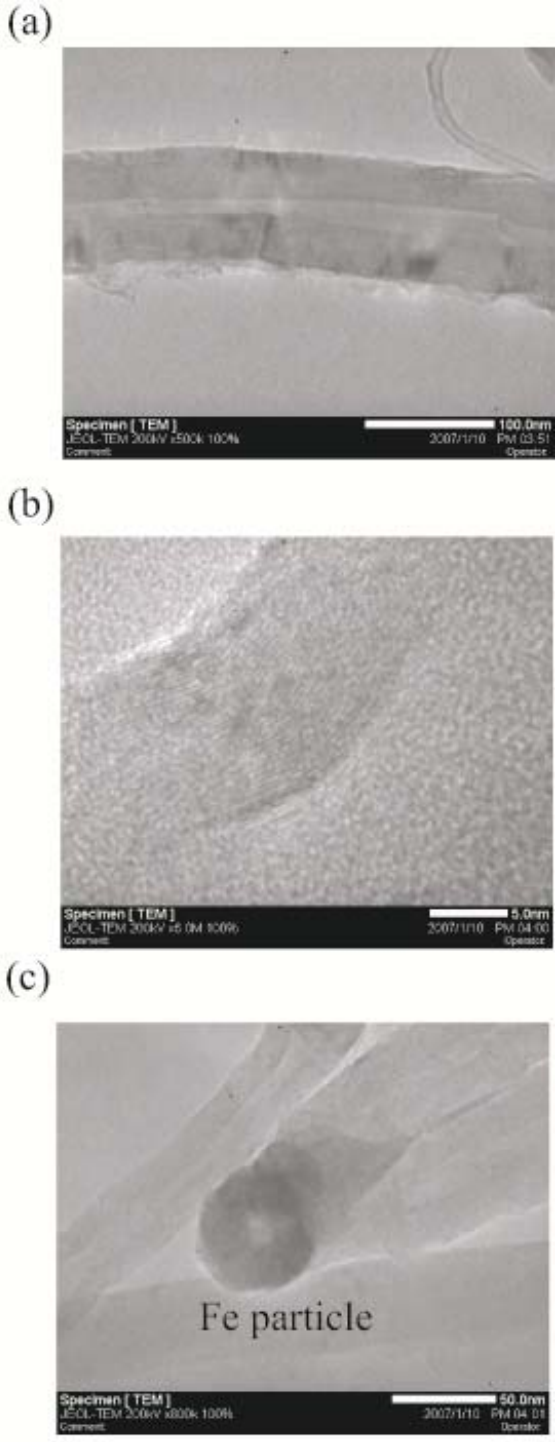

Fig. 4.4. (a) TEM image of CNTs at 850 ^{o}C. (b) HRTEM image of the wall of the CNTs at 850 ^{o}C. (c) TEM image of the CNTs containing catalytic Fe particle.

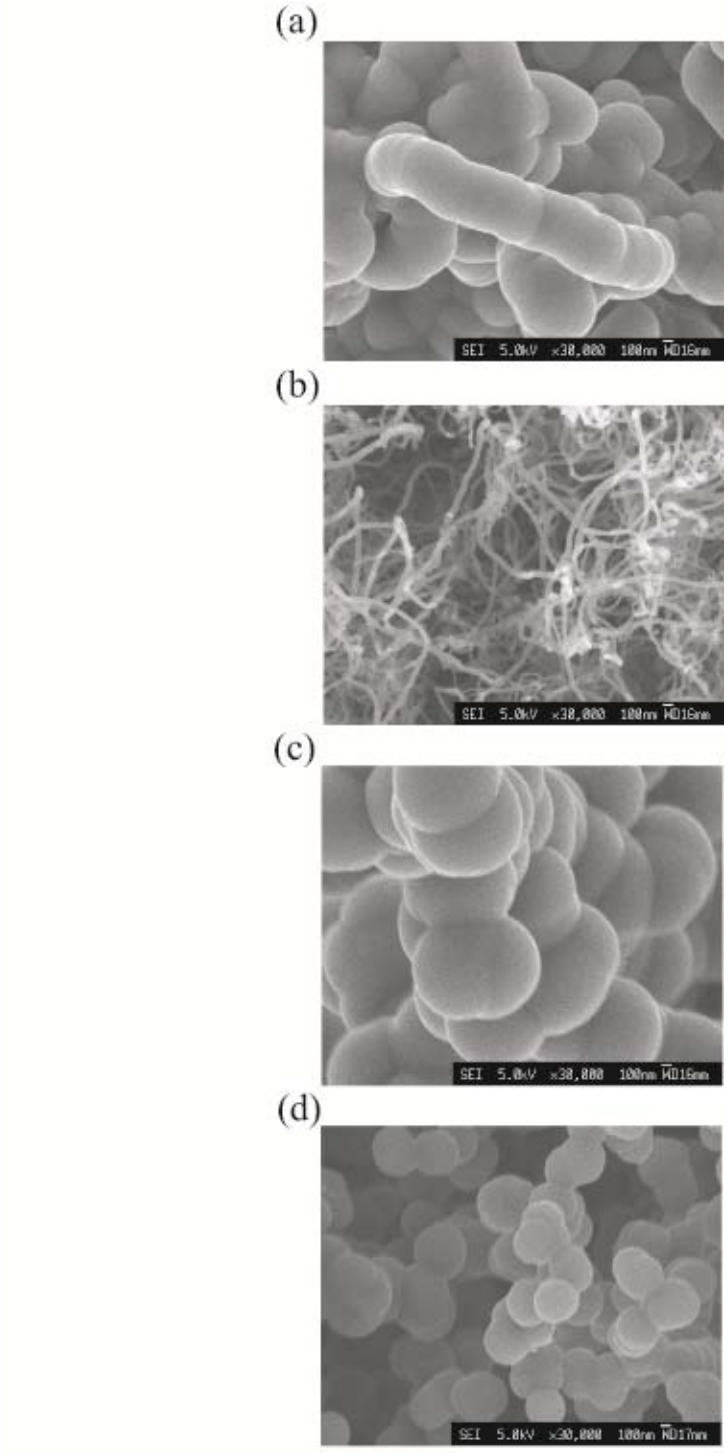

Fig. 4.5. FE-SEM images of CNTs and CNBs synthesized under the C_2H_4 flow rate of 175 sccm at various temperatures. (a) 750, (b) 800, (c) 850, and (d) 990 ^{o}C.

(d) and Fig. 4.5 (d), the diameters of the CNBs decrease with the increase of the C_2H_4 gas flow rate. The SEM images revealed that the CNBs were present in a large quantity in the carbon products. Fig. 4.6 (a) shows a TEM image of the CNBs at 850 ^oC. Figs. 4.6 (b) and (c) are the high magnification TEM images of the Fig. 4.6 (a) and a XRD pattern of the CNBs. As clearly seen in Fig. 4.6 (b), the interlayer spacing is found to be 0.34 nm, which corresponds to the 002 lattice distance in hexagonal graphite. A clear peak at around 26^o can be clearly observed in the XRD pattern. The peak is assigned to 002 diffraction peak of hexagonal graphite, indicating that the CNBs are composed of the graphite layers. This agrees well with the result of the TEM image. Zhong et al reported that the catalyst particles were trapped in the center of the CNBs [27]. However, there is no hollow structure in our CNBs as in the case of MWNTs. No Fe particle can be seen in the CNBs. This indicates that the formation mechanism of the CNBs with Fe catalyst by CVD synthesis from C_2H_4 gas as a raw material is different from that by the decomposition of CH_4 gas with Co as a catalyst.

It has been reported that carbonaceous balls or mesocarbon microbeads can be produced from pitch or polymeric materials from carbonization of pitches and dispersion of mesophase pitches in proper media [28-30]. These processes require the mesophase or liquid-like phase for synthesizing the carbon materials. In our process, the CNBs are synthesized by thermal CVD from C_2H_4 gas. This means that the CNBs form follows a kind of gas-solid procedure. In our process, the role of Fe particles as

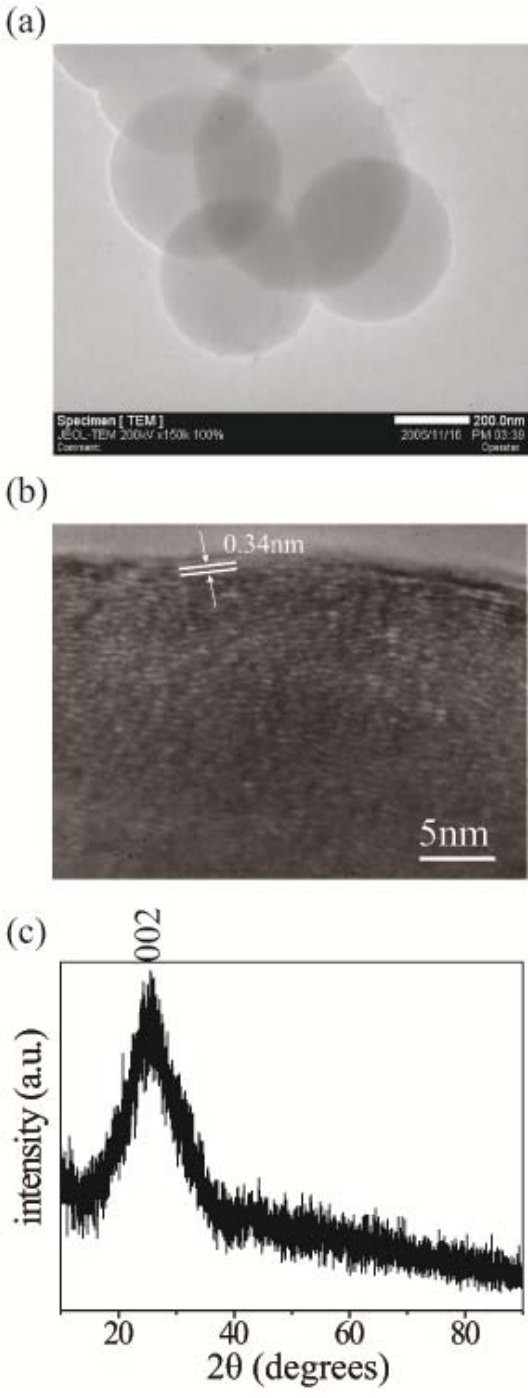

Fig. 4.6. (a) TEM images of the CNBs obtained at 850 ^{o}C. (b) HRTEM image of the CNBs obtained at 850 ^{o}C. (c) XRD pattern of the CNBs obtained at 850 ^{o}C.

catalyst is also crucial because the CNBs are not synthesized on the Si substrate uncovered with Fe. Further study would be required to reveal the formation mechanism of the CNBs in our CVD process.

Figs. 4.7 (a), (b), (c), and (d) show Raman spectra of carbon products at 750, 800, 850, and 990 ^{o}C, respectively. Two peaks around 1590 and 1350 cm^{-1} can be clearly seen in all the spectra. The peak at around 1590 cm^{-1} (G band) is attributed to the stretching modes of C-C bonds of typical graphite [31], whereas the peak at around 1350 cm^{-1} (D band) is related to the defects and disorders in structures in carbonaceous solid [32]. The value of the intensity ratio I_D/I_G is indicative of the graphitization degree of carbon materials. The larger the value of I_D/I_G is, the lower the disorder would be [33]. Fig. 4.8 shows the values of I_D/I_G as two functions of the reaction temperature and C_2H_4 gas flow rate. The values of I_D/I_G increase with the increase of the reaction temperature and/or the C_2H_4 gas flow rate. When the values of I_D/I_G are more than ca. 0.75, implying the graphitization degree of the CNBs is not high, the CNBs were successfully synthesized. On the other hand, the CNTs were produced with the I_D/I_G values of less than 0.7.

4.3.2 Surface modification of CNBs by plasma in liquid phase

The CNBs after surface modification treatment were analyzed by FT-IR spectroscopy and compared to the as-prepared CNBs. Fig. 4.9 shows FT-IR spectra of

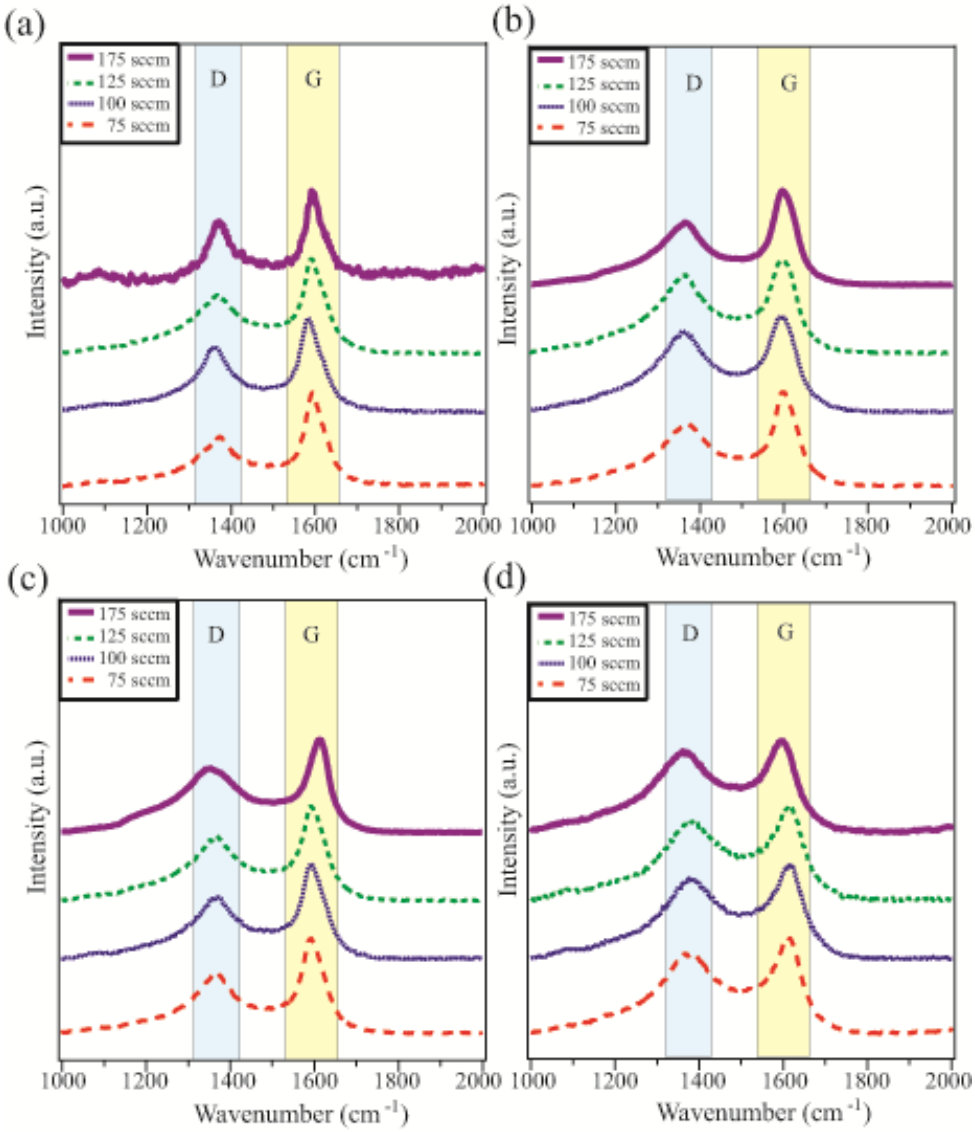

Fig. 4.7. Raman spectra of carbon products at various temperatures. (a) 750, (b) 800, (c) 850, and (d) 990 ^{o}C.

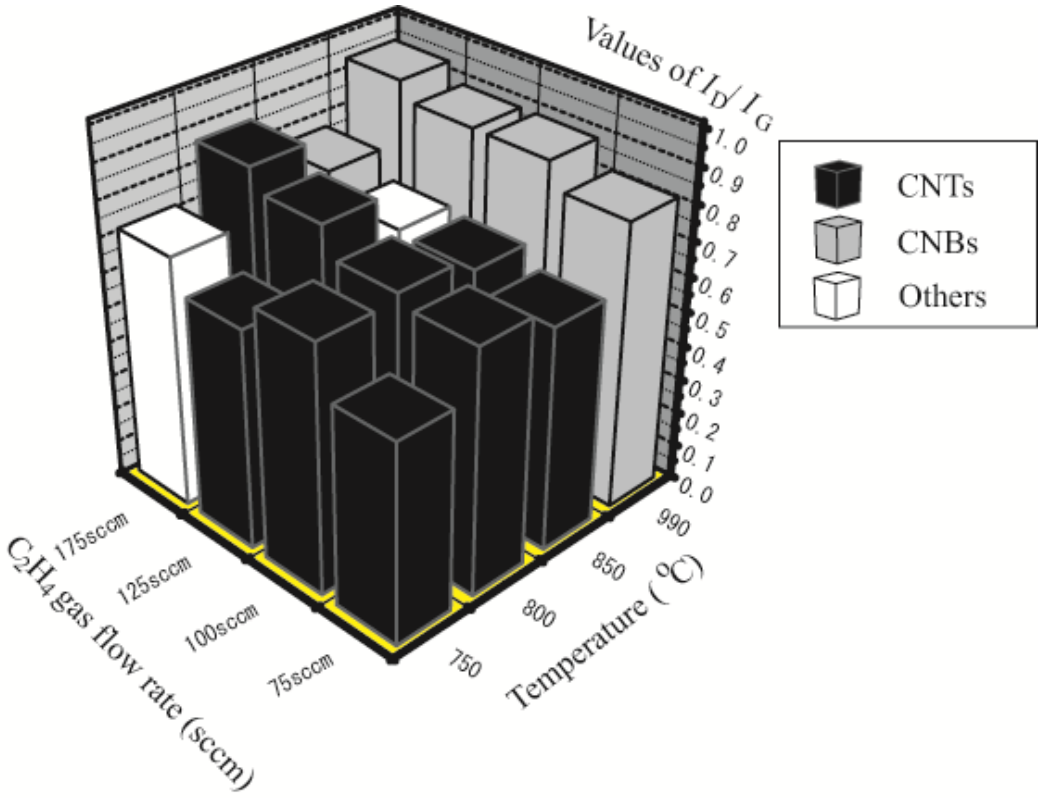

Fig. 4.8. Values of I_D/I_G as two functions of the reaction temperature and C_2H_4 gas flow rate.

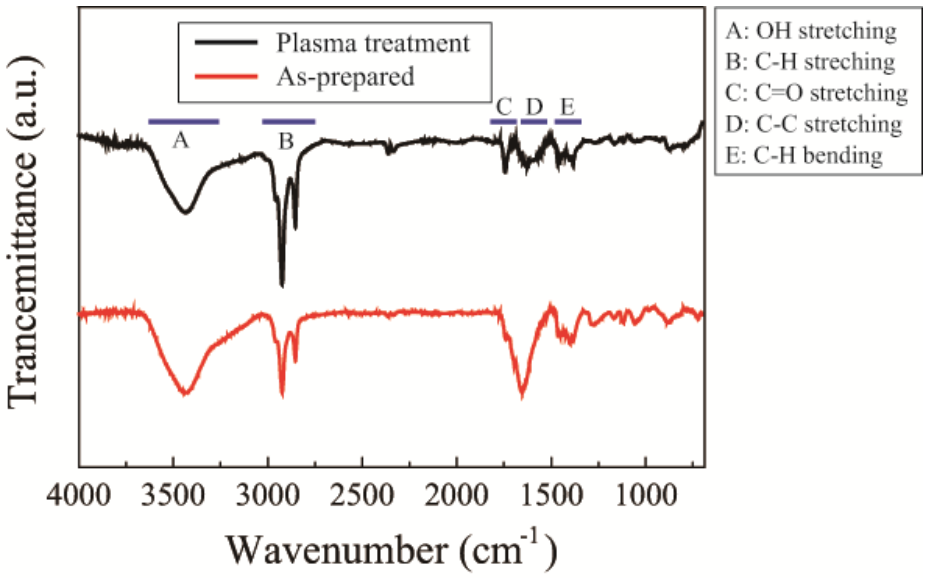

Fig. 4.9. FT-IR spectra of the CNBs before and after surface modification treatments using plasma in liquid phase.

the CNBs after surface modification treatments. In the FT-IR spectra, the absorption bands at around 3500 cm^{-1} (band A), 2900 cm^{-1} (band B), 1450 cm^{-1} (band E) are assigned to the OH stretching, the C-H stretching, and C-H bending vibrations, respectively. The intensity of the absorption bands D and E were decreased by the plasma treatment. In addition, the absorption band B was increased by the plasma treatment, indicating that a part of graphite structure in the CNBs was changed by the scission of the C-C bonds. Moreover, it is confirmed that there is a peak at around 1730 cm^{-1} only on the spectrum of the CNBs treated by plasma in liquid phase, which is originated from the carboxyl group of the carboxylic acid [34]. The carboxyl groups could be produced by the attack of OH radical produced by the plasma in liquid phase. Furthermore, the TEM image (Fig. 4.10 (a)) and Raman spectrum (Fig. 4.10 (b)) before and after plasma treatment revealed that although the CNBs surfaces were etched slightly by the plasma treatment, no change in interlayer structures and Raman spectra before and after the plasma treatment could be observed. These results prove that carboxyl groups modify the CNBs surfaces. Fig. 4.9 (a) shows the photographs of agglomerate of the CNBs before surface modification in water. Figs. 4.9 (b)-(e) show the photographs of dispersion of the COOH-modified CNBs in water, ethanol, acetone, and toluene, respectively. The as-prepared CNBs are not dispersed in water at all. On the other hand, the carboxylated CNBs are uniformly dispersed in water and these organic solvents for more than 168 h. This indicates that the surface modification of

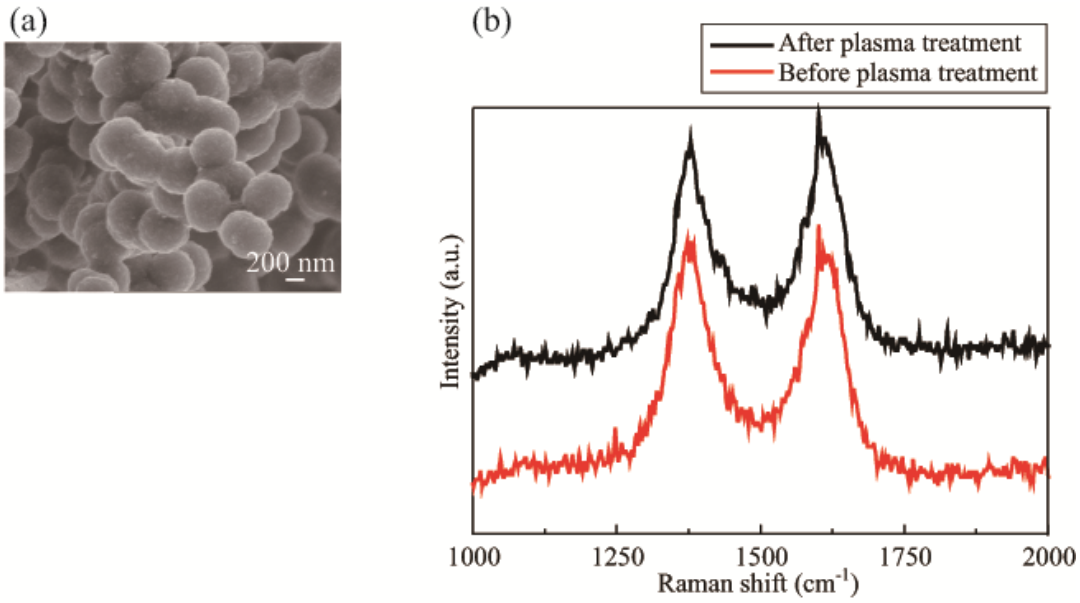

Fig. 4.10. (a) TEM image of the CNBs after plasma treatment in liquid phase. (b) Raman spectra of the CNBs before and after plasma treatment in liquid phase.

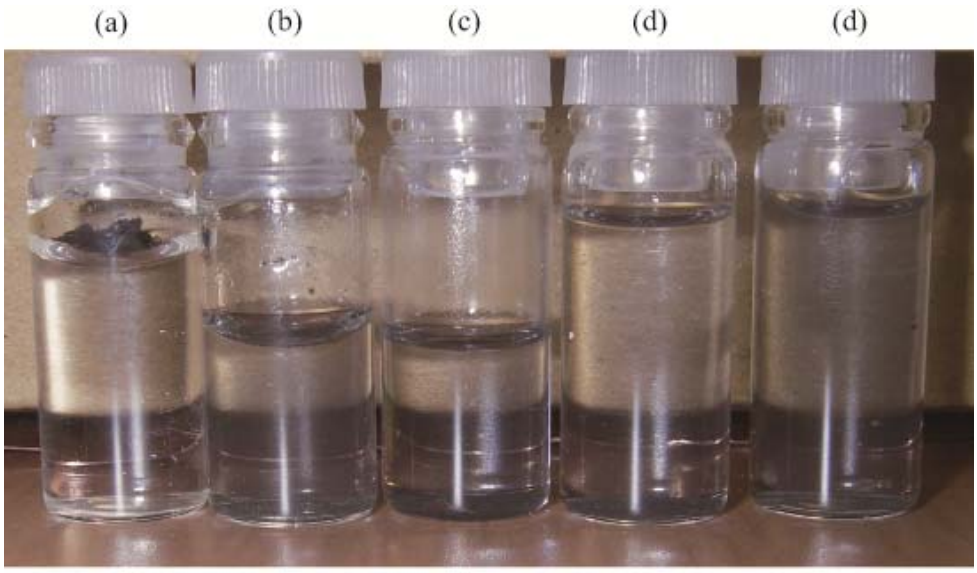

Fig. 4.11. Dispersion of the CNBs before and after treatment by the mixture of sulfuric acid/nitric acid in each solvent. (a) and (b) water, (c) ethanol, (d) acetone, and (e) toluene.

carboxyl groups to the CNBs by the plasma treatment in liquid phase leads to the improvement of dispersion property in the water, ethanol, acetone, and toluene.

4.4 Summary

In this study, the CNBs were successfully synthesized on Fe coated Si substrates using Ar and H_2 gases as carriers, and C_2H_4 gas as raw material by CVD method. The diameters and shapes of the resulting samples depended on the synthesis conditions such as reactor temperature and the flow rate of C_2H_4 gas. Most of CNTs were synthesized below 850 ^{o}C, while CNBs were produced at 990 ^{o}C. The diameters of the CNTs and CNBs were in the ranges of 30 to 100 nm and 300 to 900 nm, respectively. TEM and HRTEM images showed that the CNTs had a hollow structure inside and the wall was composed of multi graphite sheets, that is, multiwalled carbon nanotubes (MWNTs). On the other hand, the CNBs had no hollow structure inside. The interlayer spacing of the CNBs was found to be 0.34 nm. Raman spectra showed that the CNTs and CNBs had two peaks at around 1350 and 1590 cm^{-1}, which correspond to D band and G band, respectively. When the values of I_D/I_G were more than ca. 0.75, the CNBs were successfully synthesized. The carboxyl acid groups were successfully introduced to the CNBs surface by the plasma treatment in liquid phase. The COOH-terminated CNBs were uniformly dispersed in water, ethanol, acetone, and toluene. The CVD

process for the CNBs synthesis is suitable for the mass production and the plasma treatment in liquid phase is useful for the carboxylation of the CNB surface. This carboxylation process will contribute significantly to covalent attachment of the CNBs to polymer matrix.

4.5 References

[1] H.W. Kroto, J.R. Heath, S.C. O'Brien, R.F. Curl, R.E. Smalley, Nature, 318 (1985), 162.

[2] S. Iijima, Nature, 354 (1991), 56.

[3] D. Ugarte, Nature, 359 (1999), 707.

[4] A. Krishnan, E. Dujardin, M.M.J. Treacy, J. Hugdahl, S. Lynum, T.W. Ebbesen, Nature, 388 (1997), 451

[5] P.M. Ajayan, J.M. Nugent, R.W. Siegel, B. Wei, Ph. Kohler-Redlich, Nature, 404 (2000), 243.

[6] Y. Wu, P. Qiao, T. Chong, Z. Shen, Adv. Mater., 14 (2002), 64.

[7] A.C. Dillon, Nature, 386 (1997), 377.

[8] G.E. Gadd, Science, 277 (1997), 933.

[9] P.J. Briffo, K.S.M. Santhanam, P.M. Ajayan, Nature, 406 (2000), 586.

[10] P.G. Collins, A. Zettl, H. Bando, A. Thess, R.E. Smalley, Science, 278 (1997), 100.

[11] W.A. deHeer, A. Chetalain, D. Ugarte, Science, 270 (1996), 1179.

[12] C. Journet, W.K. Maser, P. Bernier, A. Loiseau, M. Lamy de la Chapelle, S. Lefrant, P. Daniard, R. Lee, J.E. Fischer, Nature, 388 (1997), 756.

[13] A. Thess, R. Lee, P. Nikolaev, H. Dai, P. Petit, J. Robert, C. Xu, Y.H. Lee, S.G.

Kim, A.G. Rinzler, D.T. Colbert, G.E. Scuseria, D. Tomanek, J.E. Fischer, R.E. Smalley, Science, 273 (1996), 483.

[14] K. Tanaka, T. Yamabe, K. Fukui, The science and technology of carbon nanotubes, Amsterdam, London and New York: Elsevier, 1999.

[15] Y.N. Xia, B. Gates, Y.D. Yin, Y. Lu, Adv. Mater., 12 (2000), 693.

[16] Z.Y. Zhong, H.Y. Chen, S.B. Tang, J. Ding, J.Y. Lin, K.L. Tan, Chem. Phys. Lett., 330 (2000), 41.

[17] Q. Wang, H. Li, L.Q. Chen, X.J. Huang, Carbon, 39 (2001), 2211.

[18] X.Y. Liu, B.C. Huang, N.J. Covolle, Carbon, 40 (2002), 2791.

[19] J. Qiu, Y. Li, Y. Wang, C. Liang, T. Wang, D. Wang, Carbon, 41 (2003), 767.

[20] H.S. Qian, F.M. Han, B. Zhang, Y.C. Guo, J. Yue, B.X. Peng, Carbon, 42 (2004), 761.

[21] X. He, F. Wu, M. Zheng, Diamond Relat. Mater., 16 (2007), 311.

[22] L.S. Schdler, S.C. Giannaris, P.M. Ajayan, Appl. Phys. Lett., 73 (1998), 3842.

[23] D. Qian, E.C. Dickey, R. Andrews, T. Rantell, Appl. Phys. Lett., 76 (2000), 2868.

[24] E.T. Thostenson, R. Zhifeng, T.-W. Chou, Comput. Sci. Technol., 61 (2001), 1899.

[25] K. Hata, D.N. Futaba, K. Mizuno, T. Nanami, M. Yumura, S. Iijima, Science, 306 (2004), 1362.

[26] H. Stig, L.-C. Carlos, S. Jens, L.H. Poul, S.C. Bjerne, R.R-N. Jens, A.-P. Frank,

K.N. Jens, Nature, 427 (2004), 426.

[27] Z. Zhong, H. Chen, S. Tang, J. Ding, J. Lin, K.L. Tan, Chem. Phys. Lett., 330 (2000), 41.

[28] S.H. Yoon, Y.D. Park, I. Mochida, Carbon, 30 (1992), 781.

[29] Y. Korai, S. Ishida, S.H. Yoon, Y.G. Wang, I. Mochida, Y. Nakagawa, C. Yamaguchi, Y. Matsumura, Y. Sakai, ¥M. Komatsu, Carbon, 35 (1997), 1503.

[30] M. Kodama, T. Fujiura, K. Esumi, K. Meguro, H. Honda, Carbon, 26 (1998) 595.

[31] A.M. Rao, E. Richter, S. Bandow, B. Chase, P.C. Eklund, K.A. Williams, Science, 275 (1997), 187.

[32] F. Tuinstra, I.L. Koeing, J. Chem. Phys., 53 (1970), 1126.

[33] G. Duesberg, I. Loa, M. Burghard, K. Syassen, S. Roth, Phys. Rev. Lett., 85 (2000), 5436.

[34] Y. Lin, A.M. Rao, B. Sadanadan, E.A. Kenik, Y.-P. Sun, J. Phys. Chem., B., 106 (2002), 1294.

Chapter 5

Characterization of platinum catalyst supported on carbon nanoballs prepared by solution plasma processing

5.1 Introduction

5.2 Experimental procedures

5.3 Results and discussion

5.4 Summary

5.5 References

5.1 Introduction

In previous Chapter 4, synthesis and surface modification methods of the carbon nanoballs (CNBs) have been established. In this chapter, the fabrication of a catalytic material for fuel cells was performed by solution plasma. The catalytic activities of the hybrid materials of Pt/CNBs, Pt nanoparticles on CNBs, were investigated using cyclic voltammetry.

Carbon nano-materials (CNMs) such as carbon nanotubes (CNTs), fullerenes and carbon fibers have been focused as attractive materials since 1980s. The CNMs have been utilized in interconnection of electronic devices [1], electron emitter [2], fuel cells [3,4] and so on. Among them, CNMs combined with Pt nanoparticles are employed in fuel cells so that fuel cells offer one of solutions for the depletion of fossil fuel. In the fuel cell systems involving CNMs, the advantages of using CNMs are their high conductivity and surface areas. On the other hand, when Pt nanoparticles as catalyst are supported on CNMs, the size decrease of Pt nanoparticles is required for the realization of high efficient electrode catalyst with low-cost performance. At the present point, conventional methods for loading of Pt nanoparticles on CNMs consists of (1) adsorption of Pt ions and (2) reduction of the ions at high temperature (>500 ^{o}C), which can obtain Pt

nanoparticles with diameter 1-10 nm on CNMs [5,6]. The conventional methods are not necessarily efficient because of the use of excess heat and processing steps.

As an improvement for the efficiency in the adsorption and reduction processes, we cast a spotlight on a technique “Solution Plasma Processing (SPP)”. Solution plasma (SP) is a discharge phenomenon in a liquid such as water or its solution. The SP provides large amount of active species such as hydrogen and hydroxyl radicals, and ions into a water medium. Using the active species, the material processing has been successfully carried out. For instance, gold nanoparticles (diameter ~ 10 nm) have been synthesized by solution plasma [7,8]. The SPP is expected for the novel loading method of Pt metal on CNMs since the high activation of CNMs and reduction of metal ions should be possible in this system.

In this study, we carried out the SPP for loading of Pt nanoparticles on CNBs, which were synthesized by thermal decomposition of ethylene [9,10]. The CNB has high surface area and high conductivity similar to CNTs. We aimed to potentiate the coinstantaneous reduction and loading of metal ions by the SP. Here, we conducted the loading of Pt nanoparticles on CNB (Pt/CNB) and investigated on an effect of additives such protective agents on Pt nanoparticles.

5.2 Experimental procedures

5.2.1 Preparation of CNBs

CNBs were synthesized by thermal decomposition of ethylene (C_2H_4) and hydrogen (H_2) gases under argon (Ar) stream [9,10]. The Ar gases were previously bubbled in water at 150 sccm. The ethylene and hydrogen gases (175 and 100 sccm, respectively) were directly introduced into a quartz tube (φ = 32 mm) heated up to 1100 ^{o}C and reacted for 30 min along with the moisten Ar gas as shown in Fig. 5.1. After the thermal decomposition of the gases, black powder was obtained on the wall of the quartz tube. The powder was collected and milled until the particles passed through a mesh (mesh size: 0.5 mm x 0.5 mm).

5.2.2 Preparation of Pt/CNBs

Pt/CNB hybrids were prepared from an aqueous solution containing hexachloro platinum (IV) acid [H_2PtCl_6] (Wako Chemical Co. Ltd.) and CNBs with poly-(vinylpyrrolidone) (PVP) (Wako Chemical Co. Ltd.) or sodium dodecyl sulfate (SDS) (Sigma-Aldrich) as a protective agent. An aqueous solution (150 cm^3) of 1.44 mM H_2PtCl_6 and PVP (3.0, 12.0, 30.0, and 60.0 mM as repeated unit) or SDS (3.0, 10.0, and 30.0 mM) were mixed

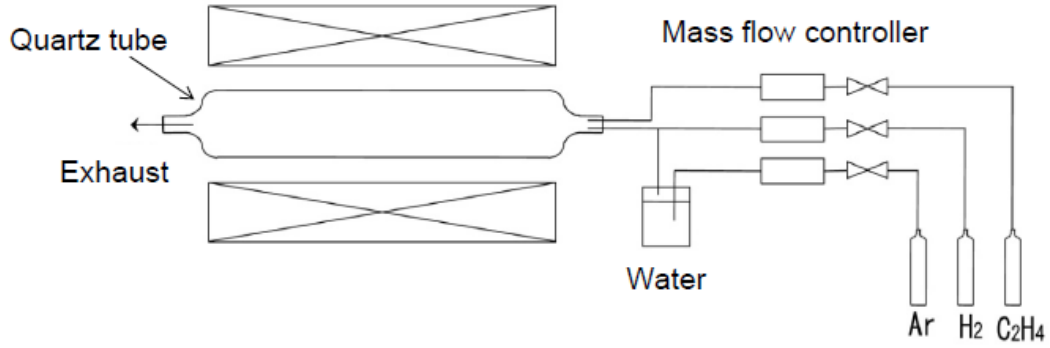

Fig. 5.1 A schematic illustration of apparatus for preparation of CNBs.

with powder of CNBs (50 mg) under vigorous stirring. Fig. 5.2 shows a schematic of the experimental apparatus for the SPP. The apparatus consists of a glass vessel (300 cm^3) filled with the mixture and two tungsten electrode (φ = 1.0 mm) with 0.5 mm gap. The bipolar-pulsed voltages were applied between the electrodes by pulsed power supply (Kurita Seisakusho Co. Ltd., MPS－06K－01C). The applied voltage was 2.4 kV. The pulse width and frequency were 2 μs and 15 kHz, respectively. The discharge was kept for 60 min. During the plasma, the mixture was stirred by magnetic stirrer and kept at 50 ^oC by a cooling chiller. The as-obtained samples were filtered with filter paper (Whatman Japan, 540) and rinsed with pure water. After the filtration, black powers were redispersed in pure water under an ultrasonic so that the final concentration of Pt/ CNB should be 0.025 mg/l. The samples were observed with a scanning electron microscope (SEM) (JEOL, JSM-6330F), a transmission electron microscope (TEM) (JEOL, JEM-2500TS) and energy dispersive spectroscopy (EDS) mapping (JEOL, EX-24055JGT).

5.2.3 Electrochemical evaluation of Pt/CNBs

For the electrochemical evaluation of catalytic activity of Pt nanoparticles, cyclic voltammetry (CV) (ALS Co. Ltd., CH Instruments

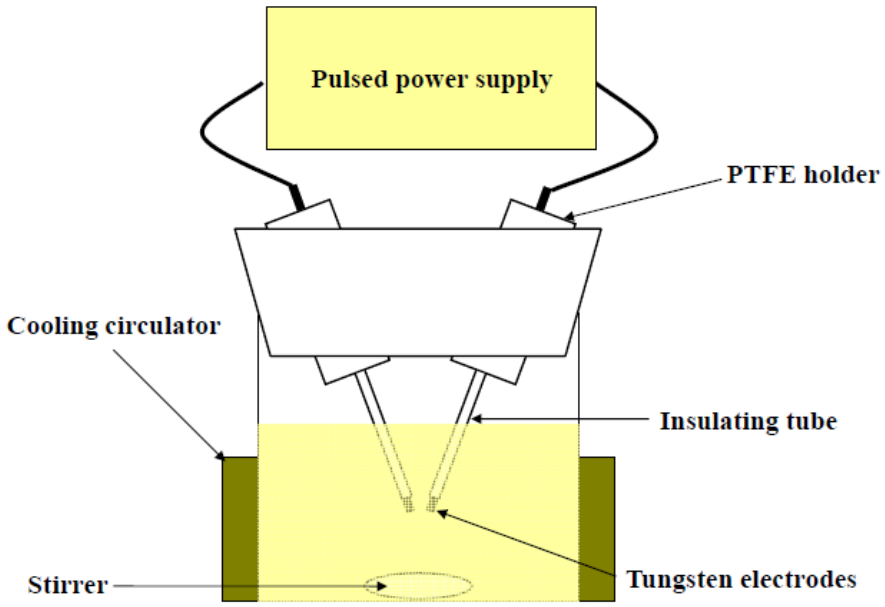

Fig. 5.2 A schematic image of an apparatus for solution plasma processing.

Electrochemical Analyzer Model 600A) was carried out [11,12]. Here, a Ag/AgCl electrode (saturated KCl aq.) and a platinum wire (φ = 0.1 mm) were used as a reference and a counter electrode, respectively. The working electrode was fabricated on a glassy carbon (GCE glassy carbon) (φ = 3 mm). A droplet (5 μl) of the aqueous dispersion of a sample (0.025 mg/l) was placed on the glassy carbon and kept until dry at ambient condition. Subsequently, the Pt/CNB on a glassy carbon was covered with Nafion by a drop and drying of 20μl of 5 % Nafion aqueous dispersion (Wako Chemical Co. Ltd.). Sulfuric acid (0.5 M) was used as an electrolyte solution, which was previously bubbled by N_2 gas for 30 min. Measurements were done under a nitrogen blanket, at a sweep rate 500 mV/s in a range between -0.2 and +1.6 V.

5.3 Results and discussion

Figs. 5.3 (a) and (b) represent SEM images of as-prepared CNBs and CNBs treated by SPP with Pt ions and PVP (12 mM), respectively. The as-prepared CNB had a spherical shape with its size distribution 200-1000 nm. In any condition, the solution before the SPP displayed yellow (color of Pt ions), although the CNBs were floated on water surface and never

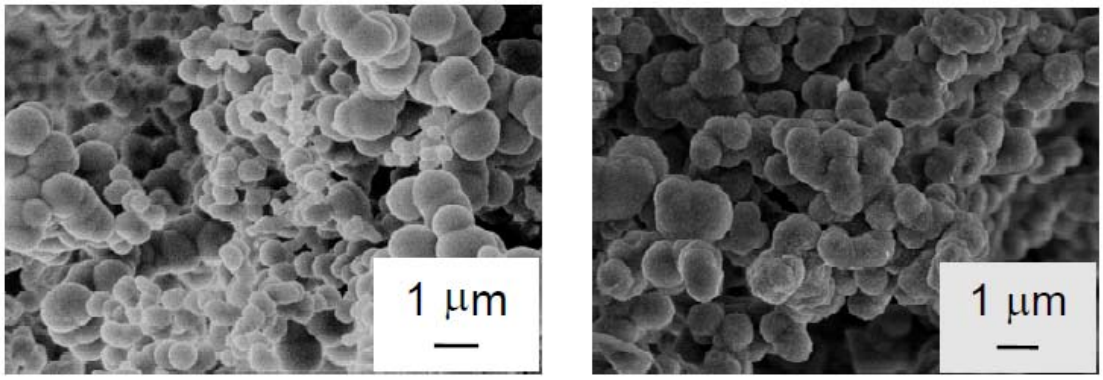

Fig. 5.3 SEM images of (a) bare CNB and (b) Pt/CNB prepared with PVP at 3.0 mM.

dispersed in water. However, after the SPP, we observed a change in the solution color to black brown, indicating the SP improved the dispersibility of CNBs in water. In microscopic observations, we could also see a morphological change on the CNB surface in the SEM images. The surface of CNBs became more roughen after the SPP, which could be resulted from the adhesion of Pt nanoparticles. Indeed, TEM images and EDS elemental mappings confirm the adhesion of Pt nanoparticles as seen in Figs. 5.4 (a)-(c). The TEM image shows black spots on the spherical CNB and the coinstantaneous elemental mapping of C and Pt reveals the presence of platinum atom on carbon spheres. This Pt/CNB electrode showed the electrochemical activity as seen in Fig. 5.4 (d). Hydrogen adsorption and desorption characteristics of Pt metal (-0.2 - 0V) were observed. It indicates the catalytic capability of the Pt nanoparticles in fuel cells.

In the present method, the loading of Pt was achieved in one pot, at single step and under ambient condition by SPP. Conventional methods contain two processes i.e. the loading and reduction processes of Pt ions [13]. Furthermore, the reduction process required extreme heating in the conventional methods. In comparison with the general processes, the present method using SPP have several advantages in simplification and high efficiency of the Pt-loading process.

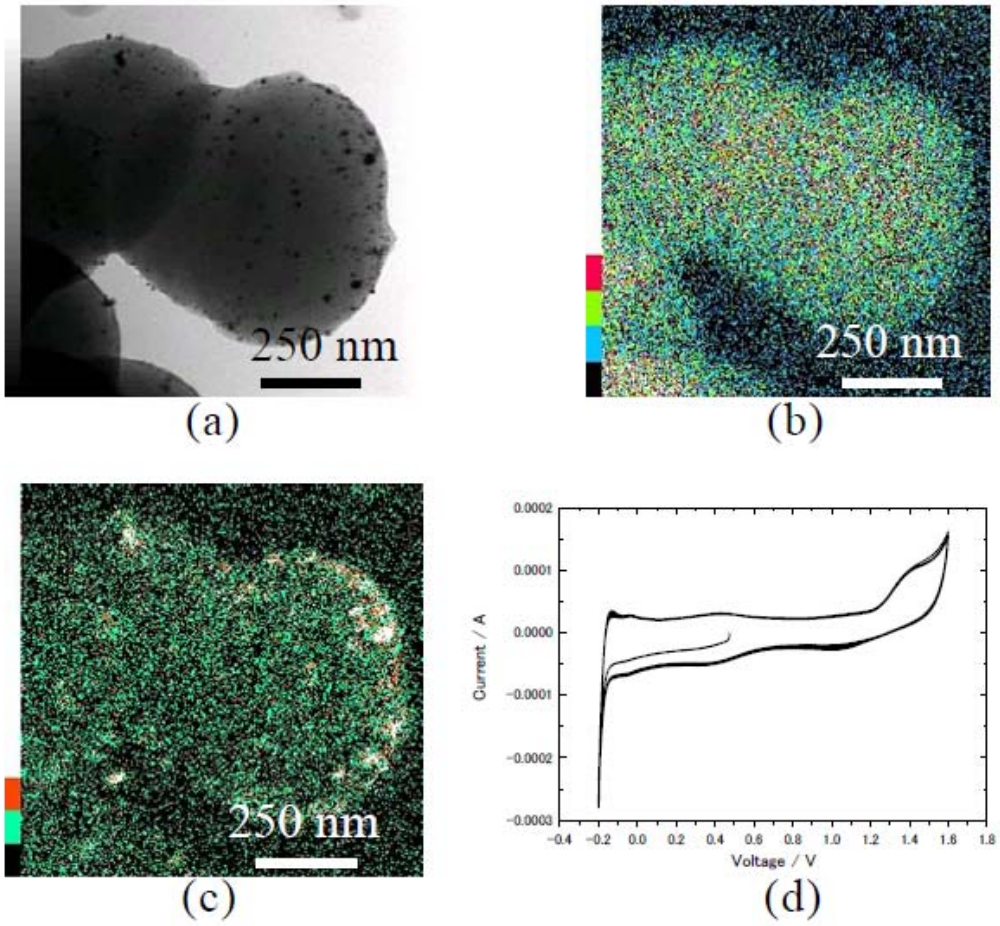

Fig. 5.4 (a) TEM image and EDS elemental mappings of (b) carbon and (c) platinum of Pt/CNB prepared with PVP at 60 mM. (d) CV curve of Pt/CNBs.

In order to find out the optimum condition for obtaining better Pt catalytic activity, we examined the preparation of Pt/CNBs with different protective agents at several concentrations. Here we employed PVP and SDS as protective agents. Furthermore we varied the concentrations 3.0, 12.0, 30.0, and 60.0 mM for PVP, and 3.0, 10.0, and 30.0 mM for SDS. Fig. 5.5 shows TEM images of Pt/CNBs prepared with PVP at the several concentrations. The images indicate the loading of Pt on CNBs at each concentration. Similarly, in the cases of the use of SDS, the Pt-loadings were also verified by the TEM observation as seen in Fig. 5.6. Fig. 5.7 represents the relationships between concentration and average diameter in both the PVP and SDS systems. In these systems, we can see the tendency that the diameter of Pt nanoparticles was reduced with increment of the concentrations.

The obtained Pt/CNBs displayed the characteristic catalytic activities evaluated by CV [11,12], which were diagrammatically shown in Figs. 5.8 (a) and (b) for PVP and SDS systems, respectively. The catalytic activity was represented by an electrochemical surface area per unit mass [$cm^2/\mu g$] calculated from the hydrogen ad-/ desorption waves. The relationships of catalytic activity with concentration were shown in Fig. 5.8 (c) in both the PVP and SDS systems. The activity was diminished as the concentration of

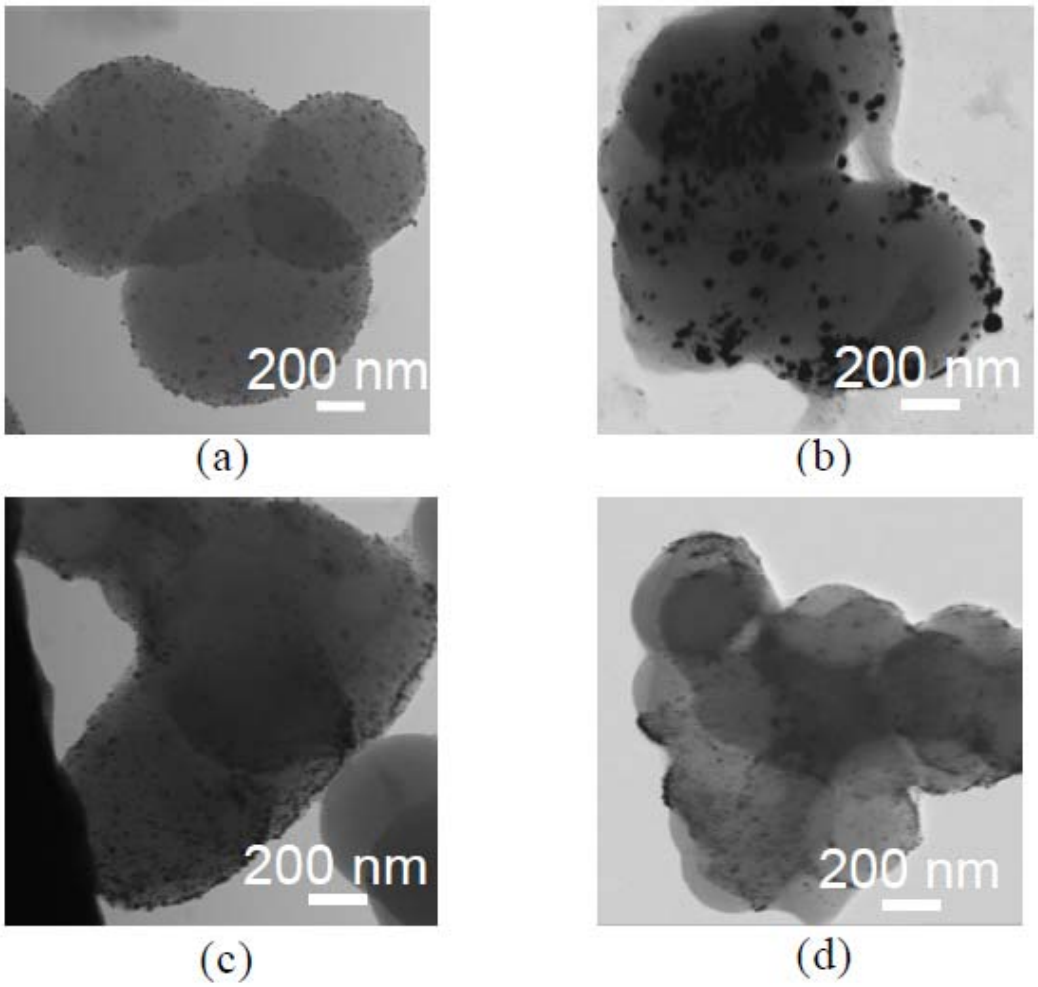

Fig. 5.5 TEM images of Pt/CNB prepared with PVP at (a)3 mM, (b)12 mM, (c)30 mM and (d)60 mM.

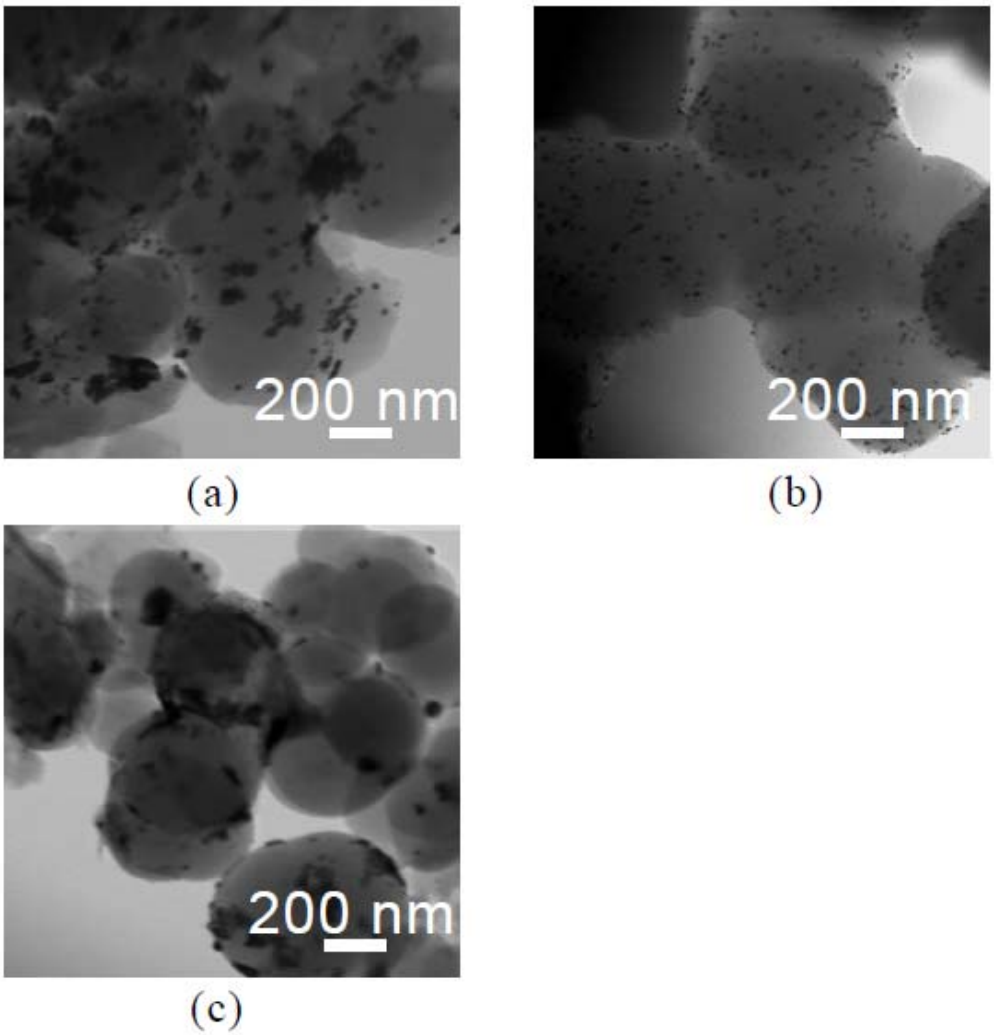

Fig. 5.6 TEM images of Pt/CNB prepared with SDS at (a)3 mM, (b)10 mM and (c)30 mM.

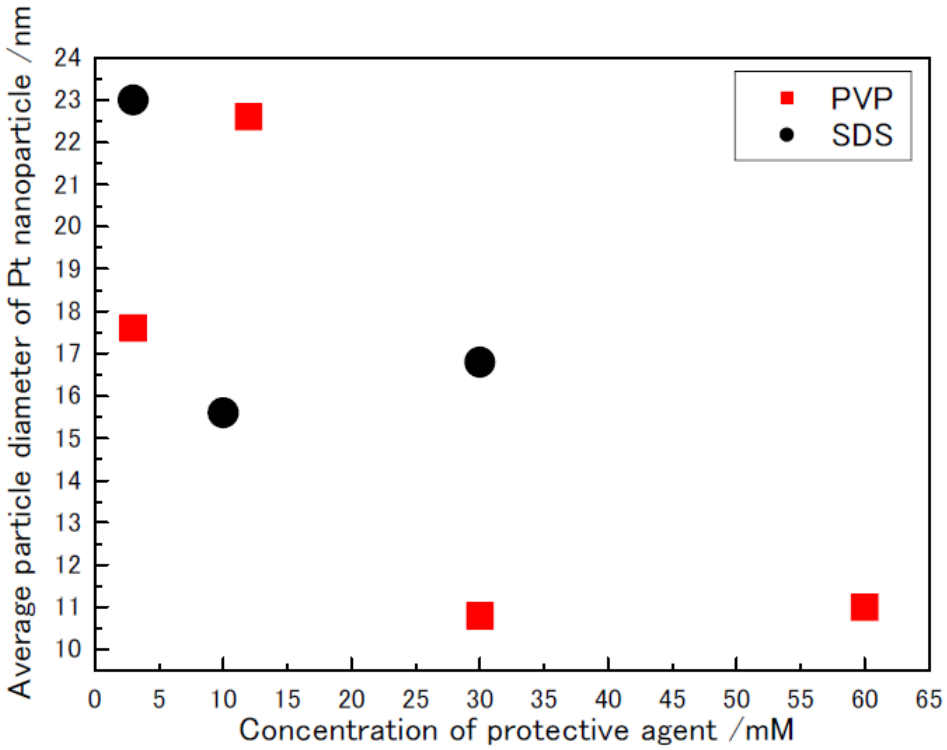

Fig. 5.7 Relationship of average diameter with concentration of PVP (red square) and SDS (black circle).

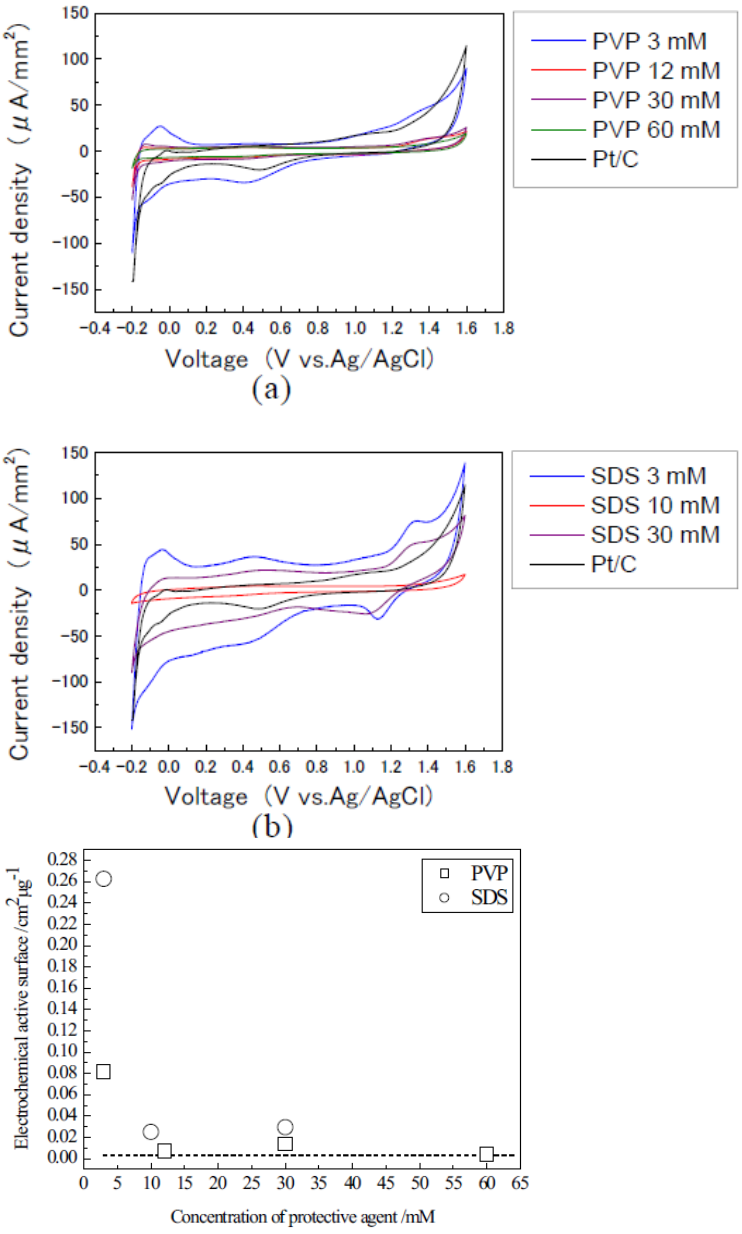

Fig. 5.8 CV curves of Pt/CNBs prepared in (a) the PVP systems and (b) SDS systems besides that of a conventional product (black line). (c) Relationship of electrochemical active surface area with concentration in PVP and SDS systems (a dot line represent the active surface area of a conventional product).

the protective agents was increased. The best catalytic activities were obtained at the 3.0 mM in both systems (0.082 $cm^2/\mu g$ and 0.263 $cm^2/\mu g$, respectively). Fig. 5.8 (c) also indicates the catalytic activity in the SDS system exceeded that in the PVP system.

In order to clarify reasons for the preference of catalytic activity in the SDS system, we compared the loaded amount of Pt nanoparticles between the PVP and SDS systems. The estimation was performed by inductively coupled plasma optical emission spectroscopy (ICP-OES) in the conditions: [PVP] and [SDS] = 3.0 mM. The loaded amounts of Pt in PVP and SDS system were evaluated as 1.58 wt% and 0.94 wt%, respectively. Although the loaded amount in use of SDS (0.94 wt%) was smaller than that prepared with PVP (1.58 wt%), the SDS-containing Pt/CNBs granted a higher catalytic activity than the PVP-containing ones. The fact indicates that the catalytic activity was not closely related to the loaded amount of Pt nanoparticles. On the other hand, since the catalytic activity of Pt nanoparticles is generally proportional to their effective surface area [11,12], from the result of Fig. 5.8, the activity in the PVP system was expected to be larger than that using SDS, where the diameter of Pt nanoparticle in PVP system (17.5 nm at 3.0 mM) was smaller than that of the correspondent SDS system (23.0 nm at 3.0 mM). However, the result of

electrochemical estimation (see Fig. 5.8 (c) at 3.0 mM) was conflict with this expectation. The activity of catalyst in these SPP systems was more dominantly dependent on chemical or physical characters of protective agents rather than the dimension and loaded amount of Pt nanoparticles. For instance, we can assume differences of chemical affinity to the nanoparticle surface among protective agents (PVP or SDS), which affects on coverage on Pt nanoparticles. Indeed, a PVP molecule is used as a good protective agent in preparation of metal nanoparticles due to the strong adsorption at the multi-point on a nanoparticle [14]. Therefore the electrochemically effective surface area in use of SDS might be larger than the PVP system.

Finally, we compared the electrochemical activity of Pt/CNBs with a conventional Pt nanoparticles supported on activated charcoal (Pt/C, Pt = 10 wt%, [Sigma-Aldrich]). The electrochemical activity of conventional Pt/C was evaluated at 0.0016 $cm^2/\mu g$ (represented by a dot line in Fig. 5.8 (c)). The activity of Pt/CNBs prepared with SDS at 3.0 mM exceeded it. Although the loaded amount of Pt in the conventional product was higher than that in the SDS system, the electrochemical efficiency of Pt/CNBs in the SDS system was dominant in comparison with the conventional product. The result shows that SPP can offer a novel process obtaining Pt/CNBs with higher electrochemical activity.

5.4 Summary

In this study, we demonstrated a novel process for loading of Pt nanoparticles on CNBs using SPP. The SPP realized a one-pot synthesis of Pt/CNB at an ambient temperature. The SDS system obtained better electrochemical activity than the PVP system, which could be resulted from a less coverage of SDS molecules on a Pt nanoparticle. Furthermore, the obtained Pt/CNB displayed more excellent catalytic activity than a conventional product.

The solution plasma provides new possibilities for nano-material synthesis and surface arrangement as shown in this study. In future, the fuel cell with higher energy-conversion efficiency can be realized by using the obtained Pt/CNB.

5.5 References

[1] G. Fedorova, A. Tselevb, D. Jimenezc, S. Latild, N.G. Kalugine, P. Barbarab, D. Smirnova, S. Roche, Physica E **40**, 1010 (2008)

[2] Chang-Kyun Parka, Jong-Pil Kima, Sung-Jun Yuna, Young-Kwang Kima, Won Kima, Jong-Uk Kimb, Jin-Seok Park, Diamond & Related Materials **17,** 1826 (2008)

[3] N. Rajalakshmi, Hojin Ryu, M. M. Shaijumon, S. Ramaprabhu, Journal of Power Sources **140**, 250 (2005)

[4] Zhenhai Wen, Qiang Wang, Qian Zhang, Jinghong Li, Electrochemistry Communications **9**, 1867 (2007)

[5] Kazuaki Yasuda, Yasuno Nishimura, Materials Chemistry and Physics **82,** 921 (2003)

[6] Dongyan Xu, Huamin Zhang, Wei Ye, Catalysis Communications **8,** 1767 (2008)

[7] Nagahiro Saito, Junko Hieda, Camelia Miron, Osamu Takai, Journal of The Surface Finishing Society of Japan **58**, 12, 810 (2007)

[8] Junko Hieda, Nagahiro Saito, Osamu Takai, Surface & Coatings Technology **202,** 5343 (2008)

[9] Tsuneyuki Itoh, Takahiro Ishizaki, Nagahiro Saito, Osamu Takai,

Proceedings of the 17th Iketani Conference the Doyama Symposium on Advanced Materials 265 (2007)

[10] T. Itoh, T. Ishizaki, N. Saito, O. Takai, Proceedings of International Symposium on Dry Proces, 257 (2007)

[11] A. Pozio, M. De Francesco, A. Cemmi, F. Cardellini, L. Giorgi, Journal of Power Sources **105,** 13 (2002)

[12] J.J. Wang, G.P. Yin, J. Zhang, Z.B. Wang, Y.Z. Gao, Electrochemica Acta **52,** 7042 (2007)

[13] Xin-dong Mua, David G. Evans and Yuan Kou, Catalysis Letters **97**, 3-4, 151 (2004)

[14] Dnniel G. Duff, Petter P. Edwards, Braian F. G. Johnson, Journal of Physical Chemistry **99**, 15934 (1995)

Chapter 6

Rapid sterilization of *Escherichia coli* by solution plasma process

6.1 Introduction

In previous Chapters 4 and 5, plasma process in liquid phase, that is, solution plasma processing has been utilized to modify the CNBs surfaces. In this chapter, to explore the diversity of the solution plasma, sterilization of *Escherichia coli* (*E.coli*) in water was performed using solution plasma.

Decontamination and sterilization of water are one of the most important issues on the environmental and medical fields [1,2]. Conventional approaches employed for sterilization of virus and bacteria in water such as chemical (chlorination by chlorine, chlorine dioxide, or chloramines, ozonization and so on) and physical (ultraviolet (UV) radiation including solar radiation, high energy particle irradiation, ultrasound treatment, ultrafiltration, heating, freezing, reverse osmosis and so on) methods and their combinations have been developed and utilized [3]. However, they are complex processes with significant limitations related to the generation of toxic side-product (e.g. chlorinated hydrocarbons known as trihalomethanes which are suspected carcinogens) or low efficiencies for large scale

applications. Moreover, most of these techniques can cause damage to the treated substrate. These drawbacks especially render such approaches counterproductive to the environmental field, which seeks to reduce hazardous compound use and production, and eliminate risk to humans. Recently, plasma technologies under atmospheric conditions are emerged as potential alternative methods for the sterilization of the bacteria in water [4-11]. The advantages of the methods have their stability to sterilize at relatively low temperatures within a short time and non-toxic nature in comparison to more traditional methods because, unlike chemical based biocides such as chlorine and ozone, the plasma treatments are a physical method used to kill all bacteria without adding any biocidal chemical.

Discharge in liquid phase also has a potential of rapid physical sterilization in water without using any chemical agent [12] because it can generate highly chemical reactive species such as OH and H radicals, shock wave, and UV light. Furthermore, it would be reasonable to expect a higher reaction rate under lower-temperature conditions with greater chemical reaction variability because the molecular density of the liquid

phase is much higher than that of the gas phase. The cold plasma in liquid-phase has been named as “Solution Plasma (SP)” [13] because we can generate a variety of plasmas by choosing the combinations of solvents and solutes in solutions. This approach would allow us to inactivate the bacteria in liquids within a short time.

In this study, we aimed to sterilize efficiently and rapidly *Escherichia coli* (*E.coli*) which is known as one of the most representative bacteria in aqueous solution by SP. In addition, the chemically active species in water generated by the SP, and the plasma parameters such as electron density, plasma density and temperature were characterized by optical emission spectroscopy.

6.2 Experimental procedures

Fig. 6.1 shows a schematic diagram of discharge system used in this study. This system consisted of two wire-type metal electrodes placed in an acrylic vessel and driven by bipolar DC pulsed power supply (Kurita-Nagoya MPS-06K06C; Kurita Co. Ltd.). The applied voltages were varied from 2.0 to 2.4 kV. The

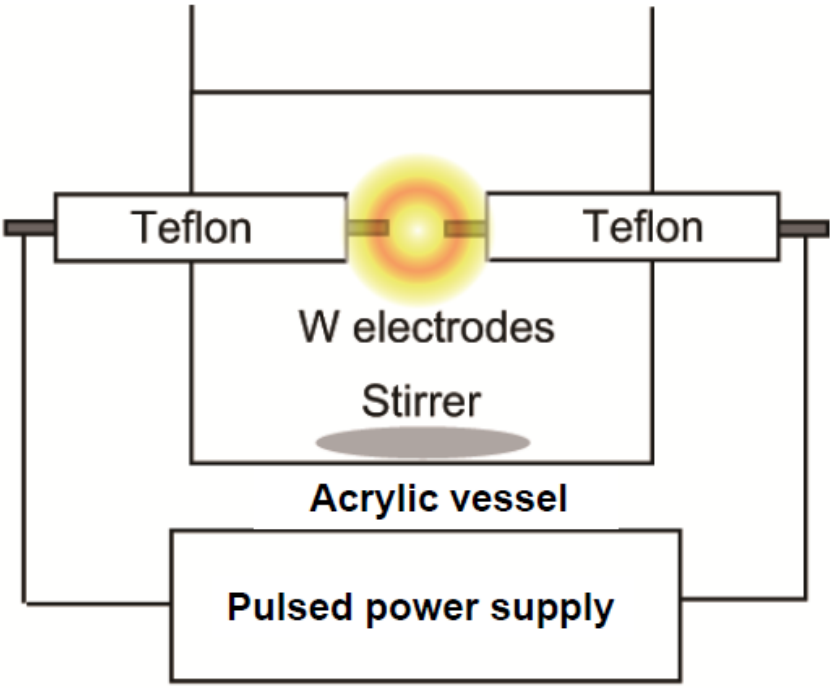

Fig. 6.1 Schematic illustration of the experimental system with the wire-to-wire electrode configuration.

pulse frequency and pulse width employed were 15 kHz and 2 μs, respectively. Tungsten wire, with a diameter of 1 mm, was used as the electrode material. The distance between the tips of the electrodes was set at 1.0 or 3.0 mm. The temperature during the discharge was measured by a digital multimeter equipped with a thermocouple. The electrical conductivity was adjusted to 500 μS/cm by Na_2SO_4 solution. The conductivity of the solution was measured by EC meter (Hanna HI991300). We selected the Na_2SO_4 as a supporting electrolyte, because the electrolyte does not affect the sterilization. Optical properties of generated plasma were observed by spectroscope (PhotoTechnica AvaSpec-3648) operated at the wavelength range of 200 to 1000 nm. UV-vis spectra was measured in wavelength range of 200 to 800 nm at the scan speed of 4 cm^{-1}.

E.coli was cultivated in a liquid culture medium for 24 h. The medium was prepared from Bacto-tryptone 10 g/l, Bacto-yeast extract 5 g/l, and Na_2SO_4 5 g/l. The culture medium containing *E.coli* was added to 400ml of the aqueous solution. Discharge in the aqueous solution was then carried out for 300 s. The solution was agitated by a magnetic stirrer at a bottom of the

acrylic vessel. During the discharge process, the samples were taken out in an interval of 1 min. Each sample of 100 μl in volume was diluted into 1 ml of ultrapure water and coated onto a cultivation dish. The cultivation dish was made from Bacto-tryptone 10 g/l, Bacto-yeast extract 5 g/l, and NaCl 5 g/l, and agar 14g/l. After cultivation process for 24 h at the temperature of 37°C, the number of surviving bacteria was determined by counting colony forming units (CFUs). The shapes of *E.coli* before and after the discharge were observed with a scanning electron microscope (SEM). *E.coli* in the aqueous solution was caught by a filter with small holes and was fixed on the filter with glutaric aldehyde and osmium tetroxide solution. The water in the bacteria was replaced by t-butanol. The filter was coated with Pt and Pd. To investigate an effect of UV light originated from discharge on the sterilization, small quartz and acrylic cells were used. The both cells were set in the acrylic vessel. The aqueous solution containing *E.coli* was then added to the cells.

6.3 Results and discussion

When the high voltage was applied between the electrodes, the bubbles originated from water vaporization were first generated at the vicinity of the electrodes. The discharge was then started in the gas phase. The discharge stably continued during the application of the high voltage.

The sterilization performance of the discharge in aqueous solution to *E.coli* was estimated by counting the CFUs after the discharge. The relation between the numbers of survivors and discharge time was shown in Fig. 6.2 (a). The decimal reduction time of *E.coli* (D value) of this system was estimated to be approximately 1.0 min. The D value of 1.0 min is faster than other microorganism sterilization procedures, evidencing that our SP process has a high potential for inactivation of *E.coli*.

To investigate the effects of the physical damages by the discharge to the *E.coli*, the shape changes were observed using SEM. Fig. 6.2 shows SEM images of *E.coli* (b) before and (d) after discharge treatment. Granular or rectangular *E.coli* with several hundred nm in diameter was clearly observed on both images. No change in shape can be seen before and after the discharge. Figs. 6.2 (c) and (e) show enlarged SEM images of the

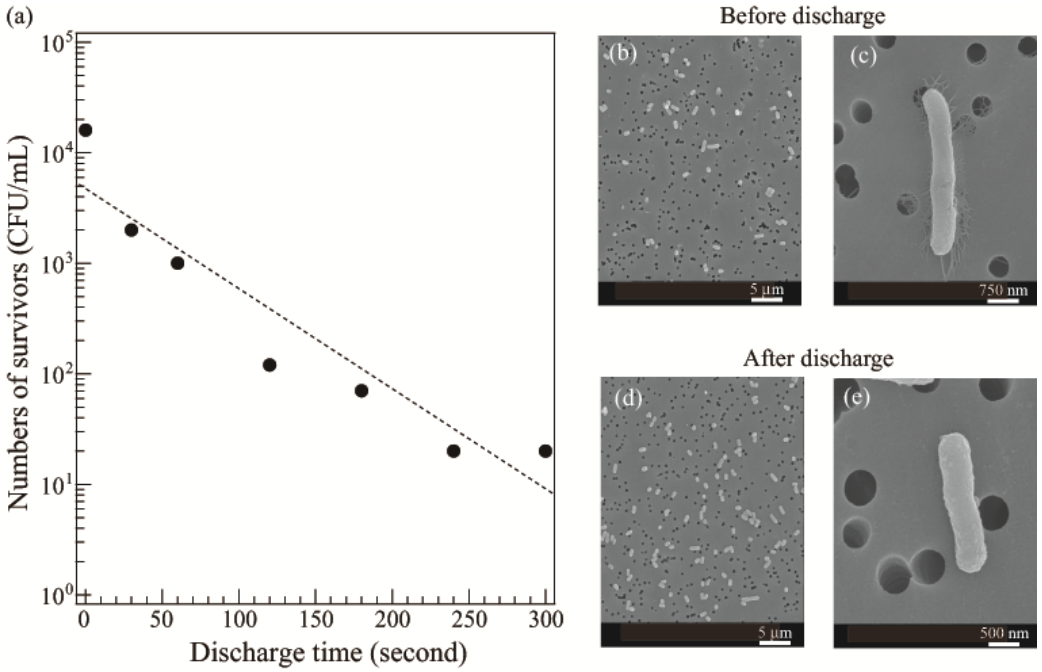

Fig. 6.2 (a) Numbers of surviving *E.coli* as a function of discharge time. SEM images of *E.coli* (b) before and (d) after discharge in aqueous solution. Enlarged SEM images of *E.coli* (c) before and (e) after discharge in aqueous solution.

E.coli before and after discharge, respectively. The shapes of most *E.coli* before and after the discharge treatment remained intact. This indicates that the discharge in the aqueous solution provides no physical damage to the *E.coli* and could inactivate the bacteria chemically or thermally. To reveal the chemical active species generated by the discharge in the aqueous solution, the optical emission spectroscopy was carried out. Fig. 6.3 (a) shows the optical emission spectrum. Some clear peaks can be observed, originating from atomic hydrogen, the hydroxyl radical (OH band at 306.4 nm), atomic oxygen (O lines at 777.9 nm, 844.6 nm and 926.2nm). These lines come from the water molecule dissociation in the electrical discharge process. The two dominant lines observed at 656 nm and 486 nm are assigned to H_α and H_β, respectively. In addition, a line attributable to atomic sodium was also clearly observed at 589 nm. Based on the optical emission spectra we estimated the electron density, temperature and plasma density of the SP. Focusing on the H_a line and assuming that broadening of this line was give by dynamic Stark effect [14], the electron density in plasma discharge could be estimated to be the orders of 10^{15} cm^{-3}. According to Lieberman

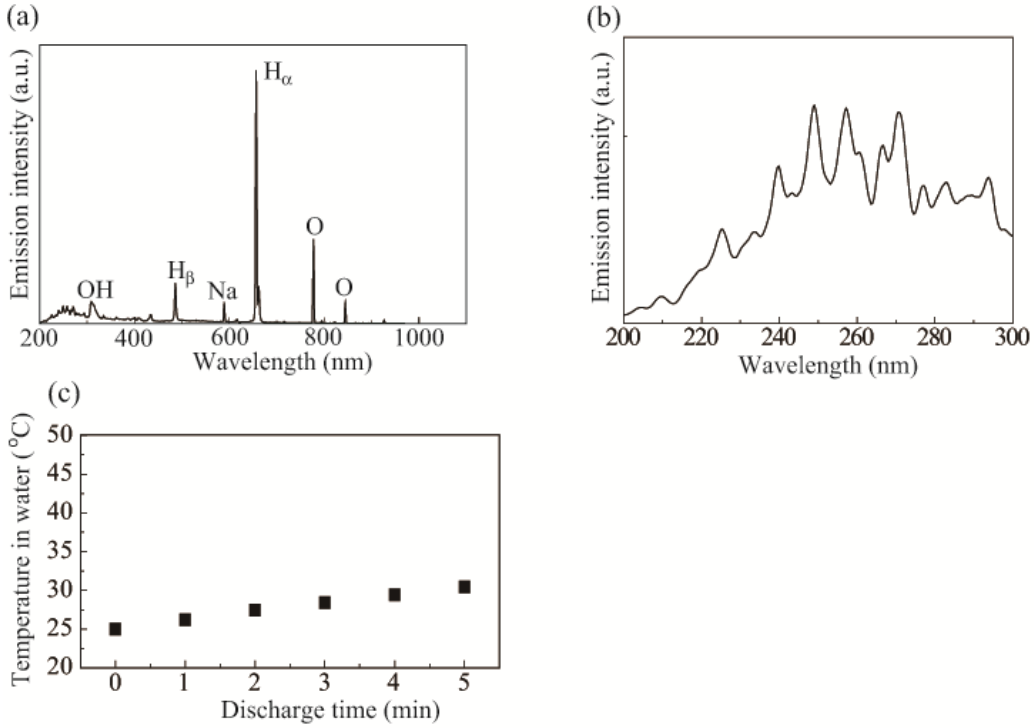

Fig. 6.3 (a) Optical emission spectrum of the discharge in aqueous solution at wavelength of 200 to 1000 nm. (b) Optical emission spectrum of the discharge in aqueous solution at wavelength of 200 to 300 nm. (c) Temperature in water as a function of discharge time.

et al [15], we could also estimate the temperature and plasma density of the discharge to be in ranges of T = 5000-7000 K and *n* = 10^{14}-10^{15} cm^{-3}, respectively. Fig. 6.3 (b) shows the enlarged optical emission spectrum ranging from 200 to 300 nm in wavelength. Several broad bands originating from UV light are clearly detected. It is known that ozone has its maximum absorption cross-section of 1.15 x 10^{-17} cm^2 at a wavelength of 254 nm [16]. The ozone is produced from oxygen ion species through the dissociation of oxygen molecules by electron impact. The recombination of oxygen molecules and oxygen radicals via three-body collisions by the following reactions:

$$e^- + O_2 \rightarrow O_2^- \rightarrow O\cdot + O\cdot + e^- \,,\; O_2 + O\cdot \rightarrow O_3 \qquad (6.1)$$

The resulting ozone molecules diffuse and could sterilize the *E.coli* in aqueous solution by possible oxidation and modification of the cell membrane. Fig. 6.3 (c) shows the temperature in the aqueous solution as a function of discharge time. As clearly seen in Fig. 6.3 (c), the change in temperature is very low. This supports that the sterilization of the *E.coli* is hardly affected by the thermal effect generated by the discharge in the aqueous solution. Thus, UV light might be an important factor for the

sterilization mechanism, so it is necessary to clarify the effect of the UV light on the sterilization.

To further investigate the effect of UV light attributable to the discharge in an aqueous solution on the sterilization, quartz and acrylic cells were used. The both cells were set in the acrylic vessel, as shown in Fig. 6.4 (a). The distance from the discharge zone to the cells was set at approximately 5cm and the distance between electrodes was set at 3.0 mm. Most UV light can pass not the acrylic cell but the quartz cell as shown in the UV-vis spectra (Fig. 6.4 (b)). Thus, we can estimate the effects of UV emission on the sterilization of the *E.coli*. Moreover, the quartz prevents active species such as ozone and radicals from attacking the samples because it allows only UV light to reach the samples. The number of surviving bacteria for the inside and outside of the both cells after the discharge was estimated as shown in Fig. 6.4 (c). The bacteria in the quartz cell were sterilized as well as bacteria in the acrylic vessel. The D values for quartz cell and acrylic vessel were estimated to be 3.0 and 3.1 min, respectively. On the other hand, no change in the numbers of surviving bacteria in the acrylic cell was clearly observed. This provides direct

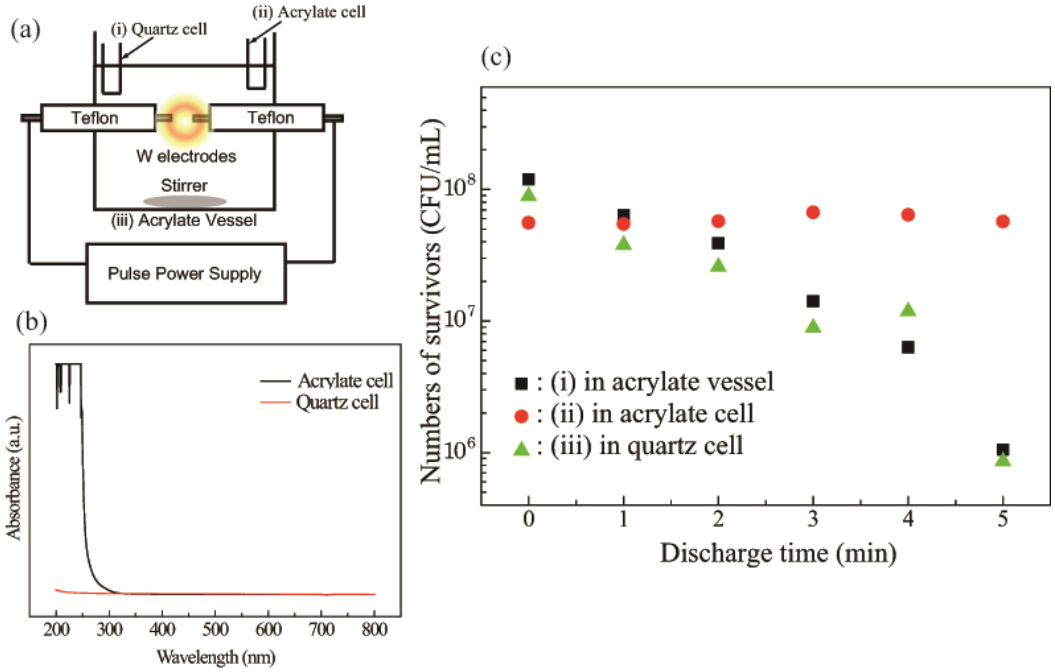

Fig. 6.4 (a) Schematic illustration of the experimental system using quartz and acrylic cells. (b) UV-vis spectrum of quartz and acrylic cells. (c) Numbers of surviving *E.coli* in quartz, acrylic cells, and acrylic vessel as a function of discharge time.

evidence that not mechanical/thermal damage and radical attack but UV light significantly contributes to the sterilization.

6.4 Summary

In this study, we revealed that the *E.coli* was successfully sterilized by the discharge in the aqueous solution, that is, SP. The D value of this system set at the electrode distance of 1.0 mm was estimated to be approximately 1.0 min. Based on the optical emission spectra, we estimated plasma parameters for SP such as electron density, plasma density, and temperature. This discharge system in the aqueous solution provides no physical damage to the *E.coli* and hardly allows the temperature increase in the aqueous solution. The important factor for the sterilization of the *E.coli* was UV light generated from the SP. This developed discharge system in an aqueous solution opens a door to the developments of treatment systems of water containing various types of bacteria with high throughput and low temperature.

6.5 References

[1] M. Korachi, Z. Turan, K. Senturk, F. Sahin, N. Aslan, J. Electrostatics, **67**, 678 (2009).

[2] S.Manolache, E.B.Somers, A.C.L. Wong, V. Shamamian, F. Denes, Environ. Sci. Technol., **35**, 3780 (2001).

[3] R.E.J. Sladek, E. Stoffels, J. Phys. D: Appl. Phys., **38**, 1716 (2005).

[4] A. Sharma, A. Pruden, Z. Yu, G.J. Collins, Environ. Sci. Technol., **39**, 339 (2005).

[5] T. Montie, K.K.-Wintenberg, R. Roth, IEEE Trans. Plasma Sci., **28**, 41 (2000).

[6] M. Moisan, J. Barbeau, S. Moreau, M. Tabrizian, J. Pelletier, A. Ricard, L.H. Yahia, Int. J. Pharm., **226**, 1 (2001).

[7] M. Laroussi, IEEE Trans. Plasma Sci., **30**, 1409 (2002).

[8] M. Laroussi, J.P. Richardson, F.C. Dobbs, Appl. Phys. Lett., **81**, 772 (2002).

[9] Y. Akishev, V. Chugunov, M. Grushin, V. Karal'nik, V. Kholodenko, N. Trushkin, Biomedical Aspect of Plasma Physics, APP Spring meeting, Bad Honnef, Germany, 37 (2003).

[10] M. Moisan, J. Barbeau, M.-C. Crevier, J. Pelletier, N. Philip,

B. Saoudi, Pure Appl. Chem. **74**, 349 (2002).

[11] M. Boudam, M. Moisan, B. Saodi, C. Popovici, N. Gherardi, F. Massines, J. Phys. D: Appl. Phys. **39**, 3494 (2006).

[12] Y.Akishev, M. Grushin, V. Karalnik, N. Trushkin, V. Kholodenko, V. Chugunov, E. Kobzev, N. Zhirova, I. Irkhina, G. Kireev, Pure Appl. Chem. **80**, 1953 (2008).

[13] N. Saito, J. Hieda, O. Takai, Thin Solid Films, **518**, 912 (2009).

[14] P. Bårmann, S. Kröll, A. Sunesson, J. Phys. D: Appl. Phys. **29**, 1188 (1996).

[15] M.A. Lieberman, A.J. Lichtenberg, Principles of Plasma Discharges and Material Processing, John Willey & Sons Inc., New York, p. 9 (1994).

[16] Y. Katrib, S. T. Martin, H. M. Hung, Y. Rudich, H. Zhang, J. G. Slowik, P. Davidovits, J. T. Jayne, D. R. Worsnop, J. Phys. Chem. A **108**, 6686 (2004).

Chapter 7

Conclusions

Conclusions

The aim of this study described in this doctoral dissertation is to establish the basic process conditions for high functionalization of biomaterial, sensor device, energy material, and sterilization treatment using plasma chemical process and to investigate their characteristics. In this dissertation, “plasma in gas phase” and “plasma in liquid phase” have been treated in Chapters 2-3 and 4-6, respectively.

The topic of “plasma in gas phase” in this dissertation was to perform surface modification of organic and inorganic materials to impart high functionalization to their materials and to estimate their highly functionalized materials surface in terms of bioactivity and detection sensitivity. That of “plasma in liquid phase” in this dissertation was to modify the CNBs surface and improve the functionalization of the CNBs. In addition, a novel functional material, i.e., Pt/CNBs hybrid material, was successfully fabricated and the catalytic activity of the Pt/CNBs hybrid material was estimated using cyclic voltammetry. Moreover, sterilization technology of *Escherichia coli* using the plasma in liquid phase was developed.

The conclusions of respective studies are as follows:

(1) The study of “Hydrophilicity and bioactivity of a polyethylene terephthalate surface modified by plasma-initiated graft polymerization” in Chapter 2 can be

summarized and concluded as follows:

Hydrophilic modification of polyethylene terephthalate (PET) was successfully achieved by surface wave plasma treatment followed by graft polymerization with monomers such as acrylic acid (AA) and (2-hydroxyethyl) methacrylate (HEMA) in the vapor phase. The surface morphology of the PET film after Ar plasma treatment was observed using atomic force microscopy (AFM). The plasma treatment did not physically damage the PET surface. The graft reaction was confirmed by water contact angle measurements and X-ray photoelectron spectroscopy (XPS). The water contact angles of the PET surface modified with hydrophilic AA and HEMA monomers decreased from approximately 80° before treatment to less than 35°, and the hydrophilicity of the PET surface modified by hydrophilic AA and HEMA monomers was maintained for 70 h. XPS C 1*s* spectra revealed that the modified PET surface had three chemical bond states corresponding to carbon atoms of the benzene rings unbonded to the ester group, carbon atoms singly bonded to oxygen, and ester carbon atoms. 3T3 fibroblast cells were cultured on the modified PET surface. After the cells were cultured for 24 h on the untreated and styrene (St)-modified PET surfaces, the number of cultured cells was higher than the initial number of seeded cells. In contrast, the number of cultured cells on AA-modified and HEMA-modified surfaces was much lower than the initial number of seeded cells. The developed method is useful for the

surface modification of biopolymers for advanced functionalization.

(2) The study of “High sensitive detection of volatile organic compounds using superhydrophobic quartz crystal microbalance” in Chapter 3 can be summarized and concluded as follows:

A quartz crystal microbalance (QCM) chemical sensor coated with superhydrophobic film for detecting volatile organic compounds (VOCs) such as formaldehyde and toluene under ambient conditions was developed. The superhydrophobic film was deposited by means of microwave plasma enhanced chemical vapor deposition (MPECVD). The sensitivities of QCM sensor coated with superhydrophobic film to VOCs such as formaldehyde and toluene were investigated under ambient conditions. The sensitivity of the sensor to formaldehyde and toluene was considerably improved by the superhydrophobic surface modification. The surface modification promoted microscopic texturing to the film surface and thus increased the effective specific surface area of the sensor for the adsorption of formaldehyde and toluene. In addition, the adsorption of water molecules was minimized due to the superhydrophobic film deposited on the sensor surface, thus promoting the preferential adsorption of formaldehyde and toluene molecules on the QCM sensor coated with superhydrophobic film, compared to the conventional QCM sensor. Moreover, the

adsorption mechanisms of formaldehyde-water and toluene-water molecules to the superhydrophobic film were discussed. The developed surface modification method with superhydrophobic films for the QCM chemical sensor contributes to the highly-sensitive detection of VOCs under ambient conditions.

(3) The study of "Synthesis and surface modification of carbon nanoballs (CNBs)" in Chapter 4 can be summarized and concluded as follows:

The CNBs were successfully synthesized on Fe coated Si substrates using Ar and H_2 gases as carriers, and C_2H_4 gas as raw material by thermal chemical vapor deposition (CVD) method at the temperature of 850 to 990 ^{o}C. The diameters of the CNTs and CNBs were in the range of 30 to 100 nm and 300 to 900 nm, respectively. TEM and HRTEM images showed that the CNTs had a hollow structure inside and the wall was composed of multi graphite sheets, that is, multiwalled carbon nanotubes (MWNTs). On the other hand, the CNBs had no hollow structure inside. Raman spectra showed that the CNTs and CNBs had two peaks at around 1350 and 1590 cm^{-1}, which correspond to D band and G band, respectively. When the values of intensity ratio I_D/I_G were more than ca. 0.75, the CNBs were successfully synthesized. The carboxyl groups were successfully introduced to the CNBs surface by the plasma treatment in liquid phase. The COOH-terminated CNBs were uniformly dispersed in

water, ethanol, acetone, and toluene for long time. The plasma in liquid phase, that is, solution plasma, is a promising method to control the dispersibility of carbon nano-materials (CNMs) in liquid.

(4) The study of “Characterization of platinum catalyst supported on carbon nanoballs prepared by solution plasma processing” in Chapter 5 can be summarized and concluded as follows:

In order to improve the energy-conversion efficiency of fuel cells, we loaded Pt nanoparticles on carbon nanoballs (CNBs) by using solution plasma processing (SPP) involving CNB and Pt ion with a protection group. In this study, we employed poly (vinylpyrrolidone) (PVP) or sodium dodecyl sulfate (SDS) to prepare Pt nanoparticles supported on CNB (Pt/CNB) by the SPP, and the electrochemical properties as a catalyst was evaluated by cyclic voltammetry.

The CNBs were prepared by thermal decomposition process of ethylene and hydrogen gases. Color of the solution changed from yellow to dark brown as synthesis time. This change indicates the improvement of dispersibility of CNB. Moreover, TEM images and elemental mapping images showed the Pt nanoparticles supported on CNBs. The catalytic activity of the Pt/CNB in use of SDS was shown to be higher than the Pt/CNB prepared with PVP. The SDS-containing Pt/CNB also showed the higher

activity than a conventional product. The SPP provides a new possibility to develop a highly-efficient catalyst for fuel cells.

(5) The study of “Rapid sterilization of Escherichia coli by solution plasma process” in Chapter 6 can be summarized and concluded as follows:

Solution plasma (SP) which is a discharge in an aqueous solution has a potential of rapid sterilization for water without chemical agents. The discharge had the strong sterilization performance for *Escherichia coli* (*E.coli*). The decimal reduction time of *E.coli* (D value) of this system set at electrode distance of 1.0 mm was estimated to be approximately 1.0 min. Our discharge system in the aqueous solution provides no physical damage to the *E.coli* and allows the little increase in temperature of the aqueous solution. The UV light generated by the discharge was an important factor for sterilization of the *E.coli*. The SP process is promising to develop a rapid sterilization method with high safety for various bacteria in water.

This doctoral dissertation has described materials and bio-chem innovations using plasma technologies in gas phase and in liquid phase. The plasma chemical process developed in this dissertation will contribute advances in the fields of green and life innovations.

List of Publications

Publication

1. **Nina Andreeva**, Takahiro Ishizaki, Nagahiro Saito, Creating biointerface on polymer by plasma-initiated graft polymerization, *Trans. Mater. Res. Soc. J.*, in press (2012).
2. Takahiro Ishizaki, **Nina Andreeva**, Nagahiro Saito, Cell adhesion behaviors on polyethylene terephthalate surface modified by surface-wave plasma-initiated graft polymerization, TechConnect World 2011 Proceedings: *Nanotechnology* Vol 1, 4, 437-440 (2011).
3. **Nina Andreeva**, Takahiro Ishizaki, Pavel Baroch, Nagahiro Saito, High sensitive detection of volatile organic compounds using superhydrophobic quartz crystal microbalance, submitted to *Sensor and Actuators B: Chemicals*.
4. **Nina Andreeva**, Takahiro Ishizaki, Pavel Baroch, Nagahiro Saito, Synthesis and surface modification of carbon nanoballs, submitted to *Mater. Chem. Phys*.
5. **Nina Andreeva**, Takahiro Ishizaki, Pavel Baroch, Nagahiro Saito, Rapid sterilization of *Escherichia coli* by solution plasma process, submitted to *Jpn. J. Appl. Phys*.

Presentation

1. **Nina Andreeva**, Takahiro Ishizaki, Nagahiro Saito, Creating biointerface on polymer by plasma-initiated graft polymerization, The 20th MRS-Japan Academic Symposium, 20-22 December 2010, Yokohama, Japan.
2. **Nina Andreeva**, Takahiro Ishizaki, Nagahiro Saito, Cell adhesion behaviors on polyethylene terephthalate surface modified by surface-wave plasma-initiated graft polymerization, TechConnect World, 13-16 June 2011, Hynes Convention Center, Boston, MA., U.S.A.
3. **Nina Andreeva**, Takahiro Ishizaki, Nagahiro Saito, Adhesion control of bacteria with micropatterned superhydrophobic/superhydrophilic and superhydrophobic/poly(ethylene glycol) surfaces, 20th International Materials Research Congress, 14-19 August 2011, Cancún, Mexico.